

The University of Maine

DigitalCommons@UMaine

---

Electronic Theses and Dissertations

Fogler Library

---

Fall 8-21-2020

## Beyond the Brain: a Study of $\alpha$ -synuclein's Role in Bone and Adipose Tissue

Carolina A. Figueroa

University of Maine, carolina.figueroa@maine.edu

Follow this and additional works at: <https://digitalcommons.library.umaine.edu/etd>



Part of the [Behavioral Neurobiology Commons](#), and the [Biochemical Phenomena, Metabolism, and Nutrition Commons](#)

---

### Recommended Citation

Figueroa, Carolina A., "Beyond the Brain: a Study of  $\alpha$ -synuclein's Role in Bone and Adipose Tissue" (2020). *Electronic Theses and Dissertations*. 3261.

<https://digitalcommons.library.umaine.edu/etd/3261>

This Open-Access Thesis is brought to you for free and open access by DigitalCommons@UMaine. It has been accepted for inclusion in Electronic Theses and Dissertations by an authorized administrator of DigitalCommons@UMaine. For more information, please contact [um.library.technical.services@maine.edu](mailto:um.library.technical.services@maine.edu).

BEYOND THE BRAIN: A STUDY OF  $\alpha$ -SYNUCLEIN'S ROLE IN BONE AND ADIPOSE  
TISSUE

By

Carolina Andrea Figueroa Amenábar

B.S., University of Chile, 2009.

M.S., University of Chile, 2015.

A DISSERTATION

Submitted in Partial Fulfillment of the

Requirements for the Degree of

Doctor of Philosophy

(in Biomedical Sciences and Engineering)

The Graduate School

The University of Maine

August 2020

Advisory Committee:

Clifford Rosen, MD, Maine Medical Center Research Institute, Mentor

Aaron Brown, PhD, Maine Medical Center Research Institute

Robert Burgess, PhD, Maine Medical Center Research Institute

Juan Pablo Rodriguez, PhD, Universidad de Chile

Calvin Vary, PhD, Maine Medical Center Research Institute

# BEYOND THE BRAIN: A STUDY OF $\alpha$ -SYNUCLEIN'S ROLE IN BONE AND ADIPOSE TISSUE

By Carolina Andrea Figueroa Amenábar

Dissertation Mentor: Dr. Clifford J. Rosen

An Abstract of the Dissertation Presented in  
Partial Fulfillment of the Requirements for the  
Degree of Doctor in Philosophy  
(in Biomedical Sciences and Engineering)  
August 2020

$\alpha$ -Synuclein is a polypeptide encoded by the *Snca* gene, highly expressed in neurons, but it is also found in bones and adipose tissue. Co-expression analysis showed that *Snca* regulates skeletal homeostasis, and its deletion reduced estrogen deficiency-induced bone loss and weight gain. It is a major component of Lewy bodies (LB) in Parkinson's disease (PD), leading to progressive immobilization and a range of nonmotor symptoms, including osteopenia, body composition alterations and insulin resistance. This thesis aimed to determine  $\alpha$ -Synuclein's intrinsic role in bone and adipose homeostasis.

We discussed the PD pathophysiology emphasizing aspects of bone health and metabolism. By using *in vivo* models we showed conditional deletion of *Snca* in

osteoblasts is insufficient to reduce bone loss after estrogen deficiency, however, sufficient to reduce weight gain and decrease marrow adipocyte expansion.

Prrx1Cre off-target effects led to decreased  $\alpha$ -Synuclein expression in the brain, decreased serum catecholamines, and behavioral phenotypes. Mutant mice experienced a mild improvement in bone microarchitecture. Although not protected from diet-induced obesity, mutants showed smaller adipocytes in the inguinal fat, decreased adipogenesis and higher oxidative capacity, however, decreased insulin sensitivity. Interestingly, AdipoCre;Snca<sup>fl/fl</sup> mice showed no significant increase in inguinal adipose accrual, decreased weight gain and increased insulin sensitivity.

*In vitro* models of loss of  $\alpha$ -Synuclein led to fragmented mitochondria, decreased adipogenesis, and pAKT and, increased levels of AKT, pIR $\beta$  and pSHC. Mutated  $\alpha$ -Synuclein overexpression (A53T<sup>tg/tg</sup>) led to higher adipogenesis, mitochondria size and increased levels of pAKT/AKT. There was no change in colocalization of  $\alpha$ -Synuclein to mitochondria in cells with differential  $\alpha$ -Synuclein expression. After insulin treatment,  $\alpha$ -Synuclein relocated to the nuclei in controls, however, this response was not seen in A53T<sup>tg/tg</sup>.

This work showed  $\alpha$ -Synuclein regulates adipose tissue cell autonomously and it does affect, mildly, bone microarchitecture through its actions on osteoblasts. Moreover, we showed  $\alpha$ -Synuclein regulates insulin response by affecting the levels of pAKT/AKT and phosphorylated insulin receptor  $\beta$ .

Future research is essential to understand the local and systemic effects of  $\alpha$ -Synuclein signaling on bone remodeling and adipose metabolism to shed light into possible treatment targets for osteoporosis and insulin resistance in PD patients.

## DEDICATION

To my dad,

who taught me the most important lessons in life.

To Motita,

For waiting long and endless hours, for many years.

## ACKNOWLEDGEMENTS

I would like to express my deepest gratitude to my mentor Dr. Cliff Rosen for taking me as a student and assigning this project to me. The completion of this work would not have been possible without his support and nurturing. Also, special thanks to the Rosen lab members who had provide me with training and assistance throughout the duration of this project.

I would like to extend my sincere thanks to the members of my committee that have been crucial in the development of this project.

Thanks to GSBSE of University of Maine for letting me be part of its student community and special thanks to MMCRI for its support.

## TABLE OF CONTENTS

DEDICATION.....	v
ACKNOWLEDGEMENTS.....	vi
LIST OF FIGURES.....	viii
ABBREVIATIONS.....	xxviii
CHAPTER	
1. INTRODUCTION.....	1
1.1. Pathophysiology of Parkinson's Disease.....	2
1.2. Motor Alterations and Disease Progression.....	2
1.3. Sleep Disorders and Sensory Abnormalities.....	4
1.4. Autonomic Alterations in PD.....	4
1.5. Body Composition and Disease Progression.....	5
1.6. Cognitive and Neurobehavioral Alterations.....	6
1.7. Bone strength, Quality (and Loss) in Parkinson's Disease Patients.....	6
1.8. Parkinson's Disease, Falls and Neuroendocrine Mediators.....	11
1.9. Animal Models of PD and Their Implications for Understanding Skeletal Morbidity.....	14
1.10. Osteoporosis Treatments for PD Patients.....	17

2. MATERIALS AND METHODS.....	21
2.1. Animals .....	21
2.2. Induction of Estrogen Deficiency .....	21
2.3. Diet Induced Obesity (DiO) .....	22
2.4. Serum Collection and Catecholamine’s Measurement.....	22
2.5. Body Composition by DXA .....	23
2.6. Micro-Computed Tomography ( $\mu$ CT) .....	23
2.7. Osmium Tetroxide Staining .....	24
2.8. Metabolic Profile .....	25
2.9. Behavioral Tests.....	26
2.9.1. Elevated Plus Maze Test .....	26
2.9.2. Open Field Test .....	26
2.9.3. Marble Burying Test .....	27
2.9.4. Tail Suspension Test.....	27
2.10. Glucose Tolerance Test (GTT) and Insulin Tolerance Test (ITT) .....	27
2.11. Gene Expression Analysis .....	28
2.11.1. Real-time PCR.....	28
2.11.2. Western Blotting .....	29
2.12. Bone Marrow Stromal Isolation.....	31

2.13.	Adipogenesis .....	31
2.14.	Oil Red O Staining.....	32
2.15.	Osteoblastogenesis .....	32
2.16.	Alkaline Phosphatase and Von Kossa Staining.....	32
2.17.	Osteoclastogenesis .....	33
2.18.	Tartrate-Resistant Acid Phosphatase (TRAP) Staining .....	33
2.19.	Histological Sections and Hematoxylin and Eosin (H&E) Staining .....	34
2.20.	Marrow Adipocyte Analysis .....	34
2.21.	Immunohistochemistry .....	34
2.22.	Isolation of Stromal Vascular Fraction from Inguinal White Adipose Tissue (iWAT).....	35
2.23.	Seahorse- Cellular Metabolism.....	35
2.24.	Mitochondrial Labelling.....	36
2.25.	Immunofluorescence.....	36
2.26.	Imaging and Quantification Analysis.....	37
2.27.	Statistical Analysis.....	37
3.	EFFECTS OF ESTROGEN DEFICIENCY ON BONE AND ADIPOSE TISSUE IN PRRX1CRE;SNCA <sup>FL/FL</sup> MICE.....	38
3.1.	Prrx1Cre;Snca <sup>fl/fl</sup> Female Mice are Partially Protected from OVX-Induced Weight Gain.....	38

3.2.	Prrx1Cre;Snca <sup>fl/fl</sup> Female Mice are not Protected from OVX-Induced Bone Loss.....	39
3.3.	Prrx1Cre;Snca <sup>fl/fl</sup> Female Mice Showed Lower Marrow Adipose Tissue After OVX-Induced Bone Loss .....	43
3.4.	Prrx1Cre;Snca <sup>fl/fl</sup> Female Mice Showed Smaller Adipocytes and Thermogenic and Lipolytic Gene Expression Profile from White Adipose Tissue after OVX-Induced Bone Loss.....	45
4.	IMPLICATIONS OF USING PRRX1CRE ENHANCER TO TARGET OSTEOPROGENITOR CELLS.....	49
4.1.	Prrx1Cre;Snca <sup>fl/fl</sup> Male Mice Present an Anxiety-Like Response and Decreased Ambulatory Activity when fed with High Fat Diet, but showed Resistance to High Fat Diet Effect in Spontaneous Activity .....	49
4.2.	Prrx1Cre;Snca <sup>fl/fl</sup> Male Mice showed Lower Catecholamines compared to Control Mice .....	51
4.3.	Prrx1Cre;Snca <sup>fl/fl</sup> Adult Mice showed a Decreased Expression of $\alpha$ -Syn in Key Brain Regions.....	53
5.	EFFECTS OF DIET-INDUCED OBESITY IN PRRX1CRE;SNCA <sup>FL/FL</sup> .....	57
5.1.	Female and Male Mice Food Intake and Body Composition.....	57
5.2.	Bone Microarchitecture Analysis of Femurs from the Diet-induced Obesity in Prrx1Cre;Snca <sup>fl/fl</sup> .....	59
5.3.	Histological Analysis of Inguinal Adipose Tissue after HFD Study .....	65

5.4.	Metabolic Cages Activity Analysis, Glucose Tolerance Test (GTT) and Insulin Tolerance Test (ITT) .....	66
5.5.	Thermogenic Gene Expression Analysis and Adipogenic Differentiation of Inguinal Adipose Depot and Preadipocytes Metabolic Profile.....	68
6.	EFFECTS OF DIET-INDUCED OBESITY IN ADIPOQCRE;SNCA <sup>FL/FL</sup> .....	74
6.1.	Female Mice Food Intake and Body Composition .....	74
6.2.	Bone Microarchitecture Analysis of Femurs from the Diet-induced Obesity in AdipoqCre;Snca <sup>fl/fl</sup> .....	75
6.3.	Metabolic Cages Activity Analysis, Glucose Tolerance Test (GTT) and Insulin Tolerance Test (ITT) .....	75
6.4.	Histological Analysis of Inguinal Adipose Tissue after HFD study.....	81
6.5.	AdipoqCre;Snca <sup>fl/fl</sup> Male Mice showed No Differences in Serum Catecholamines Compared to Control Mice .....	82
7.	<i>IN VITRO</i> STUDIES IN PRIMARY CULTURE OF LOSS AND GAIN OF FUNCTION .....	83
7.1.	Differentiation in Preadipocytes from Inguinal Adipose Tissue from Snca <sup>-/-</sup> Mice and A53T <sup>tg/tg</sup> .....	83
7.2.	Lipid Droplet in Preadipocytes from Inguinal Adipose Tissue from Snca <sup>-/-</sup> mice and A53T <sup>tg/tg</sup> .....	84

7.3.	Mitochondria Morphology in Preadipocytes from Inguinal Adipose Tissue from Snca <sup>-/-</sup> Mice and A53T <sup>tg/tg</sup> .....	85
7.4.	Differential Subcellular Localization of $\alpha$ -Synuclein in iWAT Preadipocytes from AdipoCre;Snca <sup>fl/fl</sup> and A53T <sup>tg/tg</sup> mice.....	85
7.5.	Insulin Signaling in Preadipocytes from AdipoCre;Snca <sup>fl/fl</sup> and A53T <sup>tg/tg</sup> mice.....	86
8.	DISCUSSION.....	92
8.1.	Discussion of the Effects of Deletion of $\alpha$ -Synuclein in Osteoprogenitor Cells.....	92
8.2.	Discussion of the Implications of using Prx1Cre as Enhancer to Target Deletion in the Skeletal Limb.....	93
8.3.	Discussion of the Effects of Deletion of $\alpha$ -Synuclein in Adipocytes from the Inguinal Adipose Tissue.....	98
9.	CONCLUSIONS AND CLINICAL IMPLICATIONS.....	102
10.	FUTURE DIRECTIONS.....	105
	REFERENCES.....	106
	BIOGRAPHY OF THE AUTHOR.....	121

## LIST OF FIGURES

Figure 1. Loss of nigrostriatal circuits in Parkinson’s Disease (PD).....	3
Figure 2. Bone remodeling and dopamine.....	18
Figure 3. Prrx1Cre;Snca <sup>fl/fl</sup> female mice are partially protected from OVX-induced fat acquisition.....	40
Figure 4. Prrx1Cre;Snca <sup>fl/fl</sup> female mice are not protected from OVX-induced trabecular bone loss.....	41
Figure 5. Prrx1Cre;Snca <sup>fl/fl</sup> female mice are not protected from OVX-induced cortical bone loss.....	42
Figure 6. Prrx1Cre;Snca <sup>fl/fl</sup> female mice showed a decreased in marrow adipose tissue (MAT) after OVX-induced bone loss.....	44
Figure 7. Prrx1Cre;Snca <sup>fl/fl</sup> female mice showed smaller adipocytes from the inguinal white adipose tissue (iWAT) after OVX.....	45
Figure 8. Thermogenic genes analysis in Prrx1Cre;Snca <sup>fl/fl</sup> female mice inguinal white adipose tissue (iWAT).....	46
Figure 9. Lipolytic and mitochondrial genes analysis in Prrx1Cre;Snca <sup>fl/fl</sup> female mice inguinal white adipose tissue (iWAT).....	48

Figure 10. Activity and behavioral analysis of Prrx1Cre;Snca<sup>fl/fl</sup> mice on low and high fat diet.....52

Figure 11. Prrx1Cre;Snca<sup>fl/fl</sup> male mice showed a decreased serum levels of catecholamines than wild type mice.....55

Figure 12. Prrx1Cre;Snca<sup>fl/fl</sup> adult mice showed a decreased expression of  $\alpha$ -Syn in key brain regions.....56

Figure 13. Prrx1Cre;Snca<sup>fl/fl</sup> female or male mice are not protected from diet-induced obesity.....58

Figure 14. Prrx1Cre;Snca<sup>fl/fl</sup> female mice showed a mild improvement in trabecular bone microarchitecture after treatment with HFD.....61

Figure 15. Prrx1Cre;Snca<sup>fl/fl</sup> female mice showed no differences in cortical bone microarchitecture compared to control after HFD treatment.....62

Figure 16. Prrx1Cre;Snca<sup>fl/fl</sup> male mice showed no differences in trabecular bone microarchitecture compared to control after treatment with HFD..... 63

Figure 17. Prrx1Cre;Snca<sup>fl/fl</sup> male mice showed no differences in cortical bone microarchitecture compared to control after HFD treatment.....64

Figure 18. Prrx1Cre;Snca<sup>fl/fl</sup> female mice showed smaller adipocytes from the  
inguinal white adipose tissue (iWAT) after HFD.....65

Figure 19. Prrx1Cre;Snca<sup>fl/fl</sup> female mice have a decreased insulin sensitivity and  
higher ambulatory activity on high fat diet.....67

Figure 20. Prrx1Cre;Snca<sup>fl/fl</sup> iWAT adipocytes expressed UCP-1 and have  
higher oxidative capacity compared to controls.....70

Figure 21. Prrx1Cre;Snca<sup>fl/fl</sup> iWAT preadipocytes showed less expression of  
pro- adipogenic and mature genes.....71

Figure 22. Prrx1Cre;Snca<sup>fl/fl</sup> iWAT preadipocytes showed less expression of  
pro- adipogenic and mature genes.....71

Figure 23. Prrx1Cre;Snca<sup>fl/fl</sup> iWAT preadipocytes showed less expression  
of mitochondrial genes.....72

Figure 24. Prrx1Cre;Snca<sup>fl/fl</sup> iWAT preadipocytes showed less expression of  
β-adrenergic receptors .....73

Figure 25. AdipoqCre;Snca<sup>fl/fl</sup> female mice had a reduced body weight gain and  
fat mass accrual after diet-induced obesity.....77

Figure 26. AdipoqCre;Snca<sup>fl/fl</sup> female mice showed a mild improvement in  
trabecular bone microarchitecture after treatment with HFD.....78

Figure 27. Adipoq Cre;Snca<sup>fl/fl</sup> female mice showed no differences in cortical  
bone microarchitecture compared to control after HFD treatment.....79

Figure 28. AdipoqCre;Snca<sup>fl/fl</sup> female mice had improved insulin sensitivity and  
higher activity levels..... 80

Figure 29. AdipoqCre;Snca<sup>fl/fl</sup> female iWATs showed an impaired adipogenic  
capacity.....81

Figure 30. AdipoqCre;Snca<sup>fl/fl</sup> male mice showed no significant differences  
in catecholamines serum level compared to control mice.....82

Figure 31. iWAT preadipocytes from null Snca<sup>-/-</sup> mice and A53T<sup>tg/tg</sup> showed an  
opposite adipogenic phenotype.....84

Figure 32. iWAT preadipocytes from AdipoCre;Snca<sup>fl/fl</sup> mice showed decreased  
lipid droplet formation and high expression of lipolytic marker.....87

Figure 33. Differential expression of  $\alpha$ -Synuclein in iWAT preadipocytes  
from AdipoCre;Snca<sup>fl/fl</sup> and A53T<sup>tg/tg</sup> mice does not alter its location  
relative to mitochondria.....88

Figure 34. iWAT preadipocytes from AdipoCre;Snca<sup>fl/fl</sup> and A53T<sup>tg/tg</sup> showed  
opposite mitochondrial phenotype.....89

Figure 35.  $\alpha$ -Synuclein relocates to the nuclei after insulin treatment in  
control preadipocytes but not in A53T<sup>tg/tg</sup> preadipocytes.....90

Figure 36. Differential levels of  $\alpha$ -Synuclein induces changes in insulin signaling  
through AKT.....91

Figure 37. Proposed Role of  $\alpha$ -Synuclein in Insulin Signaling Regulation.....103

## ABBREVIATIONS

Adipoq: adiponectin

Adr $\beta$ 1: beta-1-adrenergic receptor

Adr $\beta$ 3: beta-3-adrenergic receptor

AKT: Protein kinase B

Ap2: adipocyte Protein 2

$\mu$ CT: micro-computed tomography

ACTH: adrenocorticotrophic hormone

BAT: brown adipose tissue

BMD: bone mineral density

BMI: body mass index

CIDEA: cell death inducing DFFA-like effector A

Cpt1-a: Carnitine Palmitoyltransferase 1A

DI02: thyroxine deiodinase, type II

DRP1: dynamin-related protein 1

DXA: dual-energy X-ray absorptiometry

GAPDH: glyceraldehyde 3-phosphate dehydrogenase

HSL: hormone sensitive lipase

IRS1: Insulin Receptor Substrate 1

IRS2: Insulin Receptor Substrate 1

IR $\beta$ : insulin receptor beta

iWAT: inguinal white adipose tissue

MAT: marrow adipose tissue

M-CSF: macrophage-colony stimulating factor

MSC: mesenchymal stem cell

PFA: paraformaldehyde

PPAR $\gamma$ : peroxisome proliferator-activated receptor gamma

pIRS1: phosphorylated insulin substrate 1

pAKT: phosphorylated Protein kinase B

pDRP1: phosphorylated dynamin-related protein 1

pHSL: phosphorylated hormone sensitive lipase

Prrx1: Paired-related homeobox 1

Ppib: Peptidylprolyl Isomerase B

pIR $\beta$ : phosphorylated insulin receptor beta

pSHC; phosphorylated SHC Adaptor Protein 1

pIR $\beta$ : phosphorylated insulin receptor beta

Sbrep1c: sterol regulatory element-binding protein 1c

Snca:  $\alpha$ -Synuclein gene

SHC: SHC Adaptor Protein 1

UCP-1: uncoupling protein 1

# CHAPTER 1

## INTRODUCTION

Worldwide, the elderly population continues to expand at an unparalleled rate. Approximately, 8.5% of the total population is now over 65 years and is projected to reach nearly 17% of the world's population by 2050 [1]. This aging trend presents several public health and socio-economic challenges including an increased risk for neurodegenerative and bone diseases. Parkinson's disease (PD) is the second most frequently reported neurodegenerative disease and it has an estimated prevalence of 1% in subjects over the age of 60. Moreover, the socioeconomic impact of PD is also growing [2]. As PD progresses, neurological degeneration leads to wide-spread lesions in the brain along with balance impairment and an increased risk of falls. The systemic nature of PD seriously impairs life quality; symptoms comprise movement impairment and non-motor related dysfunction, dementia, gastrointestinal disturbances, body composition alterations, including, metabolic alterations, falls and a markedly increased risk of fracture as well as low bone mineral density [3,4,5]. The vast majority of research into the pathophysiology of PD has focused on the mechanisms of PD development in the *substantia nigra* and its neurologic implications; however, little is known about how PD impacts comorbidities, particularly, energy metabolism and its association with bone mass and osteoporosis, a major complication of long-standing PD. In this thesis, we discuss the fundamental relationship between PD and bone health, with an eye towards future preventive therapies.

## 1.1. Pathophysiology of Parkinson's Disease

PD is a systemic neurodegenerative disease. It encompasses a series of comorbidities that contribute to the complexity of the disease, impairing life quality of patients. Symptoms span locomotor dysfunction including resting tremors, rigidity and bradykinesia to lesser known- non-motor features such as autonomic dysfunction, cognitive/neurobehavioral abnormalities, sleep and sensory disorders. Additionally, PD patients often experience weight loss and a greater risk of fracture which increases as the disease progresses and with treatment [6].

## 1.2. Motor Alterations and Disease Progression

The underlying pathological processes in PD progresses slowly by degeneration of a particular population of neurons in the mesencephalon. An important but not exclusive pathophysiological feature in PD is the loss of the dopaminergic neurons in the *substantia nigra pars compacta* resulting in disorganization of the basal ganglia (BG) circuits [7]. The pathological hallmark of PD is the formation of intracellular aggregates of  $\alpha$ -Synuclein in the cytoplasm in these dopaminergic neurons, known as Lewy bodies or if located in neurites, Lewy neurites [7,8]. These neurons are affected specifically in their cytoskeleton organization, which impairs its function and ultimately leads to cell death and alteration of the nigrostriatal circuit [7]. During the early stages of PD, the disease affects the dorsal motor nucleus of the vagal nerve, olfactory bulbs and nucleus, then the *locus coeruleus*, and later, the *substantia nigra* and ultimately cortical areas. The damage to the *substantia nigra* has been shown to be consistently accompanied by substantial extranigral lesions that cause impairment of the limbic system, telencephalic

cortical function and autonomic regulative mechanisms [9]. Overall, these alterations result in 4 classical cardinal (motor) features of PD that a clinical diagnosis includes: 1) bradykinesia, or slowness in movement, 2) rest tremor, 3) rigidity and 4) postural instability [3]. PD patients also experience non-motor alterations that contribute to quality of life deterioration. These are often expressed earlier than locomotor alterations, even as earlier as 20 years prior diagnosis.

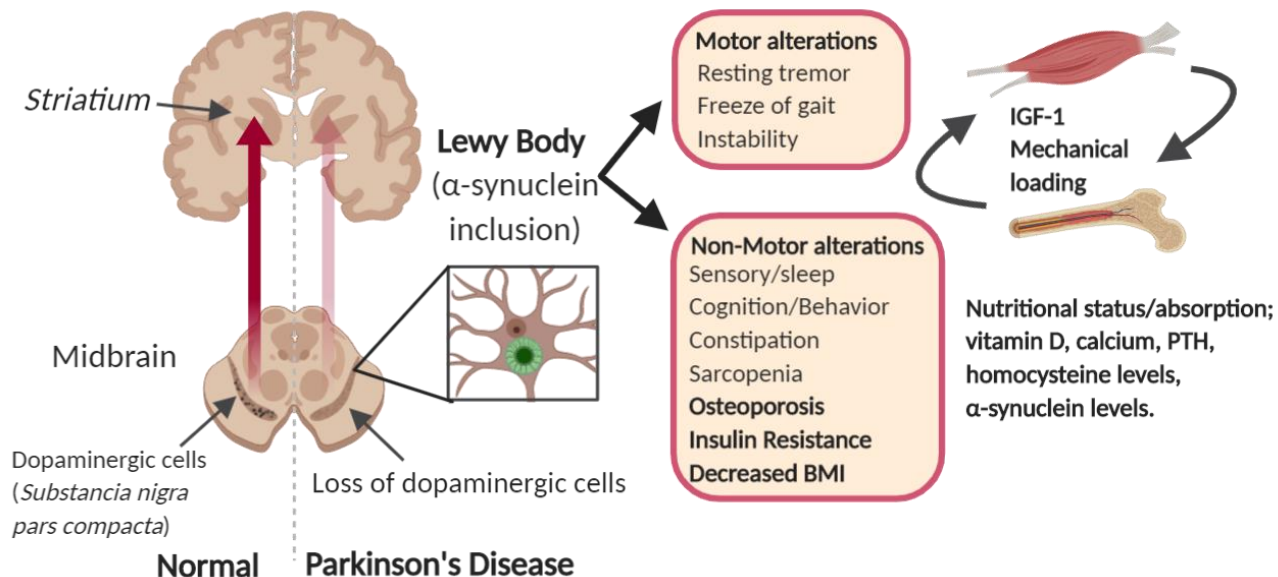


**Figure 1. Loss of nigrostriatal circuits in Parkinson's Disease (PD).**

Aggregation of  $\alpha$ -Synuclein leads to loss of dopaminergic neurons in *substantia nigra*. Disruption of nigrostriatal circuits leads to motor and nonmotor alterations. PD patients often show signs of sarcopenia that may contribute to bone deterioration. Endocrine and nutritional factors converge to overall bone impairment.

### 1.3. Sleep Disorders and Sensory Abnormalities

Patients with PD often present diverse sleep disorders. Most common alterations include insomnia, REM sleep behavior disorder (RBD), daytime sleepiness and restless legs syndrome, but frequently, pain and cramps or desire to urinate often interrupt their sleep, as well [10,11,12]. Sleep disturbances have been attributed to thalamic atrophies in PD patients and dysregulation of circadian rhythm [13,14]. It is still uncertain what are the mechanistic (s) alterations in the brainstem circuits that lead to dysfunction of glutamatergic, cholinergic and GABAergic signals in the dorsal pons within the brainstem, and how these may explain the symptom complex [15]. Clinical studies have shown that loss of REM sleep atonia is positively associated with neurodegenerative symptoms such as loss of olfactory function at early stages of neurological progression, suggesting these indicators can be used as early markers of PD [16].

### 1.4. Autonomic Alterations in PD

PD patients commonly show signs of constipation and gastrointestinal tract dysfunction during the progression of the disease. There are considerable data supporting the presence of Lewy bodies in the myenteric plexus of the intestine at early stages of the disease; this location is consistent with the fact that these regions are typically vagal terminals [17]. Analysis of immunohistochemical staining of colonic biopsies have revealed in 4 out of 5 PD patients, the presence of phosphorylated- $\alpha$ -Synuclein in the submucosal neurites of the enteric nervous system; remarkably there were no positive staining in control subjects [18]. Although, more evidence is required to fully characterize the pathophysiology of the gastrointestinal alterations in PD, the current

findings suggest that the presence of Lewy bodies in the myenteric plexus may be an early sign of peripheral involvement in PD [17]. Other autonomic alterations can lead to manifestations such as orthostatic hypotension, sweating, bladder and erectile dysfunction [19,20]. It should be noted that part of these, such as gastrointestinal dysfunction and imbalance could contribute to altered bone microarchitecture, and/or enhance the risk of falls and subsequent fractures.

### **1.5. Body Composition and Disease Progression**

Clinical studies show that PD patients often experience weight loss, sometimes preceding the PD diagnosis. Chen et al. showed that the average weight of PD patients was stable prior to the disease diagnosis, but then decreased with disease progression. Surprisingly, these patients increase their food intake, but this does not lead to a concomitant weight gain [4]. PD patients were found to be 4-fold more likely to lose 10 lbs than healthy individuals during the eight years after first diagnosis. This weight change correlated with severity of disease leading to greater nutritional risk than healthy controls [21]. Indeed, accumulating evidence suggests a negative correlation between BMI in PD patients and severity of the disease, aging, comorbidities and higher daily levodopa dosing [22, 23]. Previous studies showed that type II Diabetes Mellitus (II DM) is a risk factor for PD and that glucose metabolism alterations are often found in PD patients [5, 24, 25,26]. Not before the past couple of years, studies have returned to investigate implications of PD in metabolism, particularly, insulin response. Marques et

al, (2018) showed that glucose control was impaired in mid to later disease stages in non-diabetic PD patients, possibly as a consequence of PD dysautonomia [27].

These findings imply that alterations in body composition and glucose response in PD correlates closely with health-related quality of life and neurologic progression, an indication of the systemic nature of this disease.

### **1.6. Cognitive and Neurobehavioral Alterations**

PD patients often present signs of cognitive impairment and they are at a higher risk of dementia aside from the risk of several comorbidities such as depression, anxiety and hallucinations [23, 28, 29]. Obsessive compulsive behavior and impulse behavior are attributed to the dopamine dysregulation, but these are still not well understood [30,31].

### **1.7. Bone strength, Quality (and Loss) in Parkinson's Disease Patients**

PD and osteoporosis are two common chronic disorders, affecting a substantial portion of the elderly population. Osteoporosis is characterized by low bone mass and deterioration of bone micro-architecture, which leads to an increased risk of fracture [32, 33]. Fractures, most often due to falls, cause significant morbidity and mortality in a substantial portion of the elderly population. It has been established through observational and longitudinal studies that PD patients have a higher risk of osteoporosis and low bone mineral density when compared to controls [34]. Interestingly the levodopa dosage in patients is negatively associated with BMD in PD,

particularly relative to spine and femoral neck sites [22]. Zhao et al performed a meta-analysis of the risk of osteoporosis and bone mineral density in individuals with PD [35]. The authors found that PD patients were at higher risk for osteoporosis (OR=1.18, 95% CI= [1.09, 1.27]) than healthy controls and have lower BMD levels than healthy controls overall. Particularly, PD patients have a lower hip, lumbar spine and femoral neck BMD than healthy controls for hip, for lumbar spine, and femoral neck.

The prevalence of PD is greater in males than females by a ratio of nearly 2:1. Yet, analysis -by gender- reveal that female PD patients had lower BMD than controls, while there were no significant differences in male PD patients compared to controls. However, male PD patients are at higher risk for osteoporotic fractures than female patients. This could be due to several reasons such as differences in vitamin D levels, frequency of falls, and reduced physical activity. In regards to the former, Hagenau et al., analyzed a total of 394 studies including subjects from diverse ethnicities and found that women with PD tended to have higher mean serum 25(OH)D ( $56 \pm 1.6$  nmol/l) than men ( $50 \pm 2.6$  nmol/l,  $p= 0.05$ ) [36]. Gao et al showed in a cross-sectional study of 54 patients with PD and 59 healthy age-matched controls that PD patients had significantly lower BMD than in healthy controls, particularly in the lumbar spine. However, this study revealed that BMD scores of the spine, femoral neck, and hip were lower in females than in males in the healthy group and that within the PD group, BMD in the hip was significantly lower in females compared to males, contrary to Zhao et al (2013) [35]. Again, this study revealed a strong negative correlation between BMD in the spine, neck, and hip and severity of PD. In addition, there were negative correlations between

BMD (T-score and Z-score) and scores for PD severity such as Webster, Unified Parkinson's Disease Rating Scale for activities of daily living and motor activities (UPDRS II and III) as well as Hoehn-Yahr (H&Y) stage, and a positive correlation between BMD and Schwab and England (S&E) Scale activities of daily living score. Thus, in general, individuals with the lowest bone mass also had the most severe disease. Indeed, Gao suggested that low BMD in the spine, femoral neck, and hip may reflect the severity of PD and could be used as a surrogate marker not only of fracture risk but of disease progression [22].

The mechanisms by which PD patients develop osteoporosis it is still an area that is understudied. However, it is well known that sympathetic innervation is fundamental for integrating skeletal homeostasis with body composition mainly by suppressing bone formation and increasing bone resorption via enhanced RANKL production; thus, it is fair to speculate that PD dopaminergic alterations also could translate to compromised sympathetic innervation to the skeleton [37,38]. It has been shown that animals treated with 6-hydroxydopamine and  $\beta$ -adrenergic agonists impairs osteoblast activity in mouse calvaria and that the hematopoietic elements in the bone marrow respond to sympathetic innervation by increasing outflow of neutrophils as well as increasing sclerostin from osteocytes [39,40,41]. A recent study done by Handa et al., showed that dopamine receptors (Drd) are expressed in osteoblasts (*Drd3* and *Drd4*) and osteoclasts (*Drd1* and *Drd3*) and influence bone homeostasis [42]. *In vitro* data showed that the dopamine receptor agonist - levodopa- inhibits osteoclast differentiation and bone formation by decreasing osteoblast mineralization capacity. Animal models of PD

responded to levodopa treatment by reducing their bone formation rate and increased serum levels of homocysteine. Independently, an *in vivo* model of neurodegeneration of dopaminergic neurons, showed increased in bone resorption and suppressed bone formation [42]. In the context of the PD, neurodegeneration occurs while patients are under treatment with levodopa, thus, these results suggest both factors occur simultaneously and contribute independently to bone loss [42]. Thus, it is conceivable that PD autonomic disturbances or the treatment of the disease itself could affect bone remodeling through enhanced adrenergic signaling leading to further uncoupling of bone formation to resorption. However, there are no basic or translational studies to test these hypotheses.

Muscle mass and activity also influence overall bone health. Sarcopenia and immobilization can impair bone formation in PD patients. It has been shown that exercise promotes bone remodeling by mechanosensory interactions between muscle and bone [43]. It has been reported that loading exercises are marginally beneficial in respect to bone mineral density and microstructure. In addition, regular physical exercise may suppress sclerostin production, thereby enhancing bone formation. Studies have shown that greater lean mass was directly related to higher BMD at the femoral neck during aging and smaller muscle area was associated with reduced cortical thickness and fractures [44, 45]. Men with lower relative appendicular skeletal muscle mass (RASM) ( $<7.26 \text{ kg/m}^2$ ) had significantly lower BMD compared to the ones with higher RASM, and these subjects showed a higher risk of osteoporosis than individuals with normal RASM. A cross sectional study of 104 PD patients aged  $>65$

years old showed 55.8% of subjects had sarcopenia compared to 8.2% who were sarcopenic in the control group. Sarcopenia and frailty were positively correlated with greater motor alterations, higher frequency of falls and disease progression [46]. Thus, it seems intuitive that strategies to enhance muscle mass could prevent bone loss in PD patients, although once again there is a gap in evidence to support that tenet [44].

It has long been established that hormones are key regulators of bone homeostasis and alterations in these endocrine factors can strongly influence bone mineral density. Growth hormone is secreted by the pituitary and acts through IGF-1 to stimulate osteoblast and osteoclast proliferation and activity [47]. ACTH, another classic endocrine hormone, stimulates cortisol secretion and can bind to melanocortin receptor family, the MC2R that is expressed in osteoblasts and promote differentiation and proliferation [48]. Cortisol has several negative effects on bone by blocking calcium absorption and directly suppressing bone formation [49].

There is a limited amount of research on endocrine alterations in PD, but those few showed that untreated PD patients present hypothalamic disturbances that could lead to decreases in hypothalamic releasing factors causing reduced plasma concentration of growth hormone, adrenocorticotropic (ACTH) and cortisol compared to controls [46]. Indeed, LBs have been found in the hypothalamus as early as Braak stage 3 of PD [51, 52]. Dopamine can affect the anterior pituitary gland. PD patients with decreased levels of dopamine can have a direct effect on anterior pituitary gland secretion [53]. These

findings suggest that PD may impact bone health by alterations in the pituitary-hypothalamic axis.

Low vitamin D has been associated in cross sectional studies with osteoporosis in PD. One study showed that PD patients presented more frequently with hypovitaminosis D and secondary hyperparathyroidism [54, 55, 56] than healthy controls, either as a consequence of limited UV light exposure and/or malnutrition. On the other hand, immobilization due to severe PD could increase serum calcium from greater resorption and this would suppress PTH and subsequently renal 1,25 dihydroxyvitamin D production [57]. Loss of sense of smell and appetite, and autonomic dysfunction in the gastrointestinal tract of PD patients have been hypothesized as causative for the development of constipation and malabsorption in these patients. The latter, in turn, could lead to lower vitamin D levels from malabsorption. Notwithstanding, there are no studies that directly link vitamin D deficiency as a result of limited sun exposure and malnutrition to low bone mineral density or fractures in PD.

### **1.8. Parkinson's Disease, Falls and Neuroendocrine Mediators**

PD is a prime example of a progressive neurological condition where falls are prevalent, presumably because many risk factors converge in this disorder; however, the extent and severity of this problem is not well understood. Several studies have shown a positive association between PD and risk of falls. A meta-analysis involving 69,387 subjects showed that PD patients had an increased risk of fracture of 2-3 fold (HR hazard ratio = 2.66, 95% CI confidence interval: 2.10-3.36) compared to controls. In particular,

there is a 4-fold increased risk of hip fracture compared to healthy patients, independently of gender [58].

A cross-sectional study of PD patients and early patients with PD have shown that falls are an increasing problem as the disease progresses. Compared with age- and sex-matched controls, patients with PD are more frequent fallers, and this problem seems to be related to symptoms associated with the disease severity. Coinciding with the progressive nature of the disease, it was noted there was a 10-fold higher frequency of fallers in a cross-sectional cohort of PD patients compared with the group of patients with newly diagnosed PD. In addition, motor complications and disease severity were significantly associated with frequency of falling [2]. On a similar note, Silva de Lima et al. study showed that the incidence rate of any type of fall was found to be higher in PD patients than controls (2.1 vs. 0.7 falls/person;  $p < 0.0001$ ); moreover, the 'new fall' incidence rate after enrollment was 1.8 times higher for self-reported PD patients than controls (95% confidence interval, 1.6-2.0). Others have reported the median range for falling for non-treated PD patients was as high as 4-6 times within the 20 weeks duration of the study and can reach to an average of 20.8 falls per year in recurrent fallers [59,60]. These findings highlight PD as a prime "falling disease" [61].

Falls increase fracture risk and are the most common reason for emergency hospital admissions in PD patients [62]. Frequent fallers can be defined as patients that have fallen more than 5 times over a 6 months period and some have suggested a possible association between fall frequency and alterations in cortical areas in the brain [63].

Some have suggested that neurodegeneration leads to a cortical volume reduction and thus, a reduction in functional connectivity due to dopamine deficiency resulting in cortical inhibition through the basal ganglial network [64]. Fallers exhibit significantly longer disease duration, lower gray matter volume in the right superior temporal gyrus (STG), the right supramarginal gyrus (SMG), and part of the inferior parietal lobule (IPL), compared with non-frequent fallers. Furthermore, there is a significant linear correlation between fall frequency and gray matter volume reduction in the right IPL and right STG [63]. In addition, among patients with a high incidence of fracture, PD subjects show the most serious complications and a greater risk of mortality (2-3 fold HR increase) than those without the disease [65]. Hip fractures are a major cause of morbidity and mortality among PD patients. Importantly, hip replacement surgery in these individuals is associated with longer hospital stays, poorer mobility, and greater mortality [66]. Thus, understanding the physiological and cellular mechanisms relating the pathophysiology of PD to low bone mass and fractures is critical to developing targeted therapies.

A possible mechanism connecting PD to falls relies on the locomotor alteration they develop throughout their disease. As mentioned above, loss of nigrostriatal dopamine circuits causes postural instability, thus, greater risk of falls. Clinical evidence shows that severe dopamine loss in the basal ganglia is associated with discoordination and often increases slips and stops of movement over dynamic surfaces, that, in attempt to correct them, result in falls [67, 68]. Moreover, frequent falls could also be explained by the decrease of muscular activity leading to muscular atrophy or sarcopenia in patients. PD severity as noted previously is associated with sarcopenia (odds ratio 2.30; 95%

confidence interval 1.15-4.58) [69]. Accumulating evidence point to a strong connection between bone and muscle, and it includes endocrine and paracrine signals between them. It has previously been shown that increases in muscle growth promotes bone formation, possibly through IGF-I secretion from the muscle; IGF-1 produces a hypertrophic anabolic signaling affecting bone mass acquisition as well as muscle mass [70, 71]. Serum IGF-1 declines with age, and has been identified as a one marker of osteoporotic risk in young women [72, 73]. However, the association between levels of IGF-1 in the context of PD is controversial: IGF-1 is low in some PD patients although this may be due to multiple factors including nutritional aspects, age and coincident co-morbidities (Fig. 1) [74]. Others have shown higher IGF-1 serum levels in PD patients compared to controls and these are inversely correlated with the Unified Parkinson Disease Rating Scale for motor function (UPDRS-III) score at early stages of the disease suggesting that IGF-1 acts as a neuroprotective peptide as a compensatory mechanism to protect against further degeneration of neurological functions [75,76]. Despite these data, it remains unclear whether IGF-I can serve as an early biomarker of PD, while lower serum IGF-1 at later stages of PD could be due to the loss of muscle mass, nutritional deficiencies, concomitant morbidities and neurological damage.

### **1.9. Animal Models of PD and Their Implications for Understanding Skeletal Morbidity**

There are several genetic animal models of PD that recapitulate some of the most important aspects of the disease, such as motor symptoms, Lewy body formation,

nonmotor symptoms and disease progression. However, there is no ideal model that fulfills all these characteristics; each has advantages and limitations although these can provide great insights into the cellular and molecular mechanisms underlying the disease. A model of PD in mice is the overexpression of human  $\alpha$ -Synuclein under the Thy1 promoter driving its expression in nervous system. Its manifestations include olfactory and digestive alterations, similar to how patients present at the first stages of the disease [77]. Other commonly used genetic models of PD are mutant mice with 3 independent single mutations, A53T, A30P, and E46K, forced expression of  $\alpha$ -Synuclein by viral infections and neurodegeneration induced by neurotoxin treatments [78, 79, 80]. The primary focus in the field has been to improve understanding of the cellular and molecular mechanisms of the neurological damage and its progression, for therapy and prevention. However, the molecular mechanisms explaining how neurodegeneration leads to a variety of the systemic alterations remain understudied. Therefore, the pre-clinical literature focusing on the impact of PD in bone health is very limited. Models of the modified LRRK2 gene have shown an increased risk of genetic and idiopathic PD [81]. To date are no reports of the bone condition in these patients. Nevertheless, Berwick et al. found that LRRK2 knock out mice showed higher  $\beta$ -catenin levels in the brain, improved bone microarchitecture, an increase in tibial cortical bone and stronger bones, mediated by activation of canonical Wnt signaling in bone [82].

More recently,  $\alpha$ -Synuclein has been shown to be expressed in several tissues [42, 83]. Close to ~80% of erythroid cells within the bone marrow express  $\alpha$ -Synuclein [84]. It is also found in the blood of mice and humans, thus providing some evidence that  $\alpha$ -

Synuclein could be playing an endocrine role via the circulatory system, marrow niche and ultimately affecting bone remodeling [85]. We previously reported that  $\alpha$ -Synuclein is a hub gene in bone homeostasis [83]. Specifically, we generated a co-expression network consisting of 53 gene modules using expression profiles from intact and ovariectomized (OVX) mice from a panel of mouse inbred strains. The expression of four modules was altered by OVX, including one whose expression was decreased by OVX across all strains. This one module was enriched for genes involved in the response to oxidative stress, a process known to be involved in OVX-induced bone loss. Additionally, these genes were co-expressed in human bone marrow.  $\alpha$ -Synuclein was one of the most highly connected "hub" genes in that module. We subsequently characterized mice deficient in *Snca* and observed a 40% reduction in OVX-induced bone loss. Furthermore, protection was associated with the altered expression of that specific network module. In summary, the results of this study suggest that  $\alpha$ -Synuclein regulates bone network homeostasis and ovariectomy-induced bone loss. Furthermore, we found that  $\alpha$ -Synuclein is expressed in both osteoblasts and osteoclasts at different stages of maturation *in vitro* (Fig. 2) [83]. Moreover, gene deletion of  $\alpha$ -Synuclein partially protected against ovariectomy-induced bone loss, including greater bone volume fraction, more trabecular number and thickness, and less weight gain [83]. Pathological  $\alpha$ -Synuclein dynamics in bone tissue could explain part of the impaired skeletal status in PD as well as other comorbidities. Notwithstanding, these results shed light that disturbances in  $\alpha$ -Synuclein in the

pathophysiology of PD might extend beyond central and peripheral neurological systems.

### **1.10. Osteoporosis Treatments for PD Patients**

Despite the well-established evidence that PD patients are at a high risk of fracture and twice the risk of mortality from fractures, only few receive treatment [65]. Fractures in general occur because of falls and low BMD. Therapies to target either or both factors are fundamental to improve life quality and decrease mortality. As discussed previously levels of vitamin D have been positively correlated with BMD but its positive effects have only been demonstrated in deficient states, thus, supplementation benefits remain controversial [56, 85]. There are studies suggesting vitamin D therapy can improve muscular function, reaction time, balance and coordination in older people; this potentially could protect against falls [86, 87]. The positive effect of vitamin D was greater in osteoporotic patients with hypovitaminosis D and co-administered calcium [88]. However, more recent meta-analyses have shown that vitamin D had no effect on overall fractures, hip fractures or falls, at low or high dose suggesting that vitamin D supplementation lacks clinical benefit and could possibly have a harmful effect [89, 90]. However, PD patients are exposed often to malnutrition, thus, considering vitamin D and calcium supplementation at low dose may be of use in selected patients.

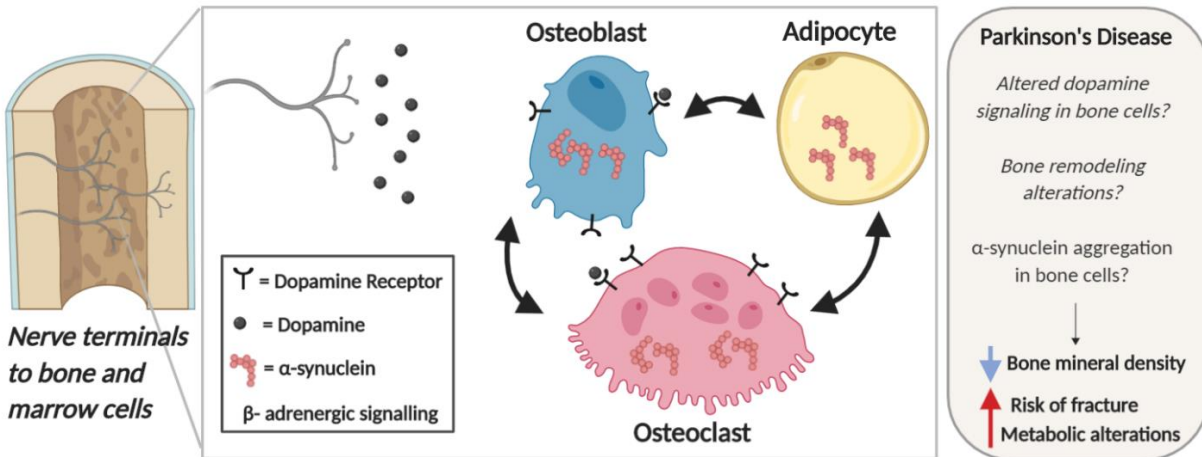


**Figure 2. Bone remodeling and dopamine.**

Osteoblasts, adipocytes and osteoclasts are the major regulators of bone homeostasis. Alteration of dopamine at central levels may be affecting bone cell signaling transduction through dopamine receptors due to decrease in dopamine levels. PD patients show higher circulating levels of  $\alpha$ -Synuclein, presence of Lewy bodies in the midbrain and in enteric terminal nerves. We postulate that  $\alpha$ -Synuclein aggregates could translate to alterations in cellular dynamic of  $\alpha$ -Synuclein in bone cells and adipocytes as possible contributing mechanism to bone impairment and metabolic alterations in PD patients.

Among possible pharmacological treatment alternatives for osteoporosis in PD patients, anti-resorptive treatments such as bisphosphonates are the most common. Bisphosphonates are pyrophosphate analogues that reduce bone resorption by directly inhibiting osteoclast activities [91]. The oral agents include alendronate, ibandronate and risedronate; all show increased bone mineral density and a markedly decreased risk of fracture [92]. Intravenous zoledronic acid, administered once per year, is the most effective bisphosphonate to date decreasing bone resorption markers and increasing BMD by 4-5% in the spine and ~3% values in the femoral neck when compared to control [93]. Fractures are reduced by 70% in the spine and ~40% in the hip along with

improvement of ~6% of BMD in total hip, lumbar spine and femoral neck [94]. Sustainable decreases in serum bone resorption markers at 6 and 12 months of infusion were demonstrated. Denosumab is another anti-resorptive agent that works through a monoclonal antibody that binds to RANKL, thereby inhibiting osteoclast maturation. It has been shown to be effective in reducing bone resorption markers and increased total hip and lumbar spine BMD [95]. However, denosumab must be administered every 6 months and there is a rebound increase in bone resorption, and potentially more vertebral fractures if the medication is stopped. Teriparatide is an anabolic agent first approved by the FDA in at? 2001 as an osteoporosis treatment targeting bone formation [96]. Intermittent PTH administration (i.e. daily injections) has been shown to effectively improve BMD and fracture risk [97]. Another anabolic drug, PTHrp analog (Abaloparatide) has been shown to prevent fractures and increase BMD in postmenopausal osteoporosis and is non-inferior to teriparatide [98, 99].

To the date there are no data whether these drugs can prevent osteoporotic fractures in PD. However, there is a new and innovative trial to address this issue. The TOPAZ (NCT03924414) trial will also address barriers to treatment of patients with PD by providing rigorous evidence about whether zoledronic acid (ZA) reduces fracture risk in patients with PD, simplifying treatment by giving ZA at home without extra medical visits and BMD testing, and overcoming poor persistence with oral therapies because one infusion may prevent bone loss for at least 2 years [65, 100, 101]. The outcome of this trial will demonstrate how a home-based fracture prevention can reach older PD

patients who would not otherwise receive treatment to reduce their high risk of fractures.

As we mentioned in this chapter, PD is characterized by non-motor clinical features that contribute to disease complexity and impaired life quality. PD disrupts nigrostriatal circuits at a central level but also, it could be impairing of catecholamine signaling to the major cellular components of bone homeostasis through the sympathetic innervation, leading to alterations in bone frailty and metabolic impairment. Nevertheless,  $\alpha$ -Synuclein is expressed locally in osteoblasts, adipocytes, and osteoclasts. Here, we aimed to clarify if  $\alpha$ -Synuclein participates in regulating bone microarchitecture by acting cell autonomously through bone cells and adipocytes.

## CHAPTER 2

### MATERIALS AND METHODS

#### 2.1. Animals

Animal studies were conducted according to the National Institutes of Health guide for the care and use of Laboratory animals. Maine Medical Center Research Institute approved all experimental procedures. *Snca<sup>fl/fl</sup>* (B6(Cg)-Sncatm1.2Vlb/J strain [103], stock #028559) mice were crossed to *Prrx1Cre* mice (B6.Cg-Tg(*Prrx1-cre*)1Cjt/J [104], stock# 005584), or to *AdipoqCre* mice (B6;FVB-Tg(*Adipoq-cre*)1Evdr/J [105], stock # 010803), all purchased from The Jackson Laboratory (Bar Harbor, ME). B6;C3-Tg(*Prnp-SNCA\*A53T*)83Vle/J (*Prnp-SNCA\*A53T*) *Prnp-SNCA\*A53T* transgenic mice express human A53T variant  $\alpha$ -Synuclein (full-length, 140 amino acid isoform) under the direction of the mouse prion protein promoter purchased at The Jackson Laboratory (Bar Harbor, ME) and B6.Cg-Tg(*Sox2-cre*)1Amc/J (*Sox2-Cre*, stock #8454, The Jackson Laboratory) from Dr Lucy Liaw Laboratory.

#### 2.2. Induction of Estrogen Deficiency

*Prrx1Cre;Snca<sup>fl/fl</sup>* and littermate controls were mice were anesthetized with Avertin and either sham operated or ovariectomized (OVX) at 8 weeks old and sacrificed at 20 weeks old and fed with phytoestrogen-free diet (D10012M, Research Diets, Inc).

### 2.3. Diet Induced Obesity (DiO)

Eight-week old female and male *Prrx1Cre;Snca<sup>fl/fl</sup>* and *AdipoqCre;Snca<sup>fl/fl</sup>* mice and littermate controls were randomly assigned treatment with high fat (60% fat) (D12492i, Research Diets, Inc.) or low fat (10% fat sucrose matched) diet (D12450Ji, Research Diets, Inc.) for 15 weeks. Total body weight was measured weekly and their food weight every two days to obtain food intake per mouse per day (grams of food/day/mouse) and converted into kilocalories for caloric intake comparison.

### 2.4. Serum Collection and Catecholamine's Measurement

Concentrations of catecholamines in biological samples were assessed by LC-MS/MS methodology as described [106]. Briefly, plasma is mixed with HPLC grade acetonitrile, vortexed and centrifuged. The supernatant is then transferred to a 96 well plate for LC/MS-MS analysis. A calibration curve is formed in mouse plasma by serial dilution and extracted via the same methodology. An Agilent 1200 system consisting of a binary pump, column compartment and auto-sampler is used for solvent delivery and sample introduction. Chromatographic separation is performed on a Phenomenex Hydro RP 2.0 x 150 mm 4  $\mu$ m column via a gradient using 0.1% formic acid in water (A) and 0.1% formic acid in acetonitrile (B). Gradient elution is 98% A from 0-1 minute, ramping to 50% A from 1.1 to 3.0 minutes, holding at 50% until 5.5 minutes, with re-equilibration at initial conditions from 5.6 to 7.5 minutes. Flow rate is 0.30 mL/min, and column temperature is 30°C. Assay range for catecholamines is 2-500 nM for dopamine, 2-2000

nM for epinephrine and 5- 5000 nM for norepinephrine. Inter-assay variability is < 14.6% across the dynamic range of the assay.

## 2.5. Body Composition by DXA

Mice were anesthetized by isoflurane inhalation and whole-body and femoral areal bone mineral density (BMD) and body composition excluding the head were analyzed by dual-energy X-ray absorptiometry (DXA). The instrument (PIXImus, GELunar Corp., Madison, WI, USA) was calibrated daily using a phantom standard provided by the manufacturer. All mice were measured at baseline (8 weeks old) and at the end time point (20 weeks old for OVX or 23 weeks for HFD study) for lean mass, fat mass, and bone mineral density using the PIXImus dual-energy X-ray densitometer (GE-Lunar, Madison, WI, USA). Whole body scans were obtained, and X-ray absorptiometry data were analyzed, following the manufacturer's supplied software excluding the skull in the analysis (Lunar PIXImus 2, version 2.1).

## 2.6. Micro-Computed Tomography ( $\mu$ CT)

A high-resolution desktop micro-tomographic imaging system ( $\mu$ CT40, Scanco Medical AG, Brüttisellen, Switzerland) was used to assess trabecular bone and cortical bone architecture in the femur. Scans were acquired using a  $10 \mu\text{m}^3$  isotropic voxel size, 70 kVp peak x-ray tube potential, 114  $\mu\text{A}$  x-ray intensity, 200 ms integration time, and were subjected to Gaussian filtration and segmentation. Trabecular bone was identified by manually contouring the endocortical region and then using a threshold of 360

mgHA/cm<sup>3</sup> to segment bone from soft tissue. Trabecular bone architecture was analyzed in a region that began 200 μm superior to the distal femoral growth plate and extended proximally 1500 μm (150 transverse slices). The segmented images were analyzed with the standard Scanco trabecular bone morphology script to measure trabecular bone volume fraction (Tb.BV/TV, %), trabecular thickness (Tb.Th, mm), trabecular number (Tb.N, mm<sup>-1</sup>), trabecular separation (Tb.Sp, mm), and connectivity density (Conn.D, 1/mm<sup>3</sup>). Cortical bone morphology was analyzed in a 500 μm (50 transverse slices) long region that began at the femoral mid-diaphysis. Cortical bone was segmented using a threshold of 700 mgHA/cm<sup>3</sup> and the standard Scanco script for cortical bone morphology was used to measure total cross-sectional area (Tt.Ar, mm<sup>2</sup>), cortical bone area (Ct.Ar, mm<sup>2</sup>), marrow area (Ma.Ar, mm<sup>2</sup>), bone area fraction (Ct.Ar/Tt.Ar, %), cortical thickness (Ct.Th, mm), cortical porosity (%), and polar moment of inertia (J, mm<sup>4</sup>).

## 2.7. Osmium Tetroxide Staining

Following μCT scanning for trabecular and cortical structure, marrow fat quantification was performed in the tibiae using osmium tetroxide. Tibiae were demineralized in 4.1% EDTA, pH 7.4, for 14 days. Then in a fume hood, the demineralized tibiae were incubated for 48 hours in a mixture containing equal volumes of 5% potassium dichromate and 2% osmium tetroxide (Electron Microscopy Sciences, Hatfield, PA) (1% final osmium tetroxide concentration). The tibiae were washed in cool tap water for 2 h to remove unbound osmium tetroxide and then μCT imaged using the previously

specified  $\mu$ CT scanner. Scans were acquired of the whole tibia using a  $10 \mu\text{m}^3$  isotropic voxel size, 55 kVp peak x-ray tube potential, 145  $\mu\text{A}$  x-ray intensity, 300ms integration time, and were subjected to Gaussian filtration and segmentation. The medullary cavity for each tibia was manually contoured in the same regions where the marrow volume was measured in the mineralized  $\mu$ CT scans of the bones. The region within the medullary contours was segmented with a threshold of 700 mgHA/cm<sup>3</sup> or 1000 mgHA/cm<sup>3</sup> in the proximal (superior to the distal tibiofibular junction) and distal (inferior to the distal tibiofibular junction) tibia, respectively, and the segmented volume was considered to be the marrow adipose tissue volume (MAT Vol, mm<sup>3</sup>). The marrow adipose tissue volume was then normalized by the volume of the marrow cavity (MV) to calculate the marrow adipose tissue volume fraction (MAT Vol/MV, %).

## **2.8. Metabolic Profile**

Mice were placed in metabolic cages (Promethion Metabolic Monitoring Cage System, Las Vegas, NV) to measure their physical activity by indirect calorimetry. The metabolic cages are located in the Physiology Core Department of Maine Medical Center Research Institute. Briefly, animals were maintained on a 12 h light/dark (L/D) cycle and were acclimated for 24 hours. All animals were housed in identical cages and bedding, given ad libitum access to food and water and provided with a running wheel of 4.5 inches (11.5 cm) in diameter (Mini-Mitter, Bend, OR) that was wired to record revolutions per second continuously using a magnetic reed switch.

## **2.9. Behavioral Tests**

Behavioral tests were conducted in a specifically equipped room using test apparatuses from Stoelting (Wood Dale, IL). Experiments were recorded with the ANY-maze™ video tracking system v5.14 (Stoelting, Wood Dale, IL) or a camcorder (Samsung HMX-F90). Videos were analyzed offline with The Observer XT v12.5 from Noldus (Leesburg, VA). Mice were group-housed after weaning (2-4 animals per cage) and had been on a 15 weeks low-fat or high-fat diet treatment at the time of testing. The experimental animals were left undisturbed in the testing room 2-3 hours prior to each test to acclimate.

### **2.9.1. Elevated Plus Maze Test**

The test apparatus for the elevated plus maze (EPM) is 45cm elevated off the ground and cross-shaped. Opposing arms are either open (open area) or surrounded by a wall (closed area). The arms are connected via the center area (neutral square). Mice were placed in the center area to start the test and were recorded for 5 min, while exploring the maze freely. Mice that fell off the maze were excluded from the tests and analysis.

### **2.9.2. Open Field Test**

The open field test (OFT) was performed in a square shaped (40 cm x 40 cm) arena with opaque walls. The center was defined as a 20 cm x 20 cm area with equal distance to the walls, while the remaining area was referred to as periphery. At the beginning of the test mice were placed in the periphery facing the center and allowed to explore the maze freely for 5 min.

### **2.9.3. Marble Burying Test**

A rat size home cage (45 cm x 23 cm) was used and filled with a 5-6 cm deep layer of corncob bedding (Envigo, South Easton, MA). Twenty-eight black marbles were spaced out equally on top of the bedding. The mouse was placed in the cage and allowed to explore it freely under low lighting. After 30 min the animal was gently removed from the cage to avoid disturbing the bedding. Marbles buried by two thirds of their diameter or more were counted as buried.

### **2.9.4. Tail Suspension Test**

Mice were suspended by their tail and fixed with adhesive tape to a shelf with their heads located approximately 8 cm above a flat surface. Animals caged together were tested in parallel. Mice were video recorded for 5 min. Immobility, movement and climbing behavior were analyzed afterwards using The Observer XT software.

## **2.10. Glucose Tolerance Test (GTT) and Insulin Tolerance Test (ITT)**

After 15 weeks of high fat diet challenge, for the glucose tolerance test mice were fasted overnight (16-18 h) with free access to water. Fasted glucose levels were measured from tail tip punctures and later measurements were acquired after mice were intraperitoneally (IP) injected with a glucose solution (1.5 g/kg body weight). For the insulin tolerance test, mice were fed ad libitum and IP injected with insulin at a dose of 1 U/kg. Glucose levels were then measured by using a Glucometer (AlphaTRAK 2 Blood Glucose Monitoring System) at 0, 15, 30, 45, 60, and 120 minutes after injection for both

tests. The area under the curve (AUC) was determined to quantify the glucose and insulin tolerance.

## 2.11. Gene Expression Analysis

### 2.11.1. Real-time PCR

Total RNA was isolated using the TRI Reagent (MRC) according to the manufacturer's instructions. cDNA was generated using the High Capacity cDNA Reverse Transcriptase Kit (Applied Biosystems, Foster City, CA) according to the manufacturer's instructions. mRNA expression analysis was carried out using an AzuraQuant Green Fast qPCR Mix LoRox with an iQ5 thermal cycler and detection system (Bio-Rad, Hercules, CA). cDNA samples were analyzed for the expression of both genes of interest and a reference gene, Cyclophilin B (*Ppib*). Fold changes in gene expression levels were estimated using the  $\Delta\Delta C_t$  method. Primers for *Prrx1* and *Snca* were purchased from Integrated DNA Technologies (Coralville, IL). Primer sequences were as follows: *Ppib*, Fwd 5'-TGG AGA GCA CCA AGA CAG ACA- 3' and Rev 5'-TGC CGG AGT CGA CAA TGA T-3'; *Prrx1*, Fwd 5'-GAC CAA CCG ATT ATC TCT CCT GG-3' and Rev 5'-CAG TCT CAG GTT GGC AAT GCT G-3'; and *Snca*, Fwd 5'-CTT TAG CCA TGG ATG TGT TCA T-3' and Rev 5'-TTG TCT TTC CAG CTG CCT CT-3'. *Ppar $\gamma$*  Fwd 5'-CAA GAA TAC CAA AGT GCG ATC AA-3' and Rev 5'-GAG CTG GGT CTT TTC AGA ATA ATA AG-3', *Adipoq* Fwd 5'- TCA CGG TGT ACA TGA AAG ATG TG -3' and Rev 5'-GAG AAC GGC CTT GTC CTT CT-3' , *Ap2* Fwd 5'- GCC AAG CCC AAC ATG ATC A-3` and Rev 5'-TTC CAC GCC CAG TTT GAA G-3', *Ucp-1* 5'- GAG GTG TGG CAG TGT TCA TTG-3' and Rev 3'-GGC TTG CAT TCT

GAC CTT CA-3', *Cpt1-a* Fwd 5'-GGC ATA AAC GCA GAG CAT TCC TG-3' and Rev 5'-CAG TGT CCA TCC TCT GAG TAG C-3' and *Sbrep1c* Fwd 5'-CGA CTA CAT CCG CTT CTT GCA G -3' and Rev 5'-CCT CCA TAG ACA CAT CTG TGC C -3', *Mcd* Fwd 5'- TGC ATG TGG CTC TGA CTG GTG A -3' and Rev 5' GGT CAG GCT GAT GGA GTA GAA G-3', *Lipe* Fwd 5'-GCT CAT CTC CTA TGA CCT ACG G -3' and Rev 5'-TCC GTG GAT GTG AAC AAC CAG G-3', *Atgl* Fwd 5'-GGA ACC AAA GGA CCT GAT GAC C-3' and Rev 5'-ACA TCA GGC AGC CAC TCC AAC A-3', *Adr $\beta$ 1* Fwd 5'-GCT CTG GAC TTC GGT AGA TGT G-3' and Rev 5'-CGT CAG CAA ACT CTG GTA GCG A-3', *Adr $\beta$ 3* Fwd 5'-AGG CAC AGG AAT GCC ACT CCA A-3' and Rev 5'-GCT TAG CCA CAA CGA ACA CTC G, *DiO2* Fwd 5'- GGT GGT CAA CTT TGG TTC AGC C-3' and Rev 5'-AAG TCA GCC ACC GAG GAG AAC T-3', *Cidea* Fwd 5'-GGT GGA CAC AGA GGA GTT CTT TC-3' and Rev 5'-CGA AGG TGA CTC TGG CTA TTC C-3', *Cited-1c* Fwd 5'-CCT CAG CTC CTG TGA GCT TT-3' and Rev 5'-CTG GGC AGA AGT CCG ATA AA-3', *Bcl2l13* Fwd 5'-ATG GCG TCC TCT ACG ACT G-3' and Rev 5'- GGT GAG GGA CCT TGT TGT TTC -3', *Bnip3* Fwd 5'- TCC TGG GTA GAA CTG CAC TTC-3' and Rev 5'-GCT GGG CAT CCA ACA GTA TTT-3', *Prkn2* Fwd 5'-TCT TCC AGT GTA ACC ACC GTC-3' and Rev 5'-GGC AGG GAG TAG CCA AGT T-3', *Drp1* Fwd 5'-CAG GAA TTG TTA CGG TTC CCT AA-3' and Rev 5'-CCT GAA TTA ACT TGT CCC GTG A -3'

### 2.11.2. Western Blotting

Brain, femur, white adipose tissue, or bone marrow tissues were homogenized in RIPA assay buffer (Cell Signaling Technology). After centrifugation, protein concentration

was measured by using the Pierce BCA protein assay kit (Thermo Scientific) according to the manufacturer's instructions. 10 µg of each sample was loaded on 4-15% Mini-PROTEAN TGX precast gels (Bio-Rad), run at 100-200 V for 50 min, and transferred to polyvinylidene fluoride membrane using the Trans-blot Turbo Transfer System (Bio-Rad) at 25 V for 7 min. The membrane was blocked in TBS plus 0.1% Tween 20 containing 5% nonfat dry milk for 1 h at room temperature, followed by incubating with primary antibody in blocking solution at 4 °C overnight:  $\alpha$ -Synuclein polyclonal antibody (Abcam, ab52168, 1:1000),  $\beta$ -actin (Santa Cruz Biotechnology, Inc., sc-47778, 1:2000), GAPDH (Cell Signaling, 5174P, 1:1000), HSL (Cell Signaling, 4107, 1:1000), pHSL S565 (Cell Signaling, 4137, 1:1000), Shc (Cell Signaling, 24325, 1:1000), pShc Tyr239/240 (Cell Signaling, 2434, 1:1000), AKT (Cell Signaling, 9272, 1:1000), pAKT S473 (Cell Signaling, 9271, 1:1000), IR $\beta$  (Cell Signaling, 3025T, 1:1000), pIR $\beta$  (3021T), pIRS1 Ser612 (Cell Signaling, 5610, 1:1000), IRS1 (Cell Signaling, 3407, 1:1000), IRS2 (Cell Signaling, 4502, 1:1000), Cyclophilin A (Cell Signaling, 2175, 1:1000), pDRP1 S616 (Cell Signaling, 3455, 1:1000), pDRP1 S637 (Cell Signaling, 4867, 1:1000), DRP1 (Cell Signaling, 5391, 1:1000)

The membrane was incubated with blocking solution with secondary antibody: anti-rabbit IgG (NA934V) or anti-mouse IgG (NA931V) horseradish peroxidase-conjugated antibodies (GE Healthcare). Western blots were developed using the SuperSignal West Dura Extended Duration Substrate (Thermo Fisher Scientific) for 1 min and exposed with the ChemiDoc Touch imaging system (Bio-Rad).

## 2.12. Bone Marrow Stromal Isolation

Both femurs and tibiae were harvested at sacrifice and muscle was removed. Bone ends were snipped and placed in a 200  $\mu$ l tip that was cut open at the bottom and placed into a 1.5 mL microcentrifuge tube. Fresh bone marrow was spun out by quick centrifuge for 14 seconds at room temperature. Pellet was resuspended in basal medium  $\alpha$ -minimal essential medium ( $\alpha$ -MEM Gibco), 10% v/v fetal bovine serum (Hyclone), 100 units/ml penicillin, 100 $\mu$ g/ml streptomycin (Gibco, 1% v/v) and incubated at 37 °C with 5% CO<sub>2</sub> in a humidified incubator. After 2 days, non-adherent cells were removed and counted for osteoclastogenic induction. Adherent cells were lifted with 0.25% trypsin and incubating at 37 °C for 3 min, and later counted for osteoblastogenic and adipogenic differentiation.

## 2.13. Adipogenesis

Adherent cells from bone marrow stromal isolation were plated in 12 well plates and switched to differentiation medium when confluent. Differentiation medium consisted in basal medium, 2  $\mu$ M insulin, 500  $\mu$ M isobutylmethylxanthine (IBMX) (Sigma-Aldrich), 1  $\mu$ M dexamethasone (Sigma-Aldrich), and 20  $\mu$ M rosiglitazone (Cayman Chemical), and changed after 48 h. At day 4, cells were switched to basal medium with only 2  $\mu$ M insulin and 20  $\mu$ M rosiglitazone.

## 2.14. Oil Red O Staining

Adipogenic differentiated BMSCs or stromal vascular fraction from inguinal adipose tissue (iWAT) were fixed by using 10% neutral buffered formalin for 15 min and washed with 60% isopropyl alcohol. Staining solution contained 3.5 mg/ml of Oil Red O (Sigma-Aldrich) in 60% isopropyl alcohol, after several filtration steps. Washed cells were incubated in staining solution for 15 min at room temperature. After washing twice with water, retained Oil Red O staining in the cells was eluted with isopropyl alcohol and quantified at OD<sub>490 nm</sub>. For quantification of total number of cells, cells were stained with 0.4% crystal violet (CV) (Sigma-Aldrich) for 10 min, then eluted with 10% acetic acid and quantified at OD<sub>650 nm</sub>.

## 2.15. Osteoblastogenesis

After cells reached confluency, they were switched to osteoblast differentiation medium composed of basal medium containing 1 mM  $\beta$ -glycerol phosphate (Sigma-Aldrich) and 1 mM ascorbic acid (Sigma-Aldrich). Change media was done every 2 days for 21 days.

## 2.16. Alkaline Phosphatase and Von Kossa Staining

After osteoblastogenic differentiation, cells were fixed in 4% paraformaldehyde for 10 min at room temperature, stained for alkaline phosphatase (alkaline phosphatase kit, Sigma-Aldrich) and subsequently for mineral deposition by applying von Kossa staining, following manufacturer's instructions.

Firstly, for alkaline phosphatase staining, cells were washed and stained with AP solution mixed with 0.5 ml of sodium nitrite solution, 0.5 ml of FRV-alkaline solution, 22.5 ml of H<sub>2</sub>O, and 0.5 ml of naphthol AS-BI alkaline solution, for 30 min protected from the light.

Secondly, for von Kossa staining, cells were washed, stained with 5% silver nitrate solution and then exposed to light for 1 h. Then, cells were washed with deionized water, and treated with 5% sodium thiosulfate solution to neutralize any residual silver nitrate.

### **2.17. Osteoclastogenesis**

After cells reached confluency, they were switched to osteoclast differentiation medium composed of basal medium containing 50 ng/ml of Receptor Activator of NF $\kappa$ B Ligand (RANKL) and 30 ng/mL of Macrophage Colony Stimulating Factor (mCSF) to bone marrow stromal basal medium. Fresh media was changed every 2 days until day 5.

### **2.18. Tartrate-Resistant Acid Phosphatase (TRAP) Staining**

For TRAP staining, osteoclasts were fixed for 30 min at room temperature with 2.5% glutaraldehyde in PBS. Cells were incubated for 1 h at 37 °C with TRAP solution, composed of 50  $\mu$ L of Fast Garnets Base Solution, 50  $\mu$ L of sodium nitrite, 4.55 mL of distilled water, 50  $\mu$ L of naphthol AS-biphosphate, 200  $\mu$ L of acetate solution and 100  $\mu$ L tartrate solution, according to the manufacturer's instructions (Sigma-Aldrich kit). After wash, purple stained cells with 3 or more nuclei were considered TRAP positive.

## **2.19. Histological Sections and Hematoxylin and Eosin (H&E) Staining**

Briefly, after deparaffinization and rehydration, 5  $\mu\text{m}$  longitudinal sections (tibias or inguinal adipose tissue) were stained with hematoxylin solution for 5 min followed by 5 dips in 1% acid ethanol (1% HCl in 70% ethanol) and then rinsed in distilled water. Then the sections were stained with eosin solution for 3 min and followed by dehydration with graded alcohol and clearing in xylene. The slides after mounted were imaged in a light microscope (Leica, Germany).

## **2.20. Marrow Adipocyte Analysis**

Histological sections of tibias were imaged after stained with H&E and loaded to the BIOQUANT OSTEO 4.0 software (Nashville, TN, USA) to quantify the bone marrow adipocytes. The analysis included the area of the trabecular bone right below the growth plate.

## **2.21. Immunohistochemistry**

The formalin-fixed tissue sections were embedded in paraffin, sectioned, and deparaffinized. Briefly, inguinal white adipose tissue sections were kept at 60°C for 10 min in the oven and then followed by deparaffinizing with xylene and hydrating with an ethanol gradient (100%–70%). Slides were heated at 100° C for 15 min for antigen retrieval and then quenched with 3% H<sub>2</sub>O<sub>2</sub> for 30 min. The slides were rinsed with water and incubated with primary antibody (UCP1 abcam 1 : 250) overnight at 4°C. For negative controls, the primary antibody was replaced by blocking solution. The slides

were rinsed and incubated with the corresponding secondary antibody for 30 min followed by 3,3'-diaminobenzidine (DAB) and hematoxylin staining, respectively. The slides were imaged by using a light microscope (Leica, Germany).

## **2.22. Isolation of Stromal Vascular Fraction from Inguinal White Adipose Tissue (iWAT)**

Freshly harvested inguinal white adipose tissue was washed in PBS, added PBS containing 1 mg/ml collagenase P (Worthington) and finely cut into small pieces and incubated for 1 h at 37 °C on a shaker. After being passed through a 70 µm cell strainer, cells were washed in PBS, spun at 1200 rpm for 5 min and resuspended in basal medium, consisting in DMEM high glucose (Gibco), 10% v/v fetal bovine serum (Hyclone), 100 units/ml penicillin, 100µg/ml streptomycin (Gibco, 1% v/v).

## **2.23. Seahorse- Cellular Metabolism**

Analysis of preadipocyte metabolism was done by using the XF Cell Mito Stress Test Kit with a Seahorse XFe96 analyzer (Agilent Technologies). Preadipocytes isolated from inguinal adipose tissue were seeded in a 96-well Seahorse XF cell culture microplate at 7000 cells/well and after 24 h started adipogenic differentiation. At day 5 preadipocytes were seeded at same density and incubated in basal media to analyze undifferentiated cell response. At day 6 of adipogenic differentiation (day 0 for undifferentiated cells), OCR and ECAR were measured following manufacturer guidelines. Briefly, medium was changed to Seahorse XF Base Medium Minimal DMEM without phenol red with 1 mM pyruvate, 2 mM glutamine, and 10 mM glucose, pH 7.4, and the cells were equilibrated

for 1 h at 37 °C in a CO<sub>2</sub>-free incubator. After measurements of the basal rate, the responses were evaluated toward the application of oligomycin (1.25 μM final concentration), FCCP (1μM), and a combination of antimycin (0.5 μM) and rotenone (0.5 μM). OCR, ECAR, and ATP production rates were calculated by the Seahorse XFe96 software, Wave version 2.6.

#### **2.24. Mitochondrial Labelling**

Stromal vascular fraction was induced adipogenesis and at day 8 of differentiation cells were exposed to 40 μM of MitoTracker® Red CMXRos (Invitrogen) for 15 min at 37 °C with 5% CO<sub>2</sub> in a humidified incubator.

#### **2.25. Immunofluorescence**

Cells cultured in 12-well plates on coverslips were fixed in 4% paraformaldehyde for 15 min at room temperature and permeabilized with block solution (0.1% Triton™ X-100, 5% bovine serum albumin in PBS) for 10 min at room temperature. Coverslips were washed in TBS + 0.1% Triton™ X-100 and primary antibodies: α-Synuclein (ab52168, abcam); Perilipin A (ab3526, abcam), were diluted in block solution and incubated 2 hr at room temperature. Cells were then washed in PBS and appropriate Alexa Fluor® IgG secondary antibodies (Invitrogen) were applied for 30 min at room temperature. Cells were counterstained with the fluorescent nuclear stain diluted in 4,6-diamidino-2-phenylindole (DAPI) diluted 1:10000. Coverslips were mounted using antifade prolong mounting medium (Molecular probes).

## 2.26. Imaging and Quantification Analysis

Cell images were taken using Leica SP8 inverted confocal microscope (Leica Microsystems, Germany) at the MMCRI confocal microscopy facility. Images were collected using a 63x objective (HC PL APO 63x/1.40 OIL CS2I) adding 4x or 2x of digital magnification. Images were deconvoluted, segmented for quantification of morphological parameters such as ROI size and eccentricity and/or co-localization analysis by calculation of Manders Coefficients using Image J.

## 2.27. Statistical Analysis

All data are expressed as the mean  $\pm$  standard error of the mean (SEM). Area under the curve (AUC) was calculated using the trapezoidal rule with baseline as the time 0min value for the glucose and insulin tolerance test. Results were analyzed for statistically significant differences using Two-way ANOVA followed by Tukey multiple comparison post hoc test or Fischer square test for *in vivo* experiments. as indicated. For *in vitro* experiments One-way ANOVA or T-test. All statistics were performed at a significance of  $\alpha=0.05$  with GraphPad Prism 8.4.2 statistical software (GraphPad Software, Inc.). Outliers were identified using the ROUT method in GraphPad Prism.

## CHAPTER 3

### EFFECTS OF ESTROGEN DEFICIENCY ON BONE AND ADIPOSE TISSUE IN PRRX1CRE;SNCA<sup>FL/FL</sup> MICE

Initially, in order to understand whether absence of  $\alpha$ -Synuclein partially protects against estrogen deficiency-induced bone loss and weight gain due to intrinsic role of the protein in osteoprogenitors, we used the Paired related homeobox 1 or Prrx1 enhancer to drive efficiently Cre recombinase expression in the early mesenchyme of the limb.

#### 3.1. Prrx1Cre;Snca<sup>fl/fl</sup> Female Mice are Partially Protected from OVX-Induced Weight Gain

To conditionally delete *Snca* in osteoprogenitor cells, we crossed Prrx1Cre mice to Snca<sup>fl/fl</sup> mice and we obtained Prrx1Cre:Snca<sup>fl/+</sup> in heterozygosis. These heterozygous mice were crossed to Snca<sup>fl/fl</sup> to obtain Prrx1Cre:Snca<sup>fl/fl</sup> mice and Snca<sup>fl/fl</sup> littermates control. The Cre allele was only carried by males in all the mating. Western blot analysis showed a decreased expression of  $\alpha$ -Synuclein in the femur (Fig.3a). We analyzed body composition by DXA at both starting (not shown) and end time points after OVX in Prrx1Cre;Snca<sup>fl/fl</sup> mice and Snca<sup>fl/fl</sup> littermate controls. There was no statistical difference in body weight between the genotypes at baseline; however, control (Snca<sup>fl/fl</sup>) mice after OVX increased their body weight on average ~3.5 fold compared to sham. Prrx1Cre;Snca<sup>fl/fl</sup> increased only ~2 fold for total body weight (Fig. 3b). This difference could be explained by less fat accrual and lean mass in Prrx1Cre;Snca<sup>fl/fl</sup> mice after OVX compared to controls (Fig. 3d).

Both femoral (not shown) and total bone mineral density (BMD) and bone mineral content (BMC) significantly decreased after OVX in *Prrx1Cre;Snca<sup>fl/fl</sup>* mice; however, there were no differences in control mice by DXA after OVX (Fig. 3e-f).

### 3.2. *Prrx1Cre;Snca<sup>fl/fl</sup>* Female Mice are not Protected from OVX-Induced Bone Loss

We next performed  $\mu$ CT imaging on the trabecular bone of the distal femur. OVX reduced bone volume fraction (BV/TV), trabecular number (Tb.N) and connectivity density (Conn.D) in *Prrx1Cre;Snca<sup>fl/fl</sup>* mice, while controls showed a similar trend, although not statistically significant, probably due to the number of animals (Fig. 4a,h,j). Mutant mice showed increased trabecular separation (Tb. Sp), but no significant changes in trabecular thickness (Tb.Th) or structural model index (SMI) after OVX (Fig. 4d,e,i). Similarly, OVX in the *Prrx1Cre;Snca<sup>fl/fl</sup>* mice reduced cortical thickness (Ct. Th) and cortical area (Ct. BA), increased marrow area (Ma. Ar) and cortical area fraction (Ct. BA/TA) with no significant changes in cortical porosity (Porosity %) or moment of inertia (pMOI) (Fig. 5). These results suggest that loss of  $\alpha$ -Synuclein may not be protective for estrogen-deficiency induced bone loss.

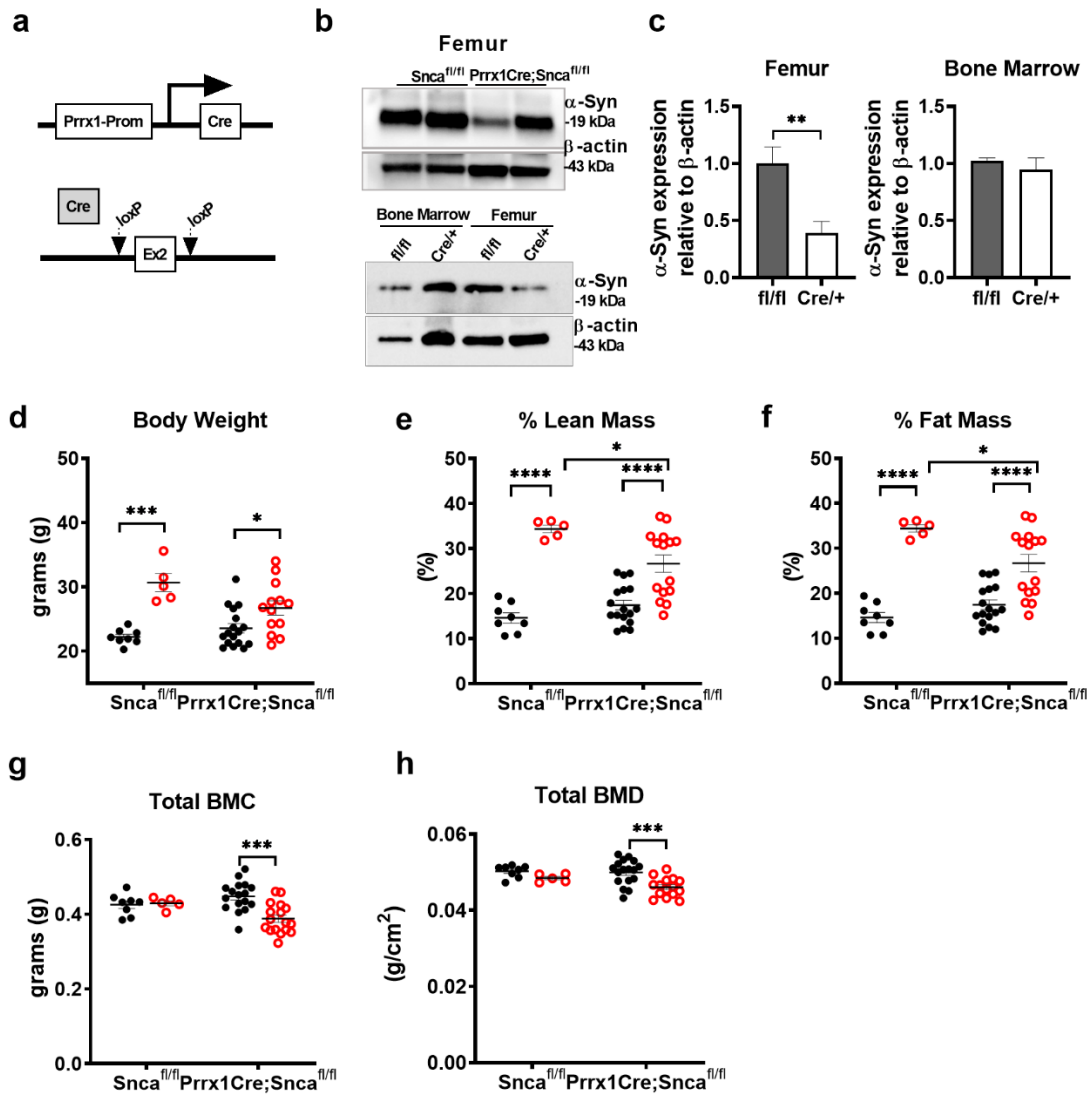


Figure 3. Prrx1Cre;Snca<sup>fl/fl</sup> female mice are partially protected from OVX-induced fat acquisition.

(a) Prrx1Cre;Snca<sup>fl/fl</sup> mice were obtained from crossed between Prrx1Cre;Snca<sup>fl/fl</sup> mice and Snca<sup>fl/fl</sup> mice to conditionally delete exon 2 of  $\alpha$ -Synuclein ( $\alpha$ -Syn) in Prrx1 expressing tissues. (b) Western blot analysis of  $\alpha$ -Syn protein expression in adult femur. (d) Body weight after 12 weeks of ovariectomization (post-OVX) (20 weeks of age), sham operation in black dots and ovariectomized (OVX) in red open circles for Prrx1Cre;Snca<sup>fl/fl</sup> mice and wild type (floxed) controls. Body composition measured at 20 weeks of age with a Lunar PIXImus Densitometer, including total (e) % lean mass and (f) % fat mass, total (h) bone mineral density (BMD) and (g) bone mineral content (BMC). Sham (black filled dots) and OVX (red circles) for each genotype is represented by scatter plot and mean  $\pm$  standard error. Two-way ANOVA and post-hoc Tukey test, \* $p < 0.05$ , \*\* $p < 0.01$ , \*\*\* $p < 0.001$ , \*\*\*\* $p < 0.0001$ .

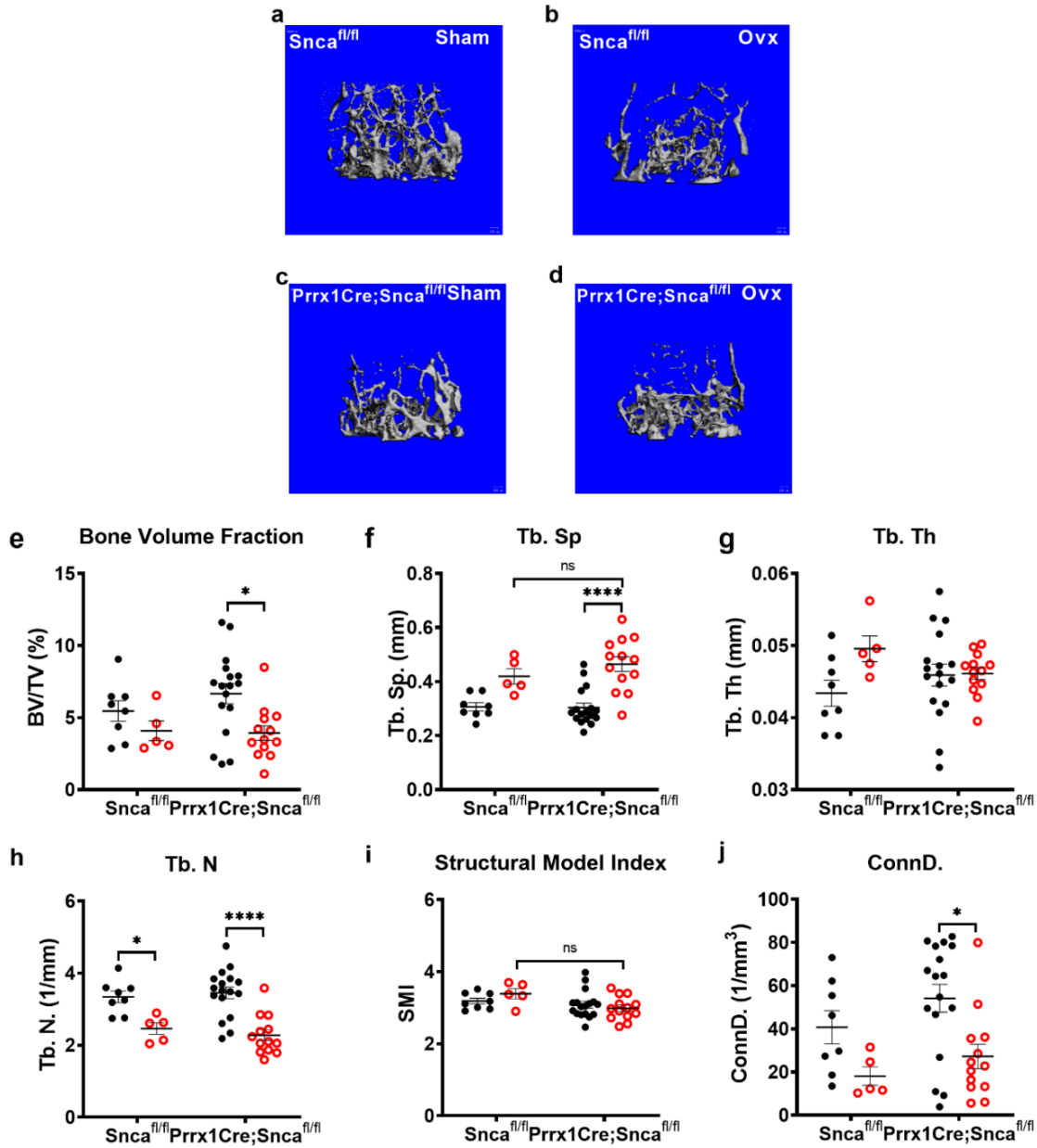


Figure 4. Prrx1Cre;Snca<sup>fl/fl</sup> female mice are not protected from OVX-induced trabecular bone loss.

Representative images of distal femur microarchitecture examined in (a) female wildtype (Snca<sup>fl/fl</sup>) and (f) Prrx1Cre;Snca<sup>fl/fl</sup> mice at 20 weeks of age for (a,f) sham and (b,g) OVX group. (c) Trabecular (Tb.) bone volume fraction (BV/TV), (d) separation (Sp), (e) thickness (Th), (h) number (N), (i) structural model index (SMI) and (j) connectivity (ConnD.) were measured by micro-CT. Sham (black filled dots) and OVX (red circles) for each genotype is represent by scatter plot and mean  $\pm$  standard error. Two-way ANOVA and post-hoc Tukey test, \*p<0.05, \*\*\*\*p<0.0001.

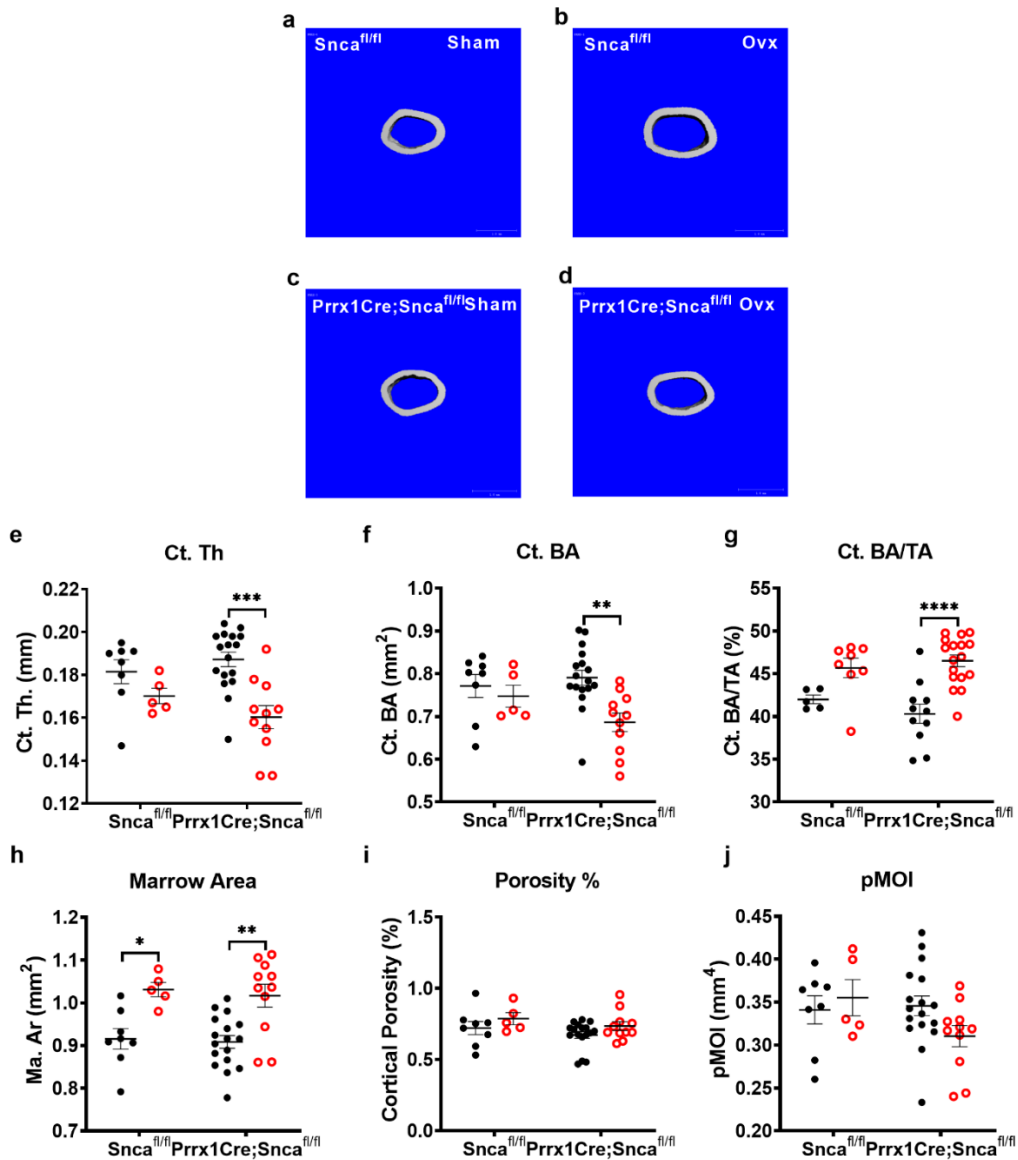


Figure 5.  $Prrx1Cre;Snca^{fl/fl}$  female mice are not protected from OVX-induced cortical bone loss.

Representative images of cortical femur microarchitecture examined in (a) female wildtype ( $Snca^{fl/fl}$ ) and (f)  $Prrx1Cre;Snca^{fl/fl}$  mice at 20 weeks of age for (a,f) sham and (b, g) OVX group. (c) Cortical (Ct.) thickness (Th), (d) bone area (BA), (e) cortical fraction (BA/TA), (h) marrow area, (i) % cortical porosity and (j) polar moment of inertia (pMOI) were measured by micro-CT. Sham (black filled dots) and OVX (red circles) for each genotype is represented by scatter plot and mean  $\pm$  standard error. Two-way ANOVA and post-hoc Tukey test, \*p<0.05, \*\*p<0.01, \*\*\*p<0.001, \*\*\*\*p<0.0001.

### 3.3. Prrx1Cre;Snca<sup>f/f</sup> Female Mice Showed Lower Marrow Adipose Tissue After OVX-Induced Bone Loss

From the 3D MAT reconstruction done by osmium- $\mu$ CT imaging of the tibia we observed that MAT volume is located primarily in the proximal metaphysis and distal tibia, and some towards the proximal diaphysis in control sham tibia, however in tibias from mutant sham mice, there was less MAT expansion to the proximal diaphysis (Fig. 6a, f, g). When controls were OVX'd, tibias showed a substantial increase in MAT towards the proximal diaphysis, meanwhile, in tibias from mutants the increase was modest, suggesting that  $\alpha$ -Synuclein could be playing a role in changes in regulated MAT (rMAT). Similarly, histological H&E tibia sections showed less adipocyte number and volume fraction, although this change did not reach significance (Fig 6b, c-e). Adherent cells from the total bone marrow is a population enriched by BMSCs. We compared its adipogenic potential from the BMSCs from both genotypes and we found that BMSCs from mutant mice showed less adipogenic differentiation, which can explain the decreased adipocyte counts in the histological sections from Fig 4b-e.

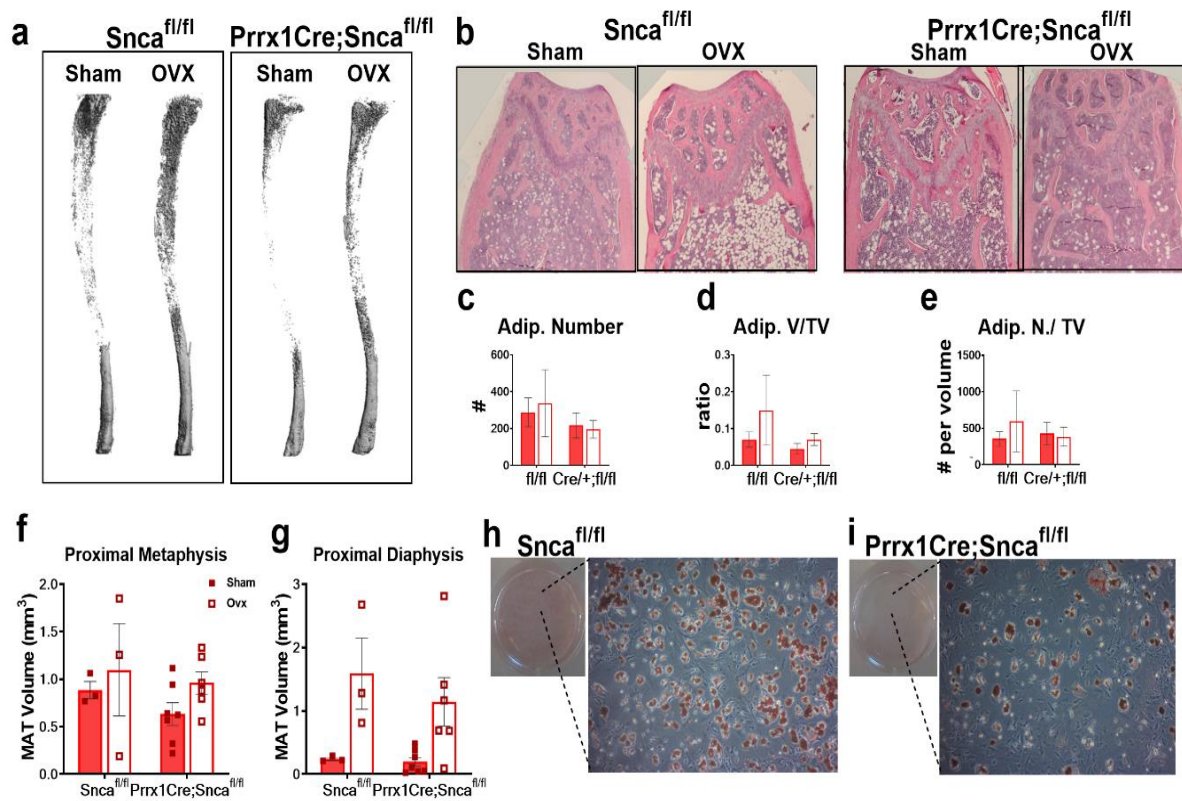
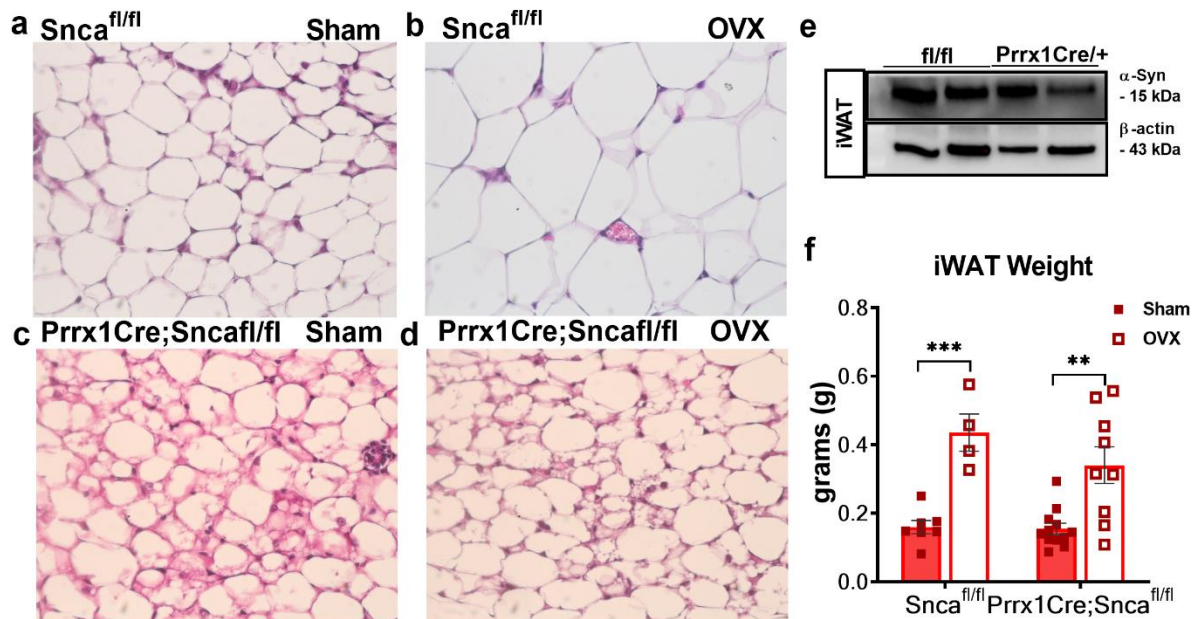


Figure 6.  $Prrx1Cre;Snca^{fl/fl}$  female mice showed a decreased in marrow adipose tissue (MAT) after OVX-induced bone loss.

Representative images of (a) Osmium tetroxide- $\mu$ CT 3D reconstruction and analysis of tibia from female wildtype ( $Snca^{fl/fl}$ ) and  $Prrx1Cre;Snca^{fl/fl}$  mice at 20 weeks of age for sham and OVX group. (b) From H&E staining of tibia sections, adipocyte (c) number, (d) adipocyte volume fraction and (e) adipocyte density were quantified by using BIOQUANT OSTEOPRO. Osmium tetroxide- $\mu$ CT MAT 3D reconstruction-based quantification included MAT volume in (f) proximal metaphysis (g) proximal diaphysis. Analysis of BMSCs adipogenic capacity from (h) control and (i) mutants was compared at day 8. Sham (red filled squares and red bars) and OVX (red empty squares, empty bars) for each genotype is represent by scatter plot and mean  $\pm$  standard error.

### 3.4. Prrx1Cre;Snca<sup>fl/fl</sup> Female Mice Showed Smaller Adipocytes and a Thermogenic and Lipolytic Gene Expression Profile from White Adipose Tissue after OVX-Induced Bone Loss

To better understand the decrease of fat mass observed in the Prrx1Cre;Snca<sup>fl/fl</sup> after OVX compared to controls, we analyzed the inguinal white adipose tissue (iWAT) of these mice. We did not observe a relevant change in  $\alpha$ -Synuclein protein levels when total iWAT lysates from 8 weeks old control and mutants were analyzed.



**Figure 7. Prrx1Cre;Snca<sup>fl/fl</sup> female mice showed smaller adipocytes from the inguinal white adipose tissue (iWAT) after OVX.**

Representative images of (a) H&E stained histological sections from iWAT pads from control Snca<sup>fl/fl</sup> sham and OVX (b) and Prrx1Cre;Snca<sup>fl/fl</sup> (c) sham and (d) OVX mice at 20 weeks. (e) Western blot from total iWAT lysates from control Snca<sup>fl/fl</sup> and Prrx1Cre;Snca<sup>fl/fl</sup> against  $\alpha$ -Synuclein and  $\beta$ -actin as reference protein. (f) Total iWAT pads were measured from both genotypes under sham or OVX conditions. Sham (red filled squares and red bars) and OVX (red empty squared, empty bars) for each genotype is represented by a scatter plot and mean  $\pm$  standard error. Two-way ANOVA and post-hoc Tukey test, \*\*p < 0.01, \*\*\*p < 0.001.

Being the primary subcutaneous fat depot in the mice, we expected that differences in total fat mass were attributable to changes in iWAT acquisition, thus, we weighted the iWAT pads and we found a mild decrease in pad size, although no statistically different from the control. By H&E staining, iWAT from the mutant after OVX had smaller adipocytes (hyperplasia).

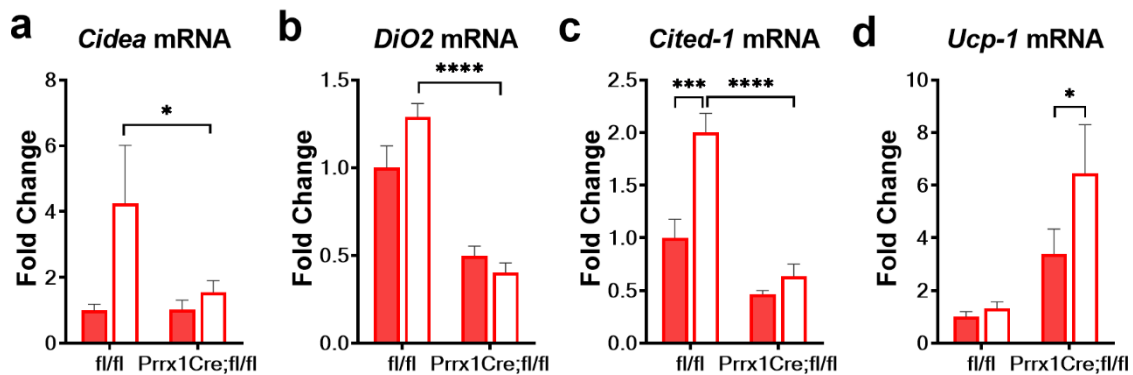


**Figure 8. Thermogenic genes analysis in *Prrx1Cre;Snca<sup>fl/fl</sup>* female mice inguinal white adipose tissue (iWAT).**

Graphs of real time PCR for (a) *Cidea* (b) *DiO2* (c) *Cited-1* and (d) *Ucp1* relative to *Ppib* gene. iWAT from Sham (red bars) and OVX (empty bars) for each genotype is represent by mean  $\pm$  standard error. Two-way ANOVA and post-hoc Tukey test, \* $p < 0.05$ , \*\* $p < 0.01$ , \*\*\* $p < 0.001$ , \*\*\*\* $p < 0.0001$ .

Gene expression analysis by real time PCR showed that iWAT from *Prrx1Cre;Snca<sup>fl/fl</sup>* female mice had a significantly decrease in transcript levels from *Cidea*, *DiO2* and *Cited-1* [107, 108]. These genes have been inversely correlated with lipolysis, metabolic rate, fatty acid synthesis/oxidation, in the literature. *Prrx1Cre; Snca<sup>fl/fl</sup>* iwats showed increased *Ucp1* expression (Fig 8a-d) suggesting mutant iWAT are more thermogenic than controls. Mutant iWATs from OVX showed an increased in *Mcd* ( $p = 0.0519$ ), an enzyme relevant in  $\beta$ -oxidation and the lipolytic enzyme *Lipe*, but no significant changes in *Atgl*,

or the oxidative enzyme *Cpt1a* or in the proadipogenic transcriptional factor *Srebp1c* relative transcript expression.

$\alpha$ -Synuclein and neurological diseases has been related to mitochondrial alterations, we examined whether decreased levels of  $\alpha$ -Synuclein were affecting genes in mitochondrial biogenesis. *Prrx1Cre;Snca<sup>fl/fl</sup>* iWATs showed decreased levels of *Drp1* and *Mfn2* ( $p= 0.1096$ ,  $p= 0.0422$  for the interaction, Two-way ANOVA), both genes are important for mitochondrial fission and fusion, respectively. Our data showed that mutant iWATs had decreased levels of *Bnip3*, a gene that has been positively associated with mitophagy.

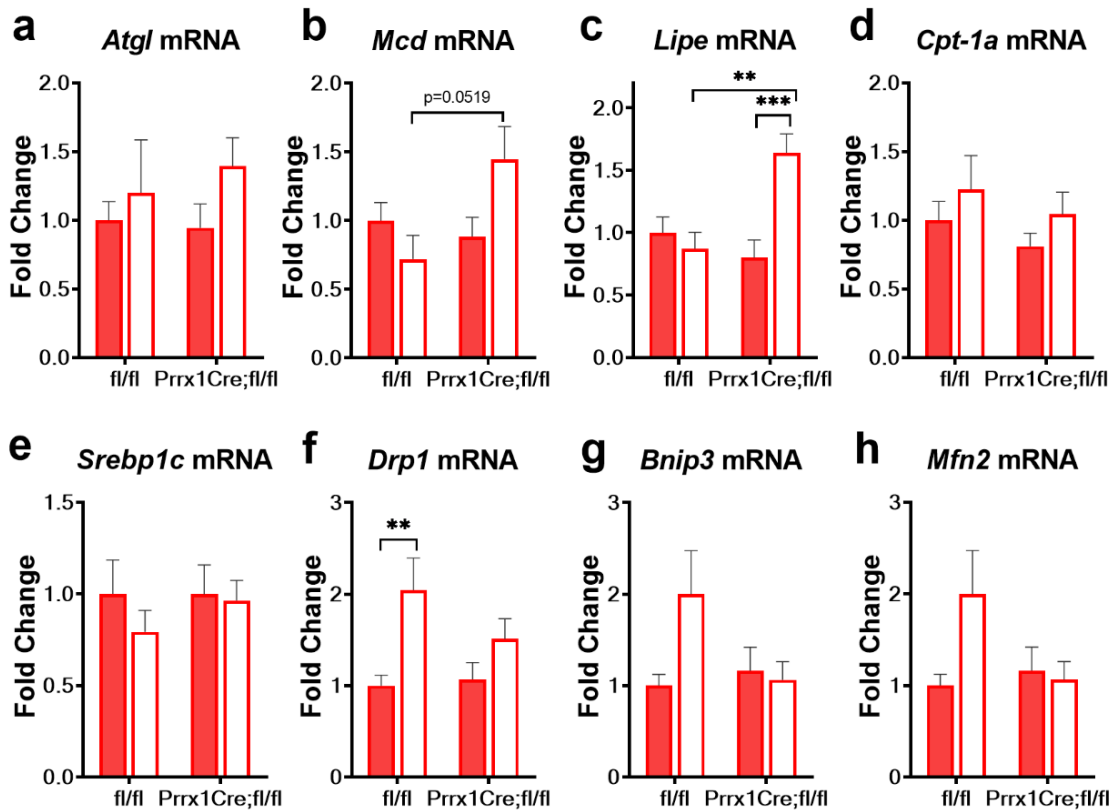


Figure 9. Lipolytic and mitochondrial genes analysis in *Prrx1Cre;Snc $\alpha$ <sup>fl/fl</sup>* female mice inguinal white adipose tissue (iWAT).

Graphs of real time PCR for (a) Adipose triglyceride lipase, *Atgl* (b) Malonyl CoA decarboxylase, *Mcd* (c) Lipase E, Hormone sensitive type, *Lipe* (d) Carnitine palmitoyltransferase 1A, *Cpt1a* (e) Sterol regulatory element-binding transcription factor 1, *Srebp1c*, (f) Dynamin related protein 1, *Drp1*, (g) BCL2 Interacting Protein 3, *Bnip3* and (h) Mitofusin-2, *Mfn2* relative to *Ppib* gene.

## CHAPTER 4

### IMPLICATIONS OF USING PRRX1CRE ENHANCER TO TARGET OSTEOPROGENITOR CELLS

#### 4.1. Prrx1Cre;Snca<sup>fl/fl</sup> Male Mice Present an Anxiety-Like Response and Decreased Ambulatory Activity when fed with High Fat Diet, but showed Resistance to High Fat Diet Effect in Spontaneous Activity

To assess if loss of  $\alpha$ -Synuclein in osteoprogenitor cells affected metabolic and activity performances, Prrx1Cre;Snca<sup>fl/fl</sup> and control mice were randomly assigned high fat diet (60%) or low fat (10%) diet treatment for 15 weeks, in both genders. At end point, females (not shown) and male mice were put in the metabolic cages for 72 hours to measure activity (Fig. 10a-e). Male and female (data not shown) mice did not show any significant changes in terms of food intake among the genotypes. However, Prrx1Cre;Snca<sup>fl/fl</sup> male mice had higher water intake ( $p=0.0703$ ) compared to male controls on a LFD, and this decreased on a HFD (Fig. 10a). These differences in water intake were not found in the females (data not shown). Control male mice on a HFD showed a decrease in distance ( $\sim 55\%$ ,  $p<0.01$ ), speed (33.5%,  $p<0.05$ ) and time (37.8%,  $p<0.05$ ) running on the wheel, as expected when compared to animals on a LFD (Fig. 10c-e). Notwithstanding, Prrx1Cre;Snca<sup>fl/fl</sup> mice maintained persistent spontaneous running activity when challenged with a HFD. Ambulatory (horizontal) activity did not change between the diets in control mice, but Prrx1Cre;Snca<sup>fl/fl</sup> mice decreased  $\sim 50\%$  ( $p<0.05$ ) in their activity when they were on a HFD, as compared to LFD, and had

significantly lower horizontal activity when compared to wild type, both on a HFD (Fig. 10b). These changes in ambulatory activity were not found in females.

We also performed a set of behavioral tests to the same cohort of female and male mice that were housed in metabolic studies, to evaluate behavioral outcomes related to anxiety and depression. We first performed an elevated plus maze test (EPM), and found that *Prrx1Cre;Snca<sup>fl/fl</sup>* mice decreased the number of entrances (entries) to the open arms of the maze, when treated with a HFD, while this change was not significant in the control mice (Fig.10f). The time spent in the open arms of the maze was not affected by the diet, in either genotype. However, *Prrx1Cre;Snca<sup>fl/fl</sup>* mice on the HFD spent less time in the open area, compared to control mice on the same diet ( $p=0.0599$ ), suggesting that a high fat diet induces an increase in anxiety-related behavior in mutant mice (Fig. 10g).

In the open field test (OFT) that *Snca<sup>fl/fl</sup>*, the high fat diet decreased the distance travelled in the center (Fig. 10h) and periphery of the field in control mice. Since mice typically reduce their activity under HFD treatment [119], these data are consistent with the decrease in the wheel activity mentioned previously (Fig. 10d-e). In contrast, the high fat diet did not affect travelled distance in mutant mice, again showing a phenotype in mutant mice that is only revealed when the experimental animals are on a high fat diet.

In the tail suspension test (TST), we found that the time mutant and control male mice spent immobile was comparable, but high fat diet treatment resulted in a significant increase in immobility in mutant mice only (Fig. 10j). No significant changes in the

immobility were observed in the female mice. We also noticed that mutant mice of both genders were more likely to climb their tails during the test when on a LFD (Fig. 10k). High fat diet lead to a reduction in tail climbing behavior in mice of both genders and genotypes, but this effect was significantly more pronounced in males than in females, and in mutant mice compared to control mice (Fig. 10k). The high fat diet also resulted in marked reduction in the duration of tail-climbing behavior in male mutant mice, but no comparable effect was observed in control mice (Fig. 10l).

In the marble-burying test, we found no significant effect of genotype or diet in the percentage of marbles buried. However, we observed that *Prrx1Cre;Snca<sup>fl/fl</sup>* males fed a HFD buried fewer marbles on average than mutant mice on LFD (Fig 10i, genotype-diet interaction  $p=0.0981$ ). Taken together, these results indicate that *Prrx1Cre;Snca<sup>fl/fl</sup>* mice decreased ambulatory activity, but did not alter their spontaneous activity as a response to diet-induced obesity. Additionally, they showed diet-dependent phenotypes of despair and anxiety.

#### **4.2. *Prrx1Cre;Snca<sup>fl/fl</sup>* Male Mice showed Lower Catecholamines compared to Control Mice**

We measured the levels of catecholamines in blood serum from female and male mice at the end point of the HFD study. Compared to control mice, *Prrx1Cre;Snca<sup>fl/fl</sup>* male mice fed on a LFD had lower levels of dopamine, epinephrine and norepinephrine, although for the latter two results did not achieve statistical significance ( $p=0.0951$  and

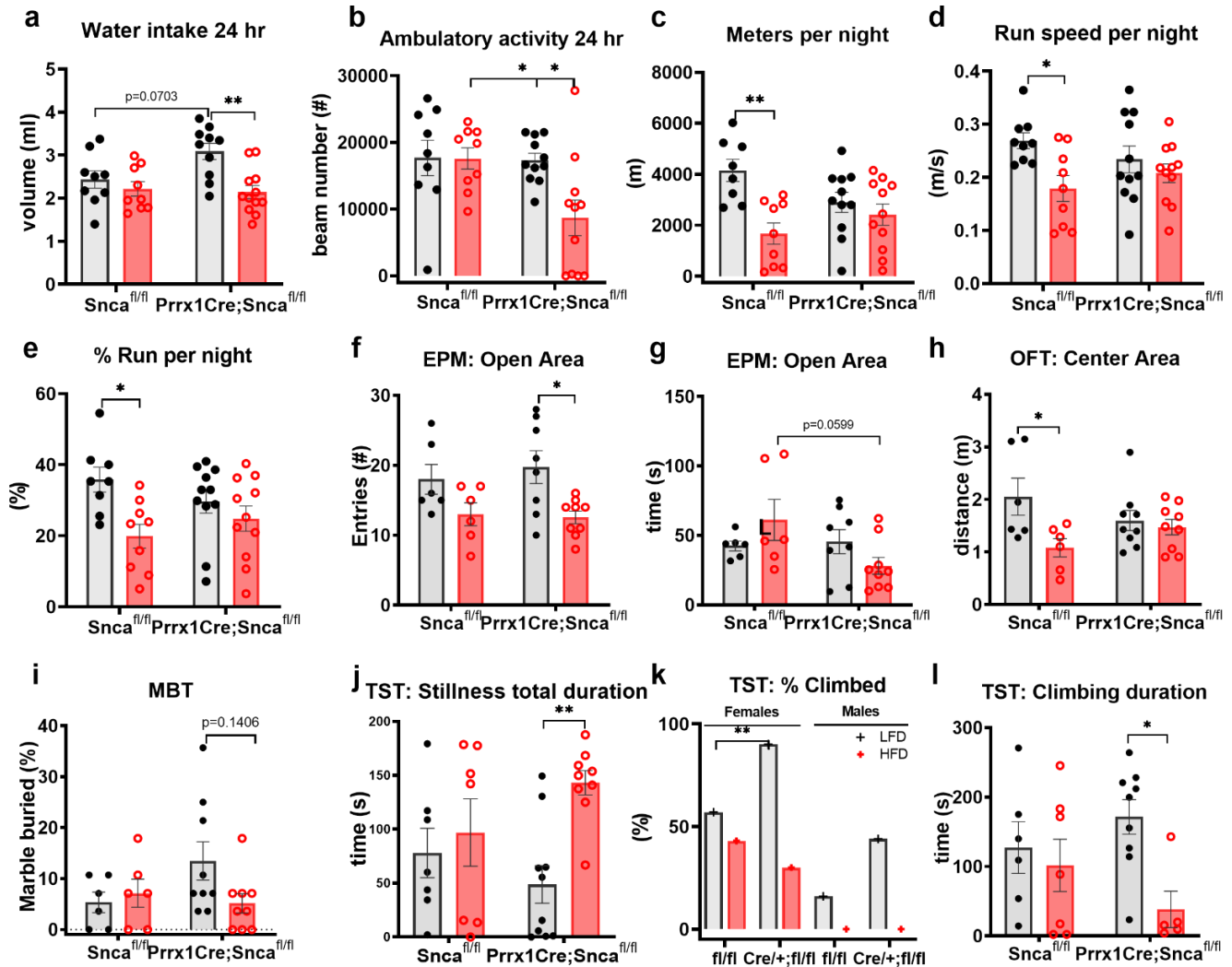


Figure 10. Activity and behavioral analysis of Prrx1Cre;Snca<sup>fl/fl</sup> mice on low and high fat diet.

Male mice activity in metabolic cages (a-f); average 24 h water intake and (b) ambulatory (horizontal) activity. Running on the wheel parameters per night (C) in meters, (d) speed and (e) % of time spent running. Activity of mice in the elevated plus maze test (EPM) (f,g); (f) number of entrances and (g) time spent in the open arms of the apparatus.. Activity in the open field test (OFT) (h) total distance traveled over central area of the apparatus. (i)Percentage of marbles buried. Activity of mice in the tail suspension test (TST) (j-l); (j) total time of immobility (stillness), (k) percentage of mice that climbed their tail (females left, males right, \*\*p<0.01 Fischer test), (l) duration of the climbing. Low fat (10%) diet (black filled dots) and high fat (60%) diet (red circles) for each genotype are represented by scatter plot and mean  $\pm$  standard error. Two-way ANOVA and post-hoc Tukey test, \*p<0.05, \*\*p<0.01.

p=0.0847, respectively) (Fig. 11b, d, f). Moreover, *Prrx1Cre;Snca<sup>fl/fl</sup>* male mice fed a HFD showed significantly lower levels of norepinephrine compared to control (Fig. 11d). These results suggest an altered sympathetic tone in *Prrx1Cre;Snca<sup>fl/fl</sup>* male mice. On the other hand, differences in females were not significant for any of the three catecholamines analyzed (Fig. 11a, c,e).

#### 4.3. *Prrx1Cre;Snca<sup>fl/fl</sup>* Adult Mice showed a Decreased Expression of $\alpha$ -Syn in Key Brain Regions

To investigate whether the behavioral and metabolic phenotypic changes of the mutant mice may derive from *Prrx1*-Cre mediated  $\alpha$ -Syn deficiency in the CNS, we used 8 week old mice to analyze *Prrx1* and *Snca* mRNA expression in selected areas of the brain and the cerebro-cortex (Fig. 12a-f). Our results indicate significant *Prrx1* expression in areas of the cortex largely corresponding to the prefrontal (Ctx1), motor (Ctx2), somatosensory (Ctx3) and piriform (Ctx4) cortices (Fig. 12b).

Mutant mice exhibited significant decrease in *Snca* expression in all those cortical regions (Fig. 12c), but the decrease was more pronounced in the Ctx2, the region that also showed higher *Prrx1* expression (Fig. 12b).

We also observed *Prrx1* expression in all brain areas tested, including the striatum, the hypothalamus and the cerebellum (Fig. 12d). In mutant mice, most of these brain regions showed an 80% or more reduction in *Snca* mRNA expression, while the

reduction was less pronounced in the olfactory bulb and the hippocampus (Fig. 12d). The changes in *Prrx1* and *Snca* brain mRNA expression were consistent with those at the protein level. *Prrx1* was detected in lysates of different brain regions of control animals (Fig. 12f, top), and we observed a consistent reduction in *Snca* protein in the whole brain and different brain regions of *Prrx1*Cre;*Snca*fl/fl mice (Fig. 12f, center and bottom), when compared those to control mice.

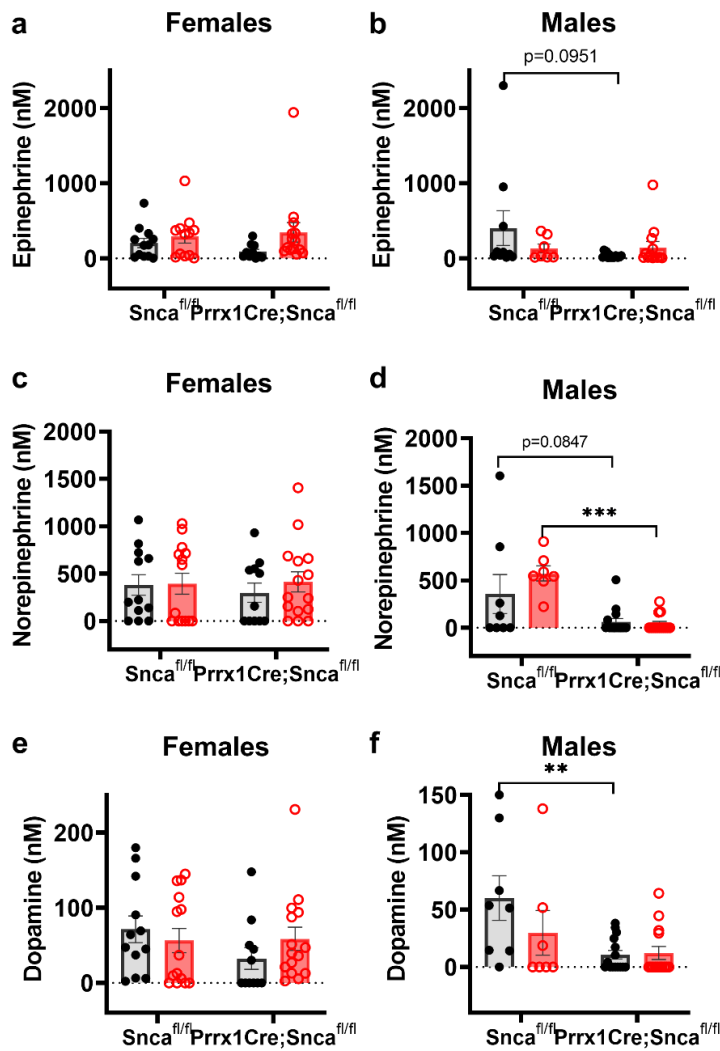


Figure 11. *Prrx1Cre;Snca*<sup>fl/fl</sup> male mice showed a decreased serum levels of catecholamines than wild type mice.

Female and male mice from both genotypes were on a low fat diet (10%, black dots) and high fat diet (60%, red circles) for 15 weeks. Catecholamines levels were measured from serological samples at the end point. (a,b) Epinephrine, (c,d) Norepinephrine and (e,f) Dopamine levels in females and males, respectively. Low fat (10% fat) diet (black filled dots, controls n=8-12, mutants n= 6-15) and high fat (60% fat) diet (red circles, controls n=7-15, mutants n=10-15) for each genotype/gender are represented by scatter plot and mean  $\pm$  standard error. Two-way ANOVA and post-hoc Tukey test, \*\*p<0.01, \*\*\*p<0.001.

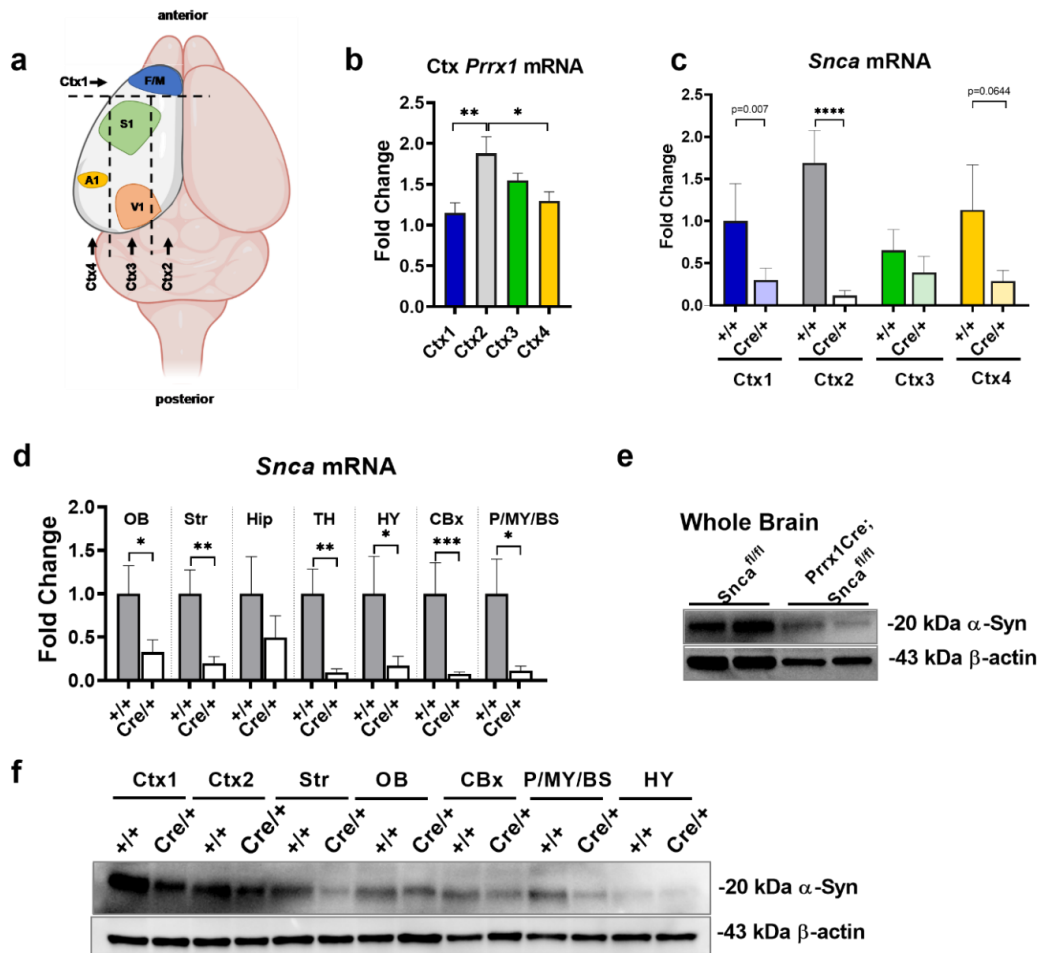


Figure 12. *Prrx1Cre;Snca<sup>fl/fl</sup>* adult mice showed a decreased expression of  $\alpha$ -Syn in key brain regions.

RT-qPCR from adult brain mice was performed to analyze *Prrx1* and *Snca* gene expression levels. (a) Scheme of cortical arbitrary areas of analysis, (b) *Prrx1* expression in cortical regions of brain, (d) *Prrx1* expression in cortex (Ctx), striatum (Str), thalamus (TH), hypothalamus (HY), hippocampus (Hip), pons/medullar/brainstem (P/MY/BS), olfactory bulb (OB) and cerebellum (CBx). expression levels decreased in (c) cortex regions, (e) olfactory bulb, striatum, hypothalamus, thalamus, hippocampus, cerebellum and pons/medullar/brainstem. (f) Western blot analysis of *Prrx1* expression in key regions of the brain, upper. Whole brains and brain regions were analyzed for  $\alpha$ -Syn expression in *Prrx1Cre;Snca<sup>fl/fl</sup>* and control mice in middle and bottom, respectively. Two-way ANOVA and post-hoc Tukey test, \* $p < 0.05$ , \*\* $p < 0.01$ , \*\*\* $p < 0.001$ , \*\*\*\* $p < 0.0001$ .

## CHAPTER 5

### EFFECTS OF DIET-INDUCED OBESITY IN PRRX1CRE;SNCA<sup>FL/FL</sup>

To further understand the weight gain protection observed in our mutant mice after the OVX study, we challenged male and female mice for 15 weeks of HFD (60% fat) or LFD (10% fat sucrose match diet) and analyzed their body composition, bone microarchitecture, metabolic profile, and adipogenic capacity of adipocyte precursors from the inguinal adipose tissue.

#### 5.1. Female and Male Mice Food Intake and Body Composition

We noticed no differences between the caloric intake in females or males (Fig. 13a, c). Interestingly, there were no differences between body weight from *Prrx1Cre:Snca<sup>fl/fl</sup>* mice and *Snca<sup>fl/fl</sup>* littermates control after the HFD treatment, in both genders (Fig. 13 b, d). Both genotypes decreased their lean and increased fat mass (Fig. 13f, k,g,l). Contrary to our previous findings from the OVX study, mutant mice showed significantly higher total BMD when fed at LFD compared to control, or either males or females (Fig. 13h, m). There were no statistical differences in total BMC between diets or genotypes.

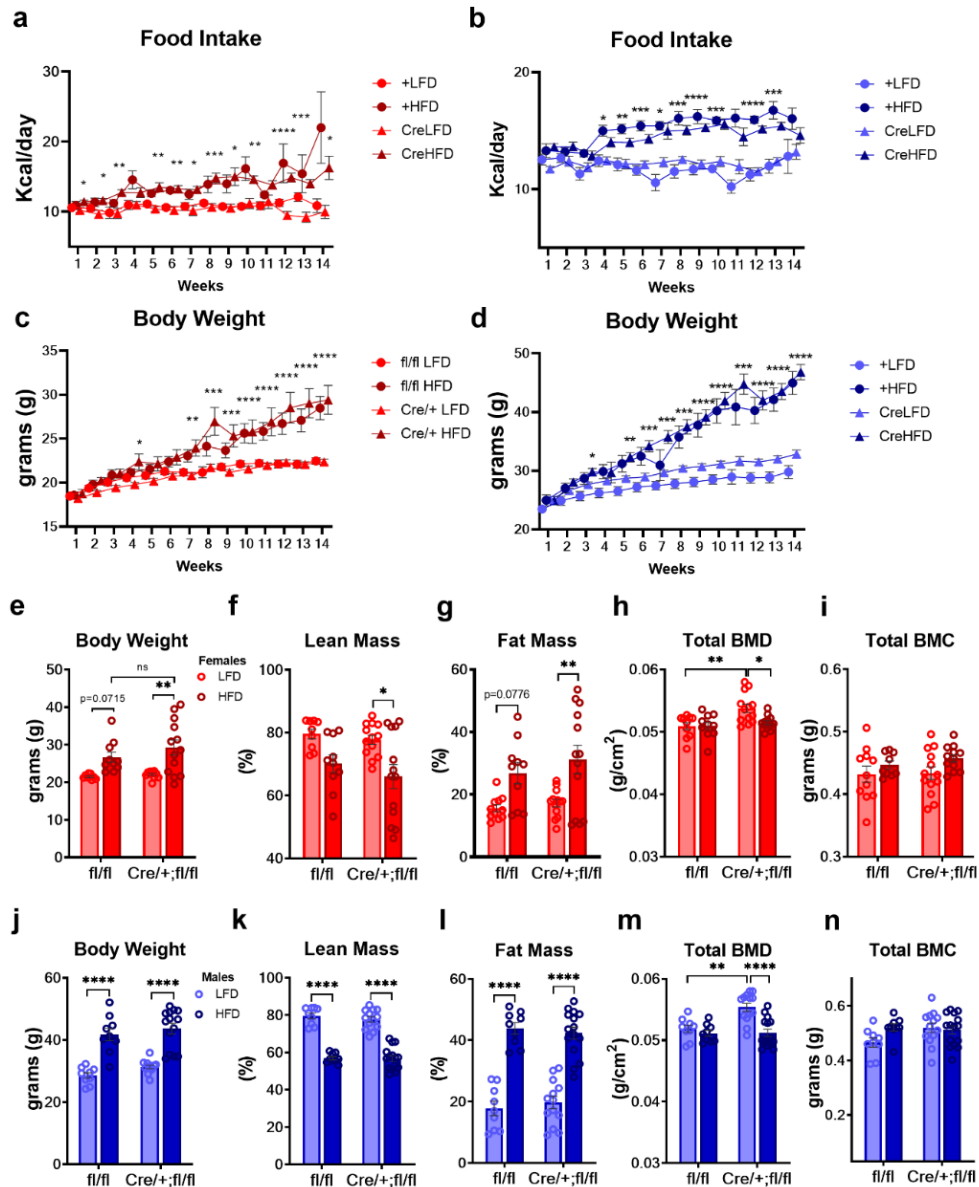


Figure 13. *Prrx1Cre;Snca<sup>fl/fl</sup>* female or male mice are not protected from diet-induced obesity.

*Prrx1Cre;Snca<sup>fl/fl</sup>* female and male mice were challenged with low fat diet (10% fat, LFD, light red/blue bars) or high fat diet (60% fat, HFD, dark red/blue bars) for 15 weeks. (a,b) Caloric intake and (c-e, d-j) body weight was measured for both genders. Body composition was measured at the end point with a Lunar PIXImus Densitometer, including total (f,k) % lean mass and (g,l) % fat mass, total (h,m) bone mineral density (BMD) and (i,n) bone mineral content (BMC). Measurements for each genotype were represented by scatter plot and mean  $\pm$  standard error. Two-way ANOVA and post-hoc Tukey test, \* $p < 0.05$ , \*\* $p < 0.01$ , \*\*\* $p < 0.001$ , \*\*\*\* $p < 0.0001$ .

## 5.2. Bone Microarchitecture Analysis of Femurs from the Diet-induced Obesity in *Prrx1Cre;Snca<sup>fl/fl</sup>*

Micro-CT imaging of the trabecular bone of the distal femur in the females showed no significant changes in femur length, connectivity density, trabecular BMD, trabecular number or separation when mice were fed on a HFD (Fig. 14e, g,h, j. i). However, there was a mild increase in trabecular bone volume fraction (Fig. 14f) and trabecular thickness (Fig. 14k) in the mutant femurs when they were fed on a HFD. In line with that, there was a significant decrease in the SMI (Fig. 14i) when mice were fed with HFD compared to LFD, as lower SMI indicate transition from rod-like to plate-like trabecular bone, this suggests an improvement in the mechanical properties of the bone (Liu XS, 2010).

Similarly, HFD in the *Prrx1Cre;Snca<sup>fl/fl</sup>* female mice showed a mild increased cortical area (Ct Ar,  $p=0.0856$ , Fig 15e), cortical thickness (Ct. Th,  $p= 0.053$ , Fig 15j) and cortical area fraction (Ct. BA,  $p=0.0977$ , Fig. 13h) and no differences in medullary (marrow) and total area (Ma. Ar, Tt. Ar. Fig 15f, g) and cortical mineral density (Ct. TMD) with no significant changes in cortical porosity (Porosity %) or moment of inertia (pMOI, Imin, Imax, Fig 15 k-n).

On the other hand, *Prrx1Cre;Snca<sup>fl/fl</sup>* male mice when fed on a HFD showed decreased trabecular BMD ( $p=0.0525$ ) and no significant changes in other trabecular parameters. Mutant mice fed on a LFD showed significantly higher femur length, increased medullar area, total area and increase in moment of inertia (Fig. 16, 17).

Overall, HFD showed a slight improvement in trabecular and cortical bone microarchitecture in the females but bone deterioration in the males. These opposite effects of the HFD may be explained by the dramatic increase in fat mass and decrease of lean mass in the males, while, in the females this phenotype was milder. Worth noting that both genders showed significantly higher total BMD when fed on a LFD by PIXImus.

These results suggest that  $\alpha$ -Synuclein may play a role in bone homeostasis through intrinsic mechanisms within the bone cells (i.e, osteoblasts, osteocytes), however, its loss does not lead to a striking bone phenotype. These outcomes suggest that  $\alpha$ Synuclein regulates bone primarily through sympathetic tone, indirectly through cross talk with other tissues such as adipose depots, or other cell types within the bone marrow, or a combination of all of the above.

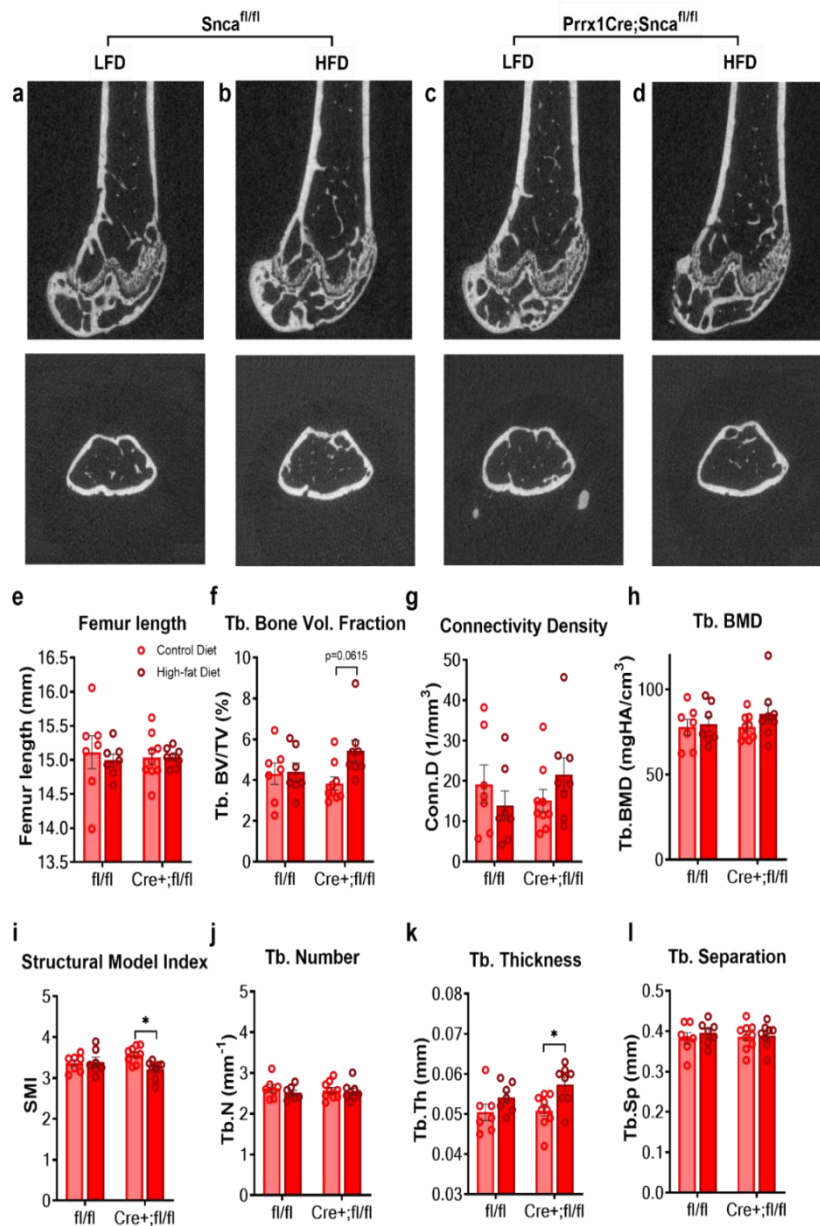


Figure 14. Prrx1Cre;Sncα<sup>fl/fl</sup> female mice showed a mild improvement in trabecular bone microarchitecture after treatment with HFD.

Representative images of distal femur microarchitecture examined in (a, b) female controls (Sncα<sup>fl/fl</sup>) and (c, d) Prrx1Cre;Sncα<sup>fl/fl</sup> mice after 15 weeks of HFD. (a, c) mice at low fat diet (LFD, pink bar) and (b, d) high fat diet (HFD, red bar). (e) Femur total length, (f) trabecular (Tb.) bone volume fraction (BV/TV), (g) connectivity density (ConnD.), (h) tb bone mineral density, (i) structural model index (SMI) (j) number (N), (k) thickness (Th), (l) separation (Sp) were measured by μCT. Data is represented by scatter plot and mean ± standard error. Two-way ANOVA and post-hoc Tukey test, \*p<0.05.

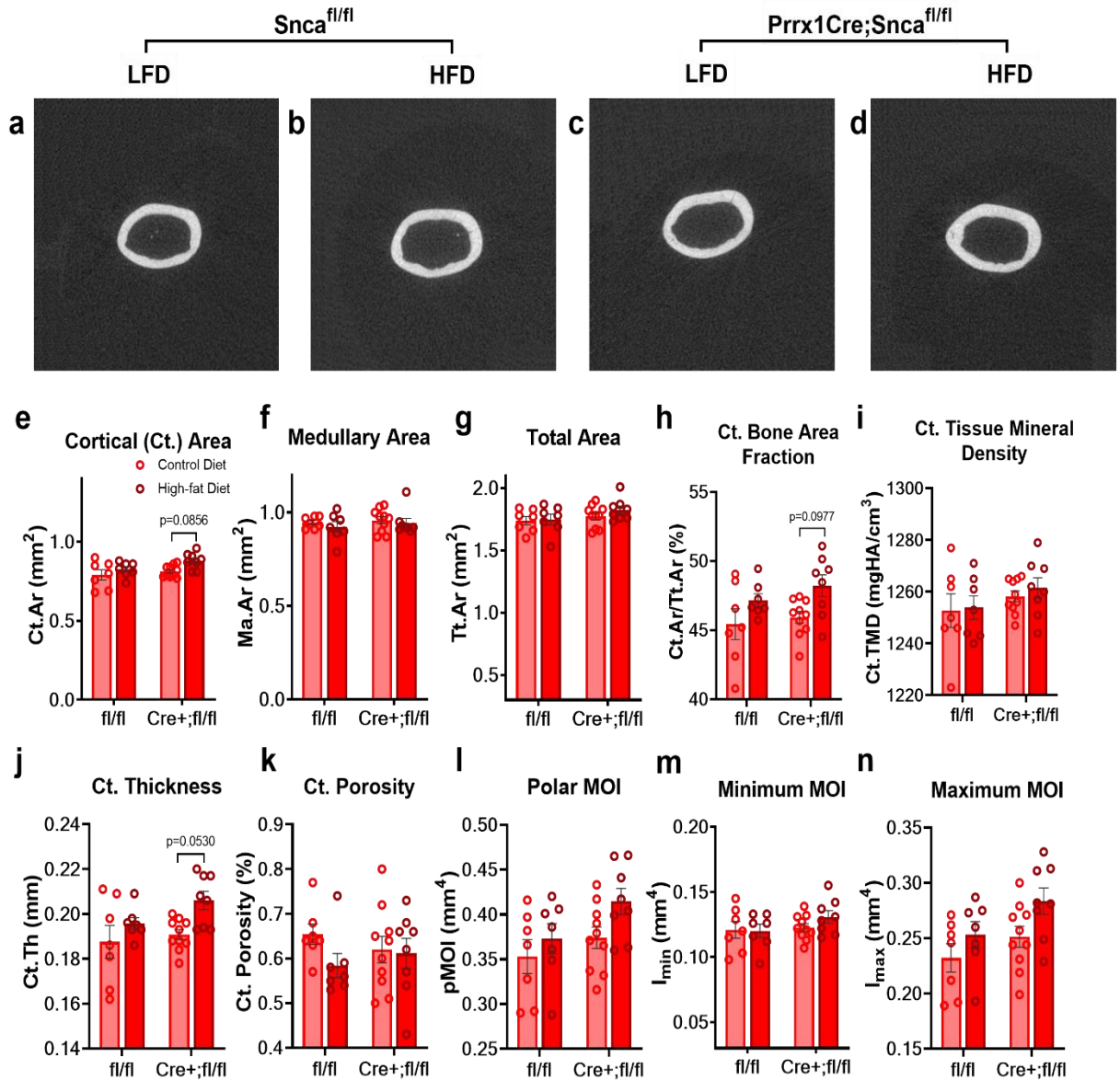


Figure 15. Prrx1Cre;Snca<sup>fl/fl</sup> female mice showed no differences in cortical bone microarchitecture compared to control after HFD treatment.

Representative images of cortical femur microarchitecture examined in (a, b) female controls (Snca<sup>fl/fl</sup>) and (c, d) Prrx1Cre;Snca<sup>fl/fl</sup> mice after 15 weeks of HFD. (a, c) mice at low fat diet (LFD, pink bar) and (b, d) high fat diet (HFD, red bar). (e) Cortical (Ct) area, (f) medullar (marrow) area, (g) total cortical area, (h) cortical bone fraction, (i) cortical mineral density, (j) cortical thickness, (k) porosity %, (l) polar moment of inertia, (m) minimum and (n) maximum moment of inertia were measured by  $\mu$ CT. Data is represented by scatter plot and mean  $\pm$  standard error. Two-way ANOVA and post-hoc Tukey test, \*p<0.05.

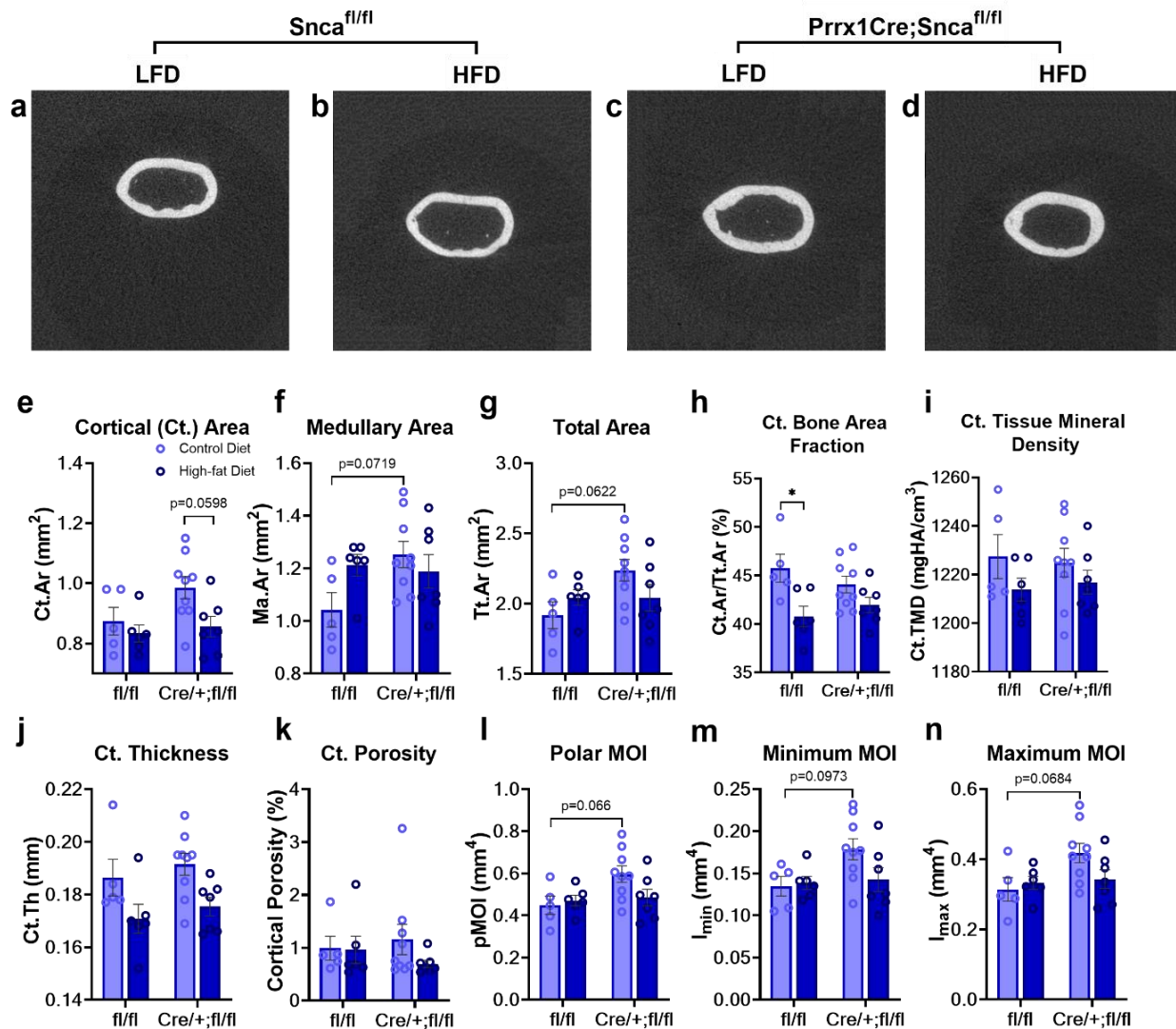


Figure 16. *Prrx1Cre;Snca<sup>fl/fl</sup>* male mice showed no differences in trabecular bone microarchitecture compared to control after treatment with HFD.

Representative images of distal femur microarchitecture examined in (a, b) male controls (*Snca<sup>fl/fl</sup>*) and (c, d) *Prrx1Cre;Snca<sup>fl/fl</sup>* mice after 15 weeks of HFD. (a, c) mice at low fat diet (LFD, light blue bar) and (b, d) high fat diet (HFD, dark blue). (e) Femur total length, (f) trabecular (Tb.) bone volume fraction (BV/TV), (g) connectivity density (ConnD.), (h) tb bone mineral density, (i) structural model index (SMI) (j) number (N), (k) thickness (Th), (l) separation (Sp) were measured by  $\mu$ CT. Data is represented by scatter plot and mean  $\pm$  standard error. Two-way ANOVA and post-hoc Tukey test, \* $p < 0.05$ .

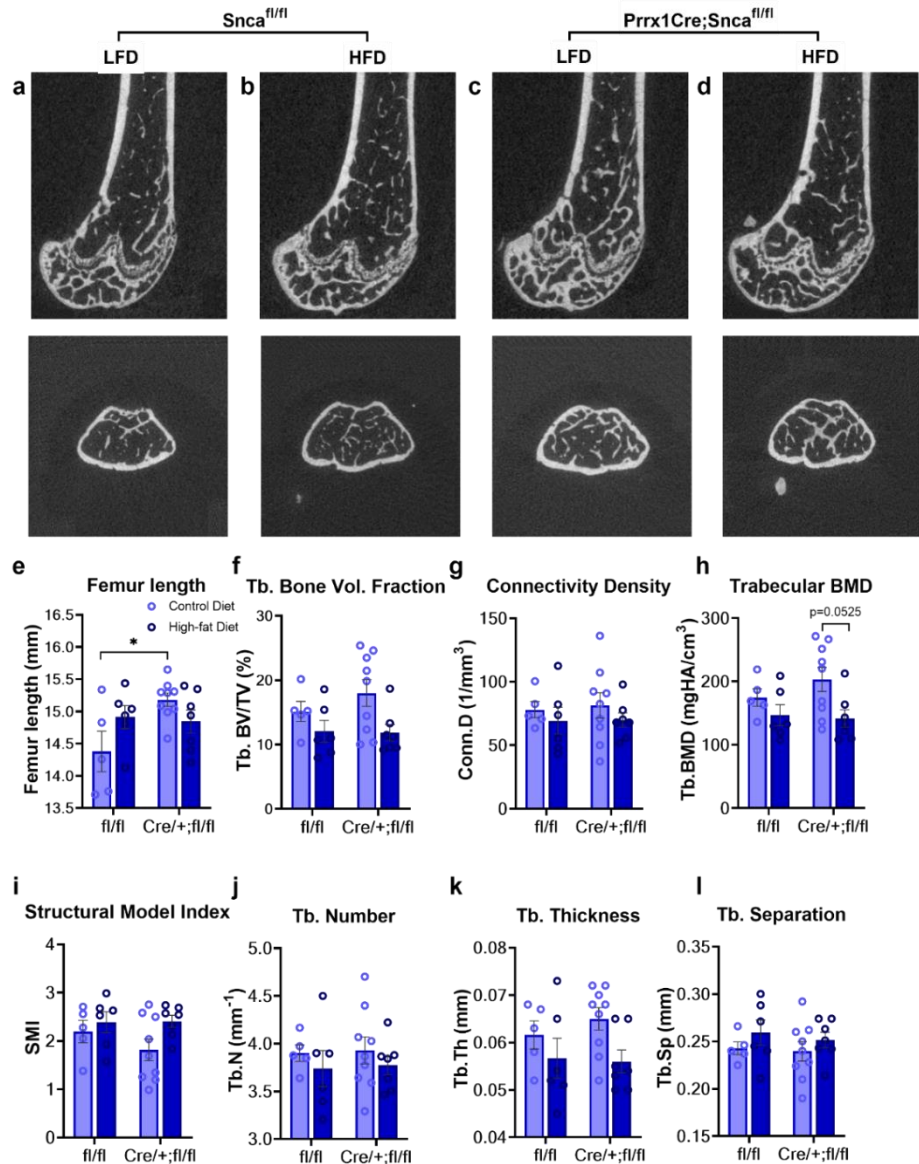


Figure 17. Prrx1Cre;Snca<sup>fl/fl</sup> male mice showed no differences in cortical bone microarchitecture compared to control after HFD treatment.

Representative images of cortical femur microarchitecture examined in (a, b) male controls (Snca<sup>fl/fl</sup>) and (c, d) Prrx1Cre;Snca<sup>fl/fl</sup> mice after 15 weeks of HFD. (a, c) mice at low fat diet (LFD, light blue bar) and (b, d) high fat diet (HFD, dark blue bar). (e) Cortical (Ct) area, (f) medullar (marrow) area, (g) total cortical area, (h) cortical bone fraction, (i) cortical mineral density, (j) cortical thickness, (k) porosity %, (l) polar moment of inertia, (m) minimum and (n) maximum moment of inertia were measured by  $\mu$ CT. Data is represented by scatter plot and mean  $\pm$  standard error. Two-way ANOVA and post-hoc Tukey test, \* $p < 0.05$ .

### 5.3. Histological Analysis of Inguinal Adipose Tissue after HFD Study

We observed at the histological H&E stained sections of iWAT an increase in size in the adipocytes from the HFD group (Fig. 18 b); however, and similar to our previous observations from the OVX study, the iWAT from the mutant mice on a HFD remained small, and with a “multilocular appearance” (Fig. 18 d). Despite of the reduced size of the iWAT adipocytes, the iWAT pad weight was not significantly different when both mice genotypes were on a HFD (Fig. 18 e).

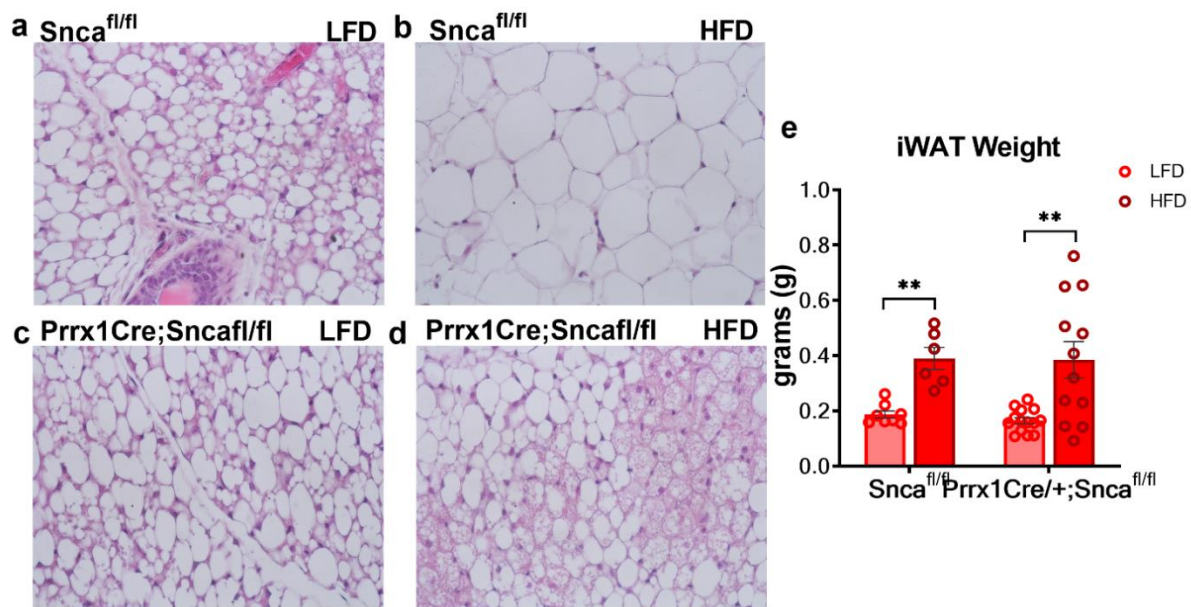


Figure 18. Prrx1Cre;Snca<sup>fl/fl</sup> female mice showed smaller adipocytes from the inguinal white adipose tissue (iWAT) after HFD.

Representative images of (a) H&E stained histological sections from iWAT pads from control Snca<sup>fl/fl</sup> LFD and HFD (b) and Prrx1Cre;Snca<sup>fl/fl</sup> (c) LFD and (d) HFD mice after 15 weeks of diet. (e) Total iWAT pads were measured from both genotypes under LFD (pink bar) or HFD (red bar). Pads weight for each genotype is represent by scatter plot and mean  $\pm$  standard error. Two-way ANOVA and post-hoc Tukey test, \*\*p<0.01.

#### 5.4. Metabolic Cages Activity Analysis, Glucose Tolerance Test (GTT) and Insulin Tolerance Test (ITT)

$\alpha$ -Synucleinopathies such as PD have been associated with alterations in metabolism and insulin impairment. We tested if partial deletion of  $\alpha$ -Synuclein had an effect in glucose and insulin response. Glucose tolerance test at the end point of the HFD challenge in female mutants showed no significant difference at a LFD or HFD (Fig. 19a) respect to controls. However, they were significantly less insulin sensitive than controls (Fig. 19b) at any diet.

Mutants had increased in  $V_{CO_2}$  (Fig. 19c) during the day and maintained their resting respiratory quotient during the day meantime the controls diminished it (Fig. 19f). They showed an increase in resting energy expenditure (Fig 19g) at night when fed on a HFD while in controls this change was not significant. There were not statistical differences in total energy expenditure (Fig. 19h). Mutants on a HFD had an increased in ambulatory activity compared to controls however they ran less in the wheel than controls ( $p=0.0958$ ) (Fig. 19d,e).

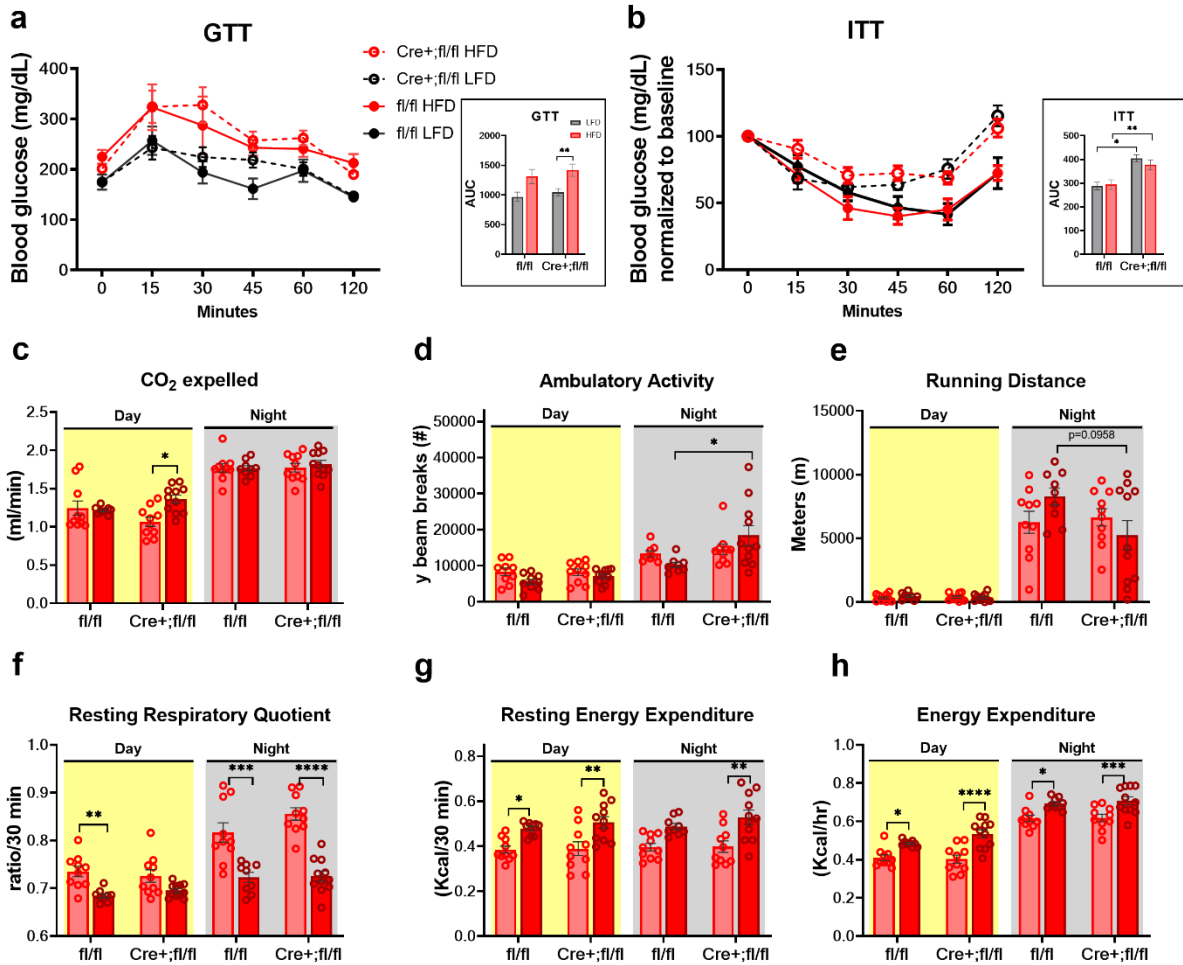


Figure 19. *Prrx1Cre;Sncα<sup>fl/fl</sup>* female mice have a decreased insulin sensitivity and higher ambulatory activity on high fat diet.

(a) Glucose tolerance test (GTT) and (b) Insulin tolerance test (ITT) were performed at the end point of the HFD treatment and analyzed the area under the curve to determine statistical differences. Metabolic analysis included measurements of (c) CO<sub>2</sub> expelled, (d) ambulatory (horizontal) activity, (e) running on the wheel parameters per night in meters, (f) resting respiratory quotient, (g) resting energy expenditure and (h) total energy expenditure. Low fat (10% fat, pink bars) diet and high fat (60% fat, red bars) diet for each genotype are represented by scatter plot and mean ± standard error. Two-way ANOVA and post-hoc Tukey test, \**p*<0.05, \*\**p*<0.01, \*\*\**p*<0.001, \*\*\*\**p*<0.0001.

## 5.5. Thermogenic Gene Expression Analysis and Adipogenic Differentiation of Inguinal Adipose Depot and Preadipocytes Metabolic Profile

Our previous findings related to the increase in resting energy expenditure and the decrease in adipocyte size “beige like” adipocytes in the iWAT from mutant mice led us to hypothesize that the phenotype could be due to an increase in the thermogenic capacity. We analyzed histological sections of iWATs from the OVX and HFD studies and immunostained with UCP-1 antibody, a mitochondrial protein responsible for the thermogenic respiration and highly expressed in the brown adipose tissue. As it is shown in the Fig. 17 a-d, we found several regions within the iWAT from the mutant mice after OVX or HFD studies that had an multilocular appearance and high expression of UCP1, brown staining in Fig. 19 b, d.

When we isolated preadipocytes from stromal vascular fraction (SVF) from iWAT, mutant cells showed significantly decrease in adipogenic differentiation (Fig. 20e,f) and increased maximal respiration and decreased coupling efficiency (Fig. 20j). These changes were not found in undifferentiated cells (Fig. 20i).

*Snca* mRNA expression time course (Fig. 20h) showed highest levels at day 8 of differentiation and mutants showed, as expected, significantly lower levels of *Snca* at that day of differentiation. *Ppar $\gamma$*  (at day 2) and *Adipoq* (at day 0, 2 and 4) were significantly lower in the mutant preadipocytes compared to control cells (Fig. 21). Contrary to our gene expression analysis from the OVX study, here we found *Atgl*, *Mcd* and *aP2* mRNA relative levels were significantly lower in the mutant preadipocytes at

day 2, 4 and day 0-2, respectively (Fig. 22). Interestingly, and supporting previous results in section 3.4, we found mutant preadipocytes had higher mRNA levels of *CPT1a*. These results suggest that *Snca* could be playing a role in the expression of master regulators of adipogenesis such as *Ppar $\gamma$* , promoting adipogenic commitment and lipid storage. Thus, in partial absence of the protein, we observed higher thermogenic capacity and expression of genes that promote  $\beta$ -oxidation.

*Drp1* and *Mfn2* mRNA relative levels were lower in mutant preadipocytes (day 2 and day 2-4) and similarly, *Bcl312* mRNA was significantly lower at day 0 and 6. *Park2*, a gene also associated with mitophagy, was also decreased in mutant preadipocytes compared to controls at day 0, 2 and 4. These results are aligned to our observations from iWAT in the OVX study suggesting that  $\alpha$ -Synuclein is associated with mitophagy and mitochondrial biogenesis as others have shown in models of neurodegeneration.

To clarify if the phenotype of these mutant cells were due to changes in sympathetic tone, we analyzed the expression of the *Adrb1* and *Adrb3* in the preadipocytes. At day 8, there is a decreased of *Adrb1* relative mRNA levels compared to controls. At day 0, 2 and 8 there was a decrease (although not statistically significant) of the *Adrb3* relative mRNA in the mutants suggesting that mutant phenotype could be, in part, due to a decrease in  $\beta$ -adrenergic signaling as result of partial loss of  $\alpha$ -Synuclein in the CNS.

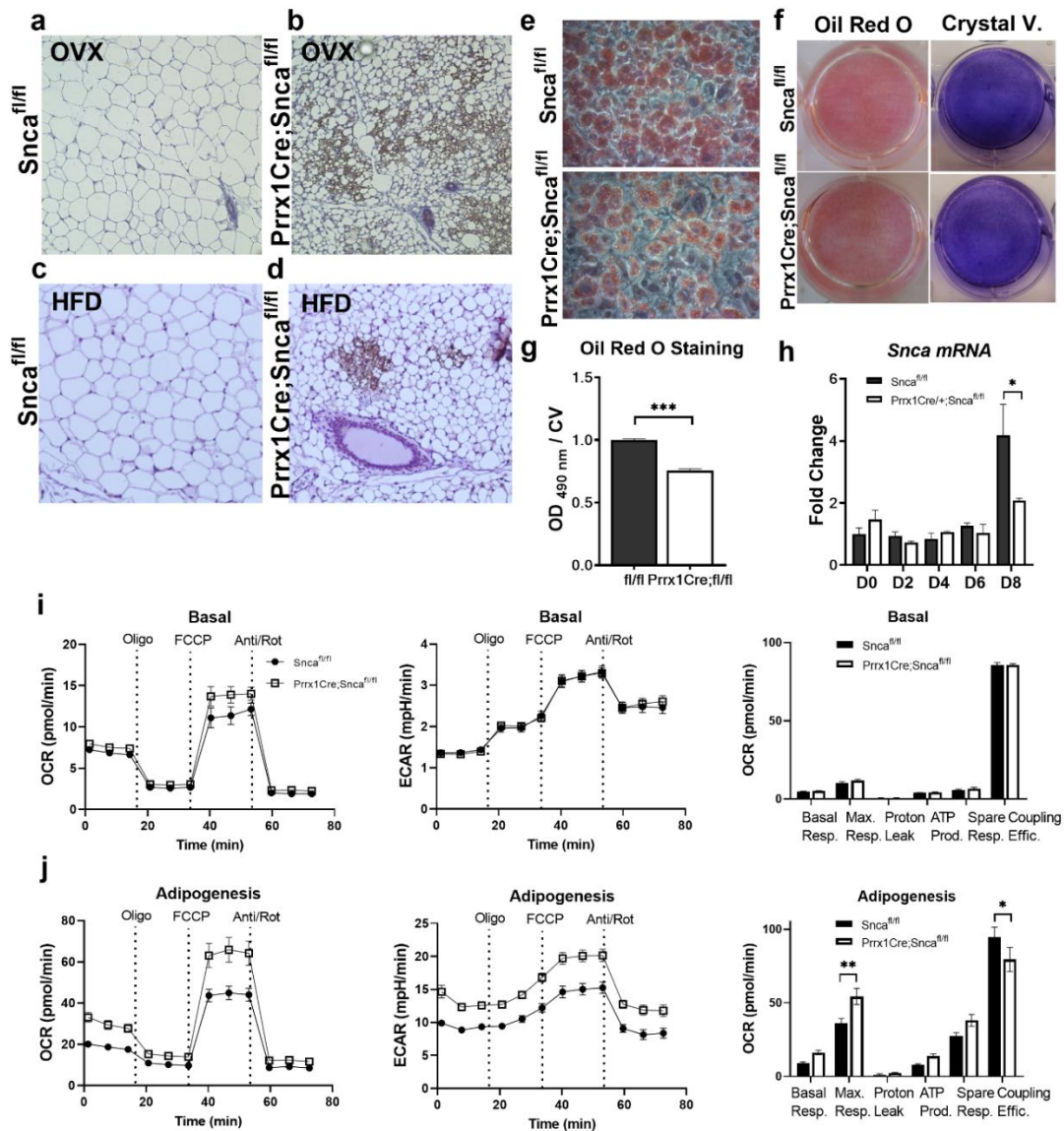


Figure 20. *Prrx1Cre;Snca<sup>fl/fl</sup>* iWAT adipocytes expressed UCP-1 and have higher oxidative capacity compared to controls.

Representative images of Immunohistochemistry of histological sections from iWAT pads from control *Snca<sup>fl/fl</sup>* (a) OVX, (c) HFD, *Prrx1Cre;Snca<sup>fl/fl</sup>* (b) OVX, (d) HFD. (k) Stromal vascular fraction (SVF) from iWAT was isolated and induced adipogenic differentiation, stained with (i) Oil Red O (ORO) and crystal violet (CV). (m) ORO staining was measured spectrophotometrically at OD= 490 nm and normalized by CV absorbance at 650 nm. (n) Relative  $\alpha$ -synuclein mRNA expression time-course from SVF after day 0, 2, 4, 6 and 8 of adipogenesis. Values for each genotype are represented by scatter plot and mean  $\pm$  standard error. For (e-j), Two-way ANOVA and post-hoc Tukey test, \* $p < 0.05$ , for (m-p), T test, \* $p < 0.05$ .

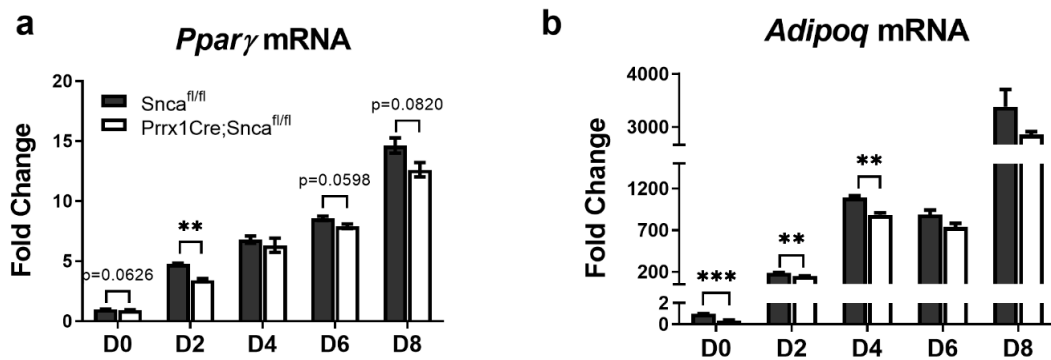


Figure 21. Prrx1Cre;Snca<sup>fl/fl</sup> iWAT preadipocytes showed less expression of pro-adipogenic and mature genes.

Relative  $\alpha$ -synuclein mRNA expression time-course from SVF after day 0, 2, 4, 6 and 8 of adipogenesis for (a) *Pparγ*, (b) *Adipoq*. Values for each genotype (controls black bars, mutants white bars) are represented by mean  $\pm$  standard error. T- test, \* $p < 0.05$

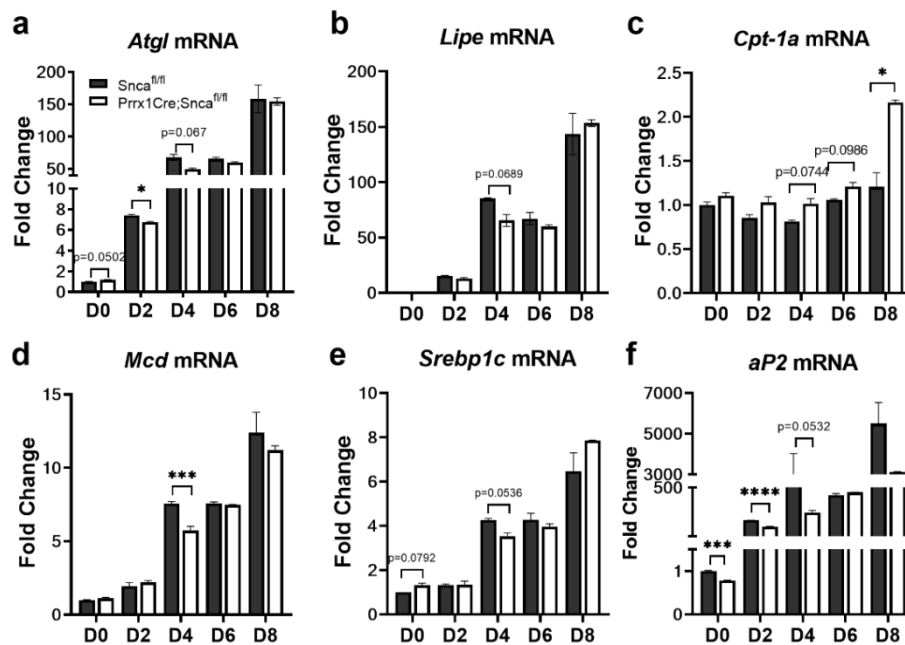


Figure 22. Prrx1Cre;Snca<sup>fl/fl</sup> iWAT preadipocytes showed less expression of pro-adipogenic and mature genes.

Relative  $\alpha$ -synuclein mRNA expression time-course from SVF after day 0, 2, 4, 6 and 8 of adipogenesis for (a) *Atgl*, (b) *Lipe*, (c) *Cpt-1a*, (d) *Mcd*, (e) *Srebp1c* and (f) *aP2*. Values for each genotype (controls black bars, mutants white bars) are represented by mean  $\pm$  standard error. T- test, \* $p < 0.05$ .

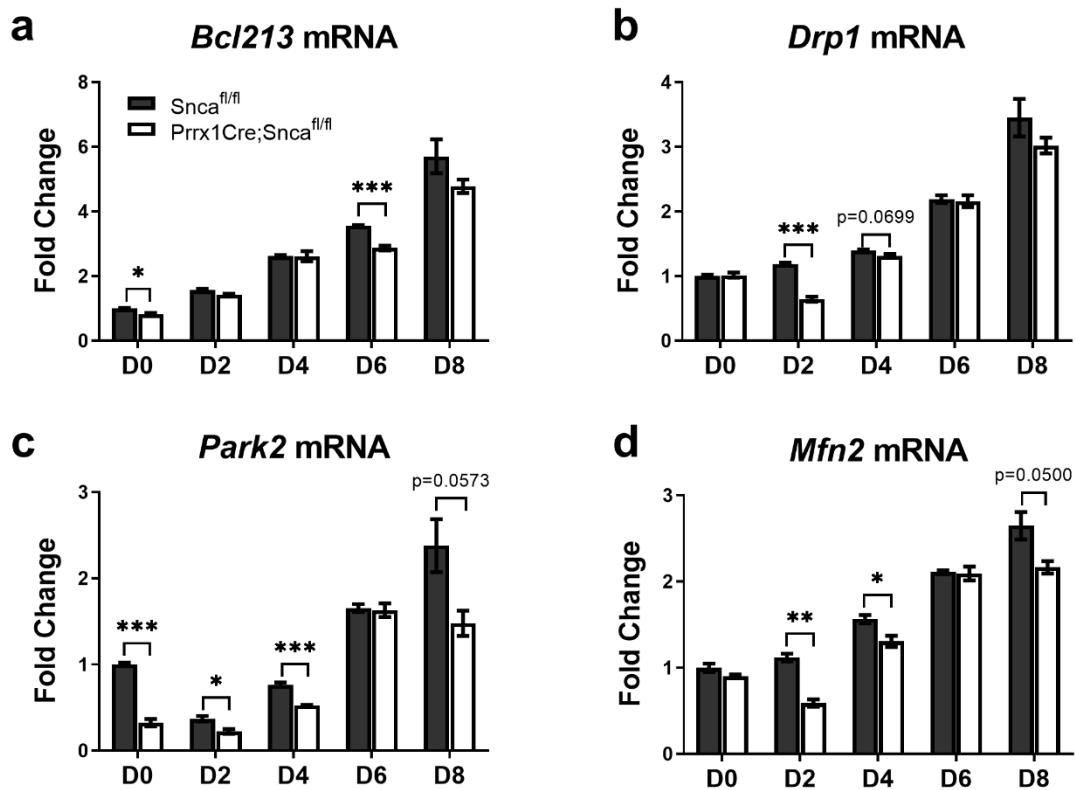


Figure 23. Prrx1Cre;Snca<sup>fl/fl</sup> iWAT preadipocytes showed less expression of mitochondrial genes.

Relative  $\alpha$ -synuclein mRNA expression time-course from SVF after day 0, 2, 4, 6 and 8 of adipogenesis for (a) *Bcl213*, (b) *Drp1* (c) *Park2*, (d) *Mfn2*. Values for each genotype (mutants black bars, control white bars) are represented by mean  $\pm$  standard error. T-test, \* $p < 0.05$ .

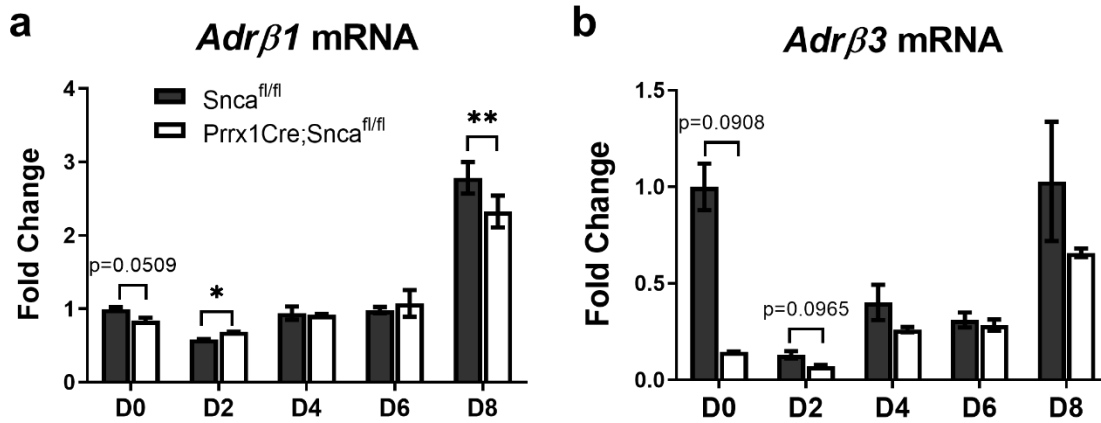


Figure 24. Prrx1Cre;Snca<sup>fl/fl</sup> iWAT preadipocytes showed less expression of  $\beta$ -adrenergic receptors .

Relative  $\alpha$ -Synuclein mRNA expression time-course from SVF after day 0, 2, 4, 6 and 8 of adipogenesis for (a) *adrβ1*, (b) *adrβ3*. Values for each genotype (controls black bars, mutants white bars) are represented by mean  $\pm$  standard error. T- test, \* $p < 0.05$ .

## CHAPTER 6

### EFFECTS OF DIET-INDUCED OBESITY IN ADIPOQCRE;SNCA<sup>FL/FL</sup>

We did not find a weight gain protection against DiO in our previous *Prrx1Cre;Snca<sup>fl/fl</sup>* model; But we still could not determine whether  $\alpha$ -Synuclein was regulating adipose metabolism cell autonomously or not, as our model presented important off-target effects that led to central *Snca* deletion. Therefore, by using Adiponectin, a mature adipocyte marker, to specifically target adipose depots with no (not reported to date) off-target effects in the CNS.

Similarly to our previous HFD studies, we challenged female and male (males not shown) *AdipoqCre;Snca<sup>fl/fl</sup>* mice for 15 weeks of HFD (60% fat) or LFD (10% fat sucrose matched diet) and analyzed their body composition, bone microarchitecture, metabolic profile, and adipogenic capacity of adipocyte precursors from the inguinal adipose tissue.

#### 6.1. Female Mice Food Intake and Body Composition

We found no differences between the caloric intake in females or males (Fig. 25b). Female *AdipoqCre;Snca<sup>fl/fl</sup>* mice had significantly lower body weight when fed on a HFD (Fig. 25c,d) compared to control. Mutants had higher lean mass and decreased fat mass when treated with HFD. Mutants showed improved total bone mineral density (BMD) and femoral BMD, but these differences were not statistically significant (Fig. 25 g, h).

## 6.2. Bone Microarchitecture Analysis of Femurs from the Diet-induced Obesity in AdipoqCre;Snca<sup>fl/fl</sup>

Micro-CT analysis of the femur microarchitecture from the AdipoqCre;Snca<sup>fl/fl</sup> mice imaging for trabecular bone of the distal femur in the females showed no significant changes in femur length, connectivity density, trabecular BMD, SMI, trabecular number or separation when mice were fed on a HFD (Fig. 26e, g-j, l). There was a mild increase in trabecular bone volume fraction (Fig. 26f) in the mutant femurs however, there were not significantly different from controls at a HFD.

There were no significant changes in cortical bone with HFD in the AdipoqCre;Snca<sup>fl/fl</sup> female mice. When animals were fed on a LFD, AdipoqCre;Snca<sup>fl/fl</sup> showed higher cortical bone mineral density compared to controls (Fig. 27i).

## 6.3. Metabolic Cages Activity Analysis, Glucose Tolerance Test (GTT) and Insulin Tolerance Test (ITT)

Similarly to our previous HFD DiO, we analyzed if AdipoqCre;Snca<sup>fl/fl</sup> mice model would also show alterations in their glucose and insulin response. Although we did not find significant differences in the AUC analysis for the GTT (Fig. 28a), we observed that mutant mice were slightly more sensitive at either LFD or HFD than controls and significantly more insulin sensitive at both diets (Fig. 28b).

Mutants had significantly lower active respiratory quotient compared to controls (Fig. 28d) during the day, suggesting that mutants can be using more fats as energy source than controls, during a LFD. However, mice of both genotypes had an active respiratory

quotient of  $\sim 0.7$  when fed on a HFD, suggesting that under those circumstances, they both turned to higher usage of fat as an energy source. Mutants on LFD during the night cycle had lower (although not significant) active energy expenditure (Fig. 28e), and significantly increase it when they were fed on a fat rich diet. There were no significant differences between the groups in resting energy expenditure (Fig. 28f), however, there was a significant increase in total energy expenditure in the mutants when we compared the mutants fed on a LFD and HFD, not seen in the controls (Fig. 28g). These results could possibly explain the “resistance” shown by the mutants to gain weight under HFD. Typically, mice on HFD tend to decrease their activity compared to LFD. Our results show that *AdipoqCre;Snca<sup>fl/fl</sup>* mice remained active; they ran significantly more than controls during the night and under HFD, they walked significantly more than control under LFD and stayed less time still than controls, under HFD during the day (Fig. 28h-k).

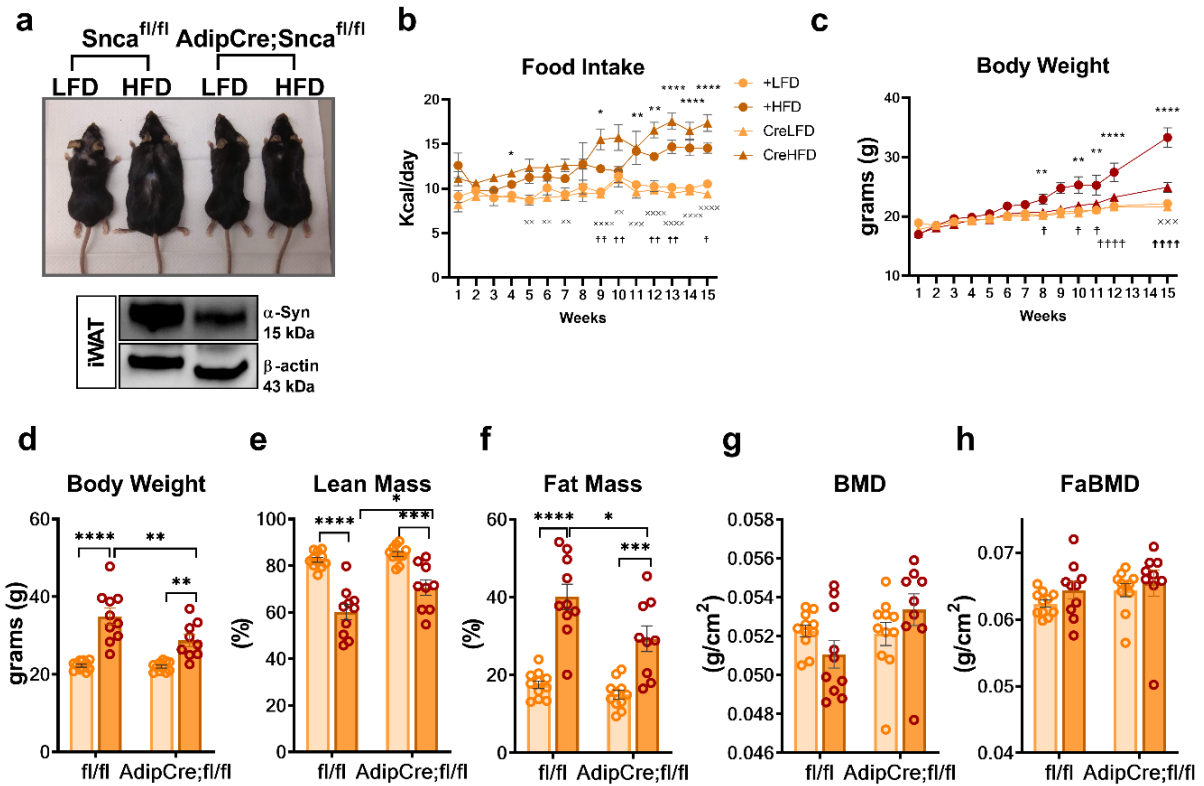


Figure 25. AdipoqCre;Snca<sup>fl/fl</sup> female mice had a reduced body weight gain and fat mass accrual after diet-induced obesity.

AdipoqCre;Snca<sup>fl/fl</sup> female and male mice were challenged with low fat diet (10% fat, LFD, light red/blue bars) or high fat diet (60% fat, HFD, dark red/blue bars) for 15 weeks. (a) Representative image of differences in size at the end point of the study. Bottom, western blot against  $\alpha$ -Synuclein in total lysates from mutant and control iWAT. (b) Caloric intake and (c) body weight was measured for thought the study and (d) at the endpoint. Body composition was measured at the end point with a Lunar PIXImus Densitometer, including total (e) % lean mass and (f) % fat mass, total (g) bone mineral density (BMD) and (h) femoral bone mineral density (FaBMD). Measurements for each genotype were represented by scatter plot and mean  $\pm$  standard error. Two-way ANOVA and post-hoc Tukey test, \* $p < 0.05$ , \*\* $p < 0.01$ , \*\*\* $p < 0.001$ , \*\*\*\* $p < 0.0001$ .

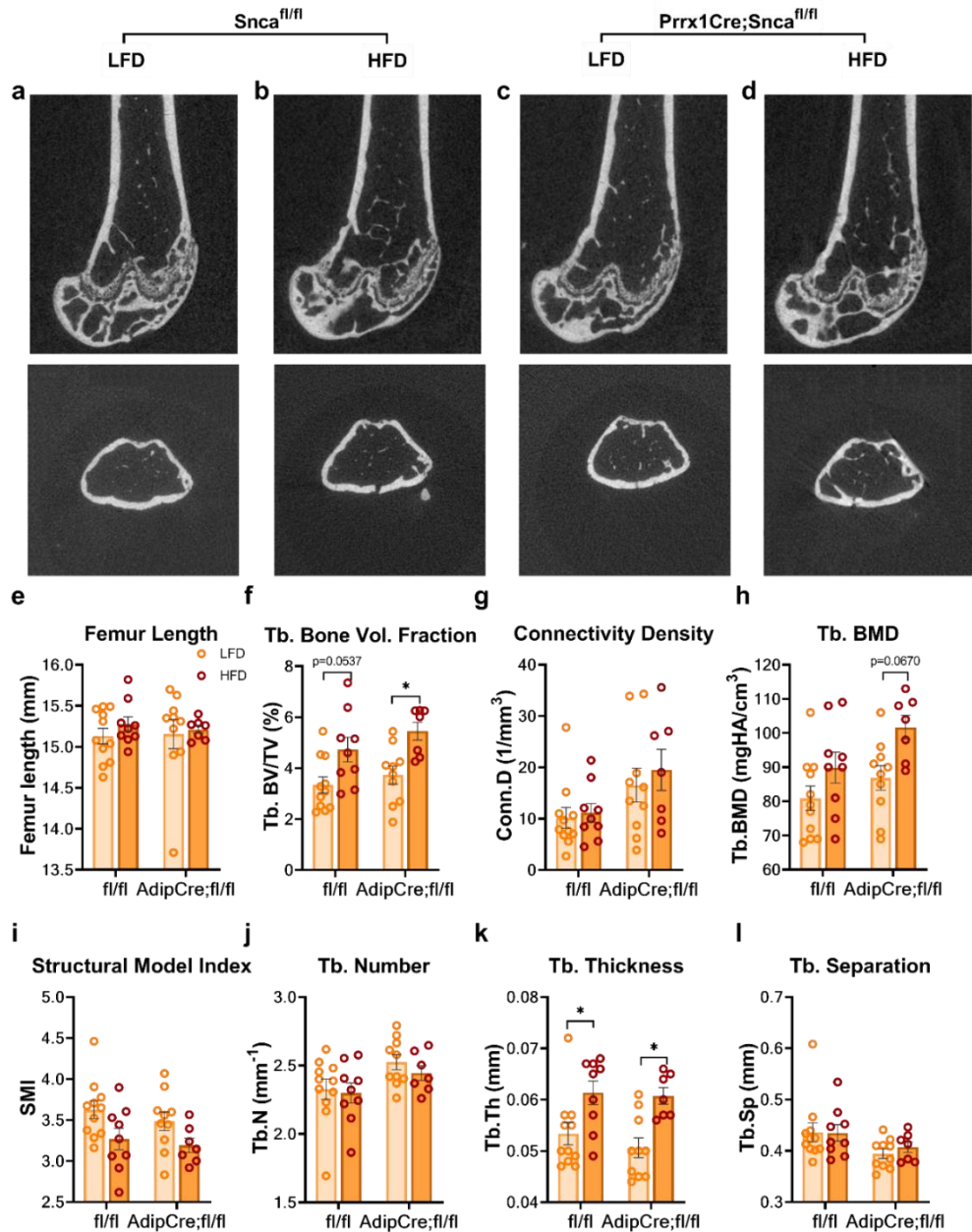


Figure 26. AdipoqCre;Snca<sup>fl/fl</sup> female mice showed a mild improvement in trabecular bone microarchitecture after treatment with HFD.

Representative images of distal femur microarchitecture examined in (a, b) female controls (Snca<sup>fl/fl</sup>) and (c, d) Prrx1Cre;Snca<sup>fl/fl</sup> mice after 15 weeks of HFD. (a, c) mice at low fat diet (LFD, pink bar) and (b, d) high fat diet (HFD, red bar). (e) Femur total length, (f) trabecular (Tb.) bone volume fraction (BV/TV), (g) connectivity density (ConnD.), (h) tb bone mineral density, (i) structural model index (SMI) (j) number (N), (k) thickness (Th), (l) separation (Sp) were measured by  $\mu$ CT. Data is represented by scatter plot and mean  $\pm$  standard error. Two-way ANOVA and post-hoc Tukey test, \* $p < 0.05$ .

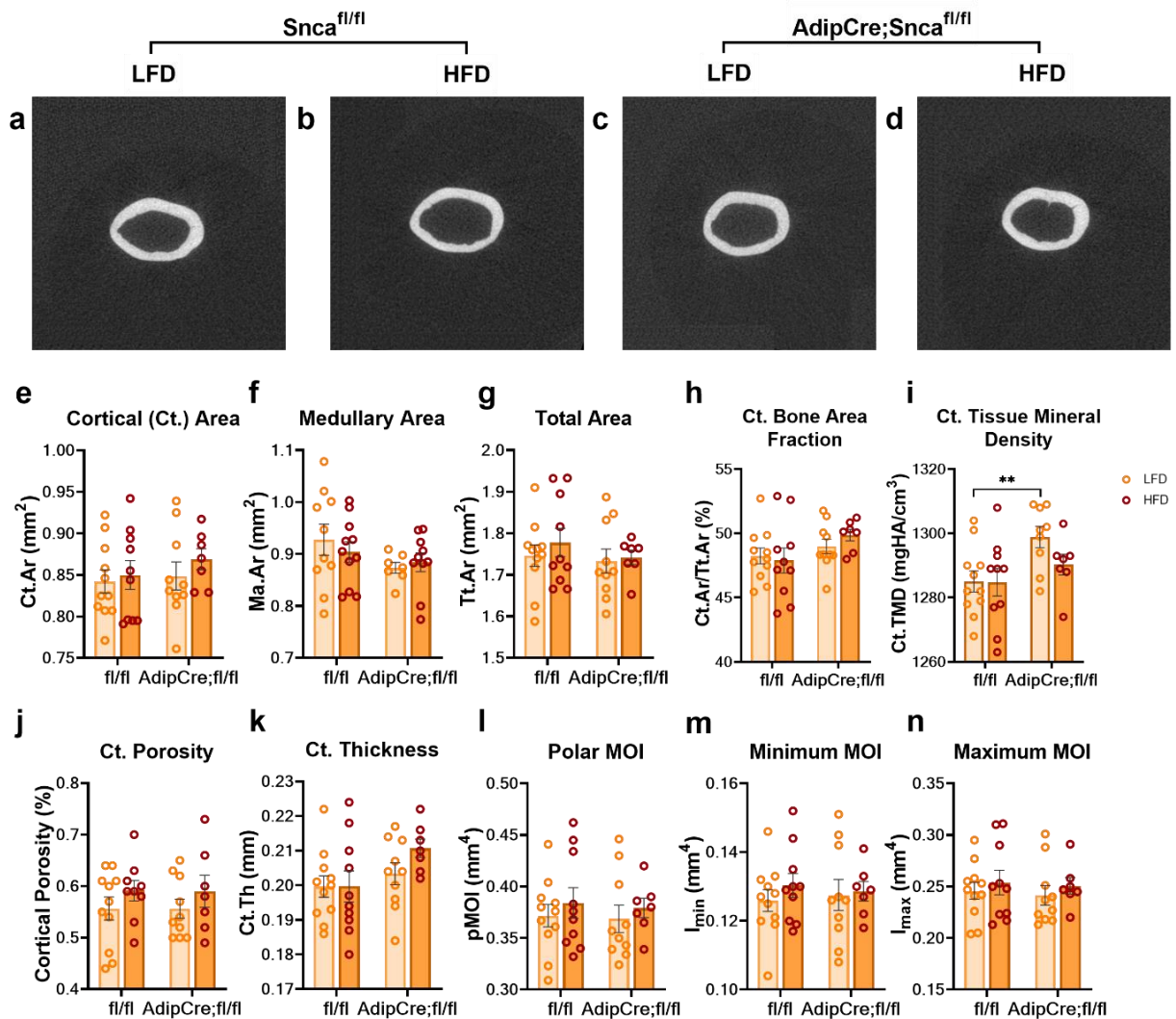


Figure 27. Adipoq Cre;Snca<sup>fl/fl</sup> female mice showed no differences in cortical bone microarchitecture compared to control after HFD treatment.

Representative images of cortical femur microarchitecture examined in (a, b) controls (Snca<sup>fl/fl</sup>) and (c, d) AdipoqCre;Snca<sup>fl/fl</sup> mice after 15 weeks of HFD. (a, c) mice at low fat diet (LFD, light brown) and (b, d) high fat diet (HFD, dark brown). (e) Cortical (Ct) area, (f) medullar (marrow) area, (g) total cortical area, (h) cortical bone fraction, (i) cortical mineral density, (j) cortical thickness, (k) porosity %, (l) polar moment of inertia, (m) minimum and (n) maximum moment of inertia were measured by  $\mu$ CT. Data is represented by scatter plot and mean  $\pm$  standard error. Two-way ANOVA and post-hoc Tukey test, \*p<0.05.

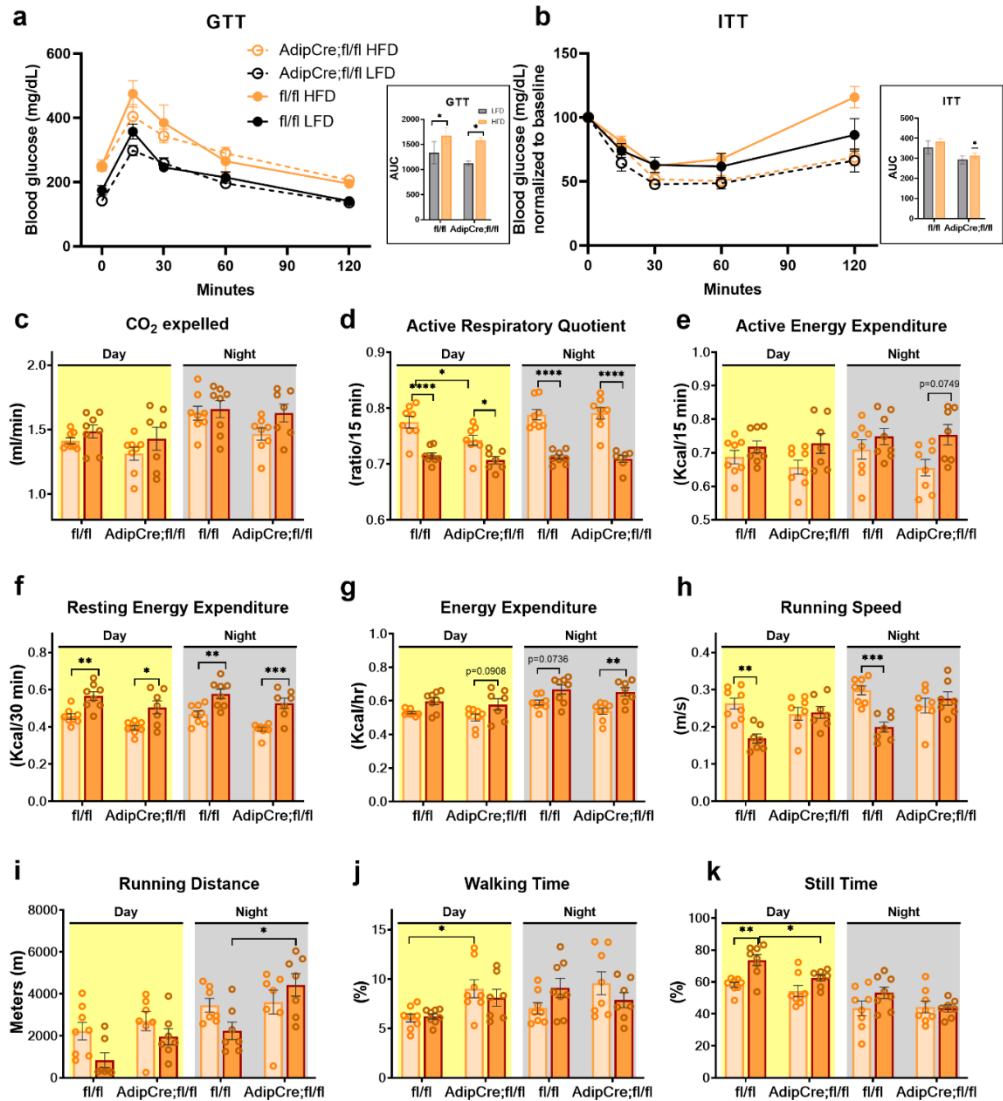


Figure 28. AdipoqCre;Snca<sup>fl/fl</sup> female mice had improved insulin sensitivity and higher activity levels.

(a) Glucose tolerance test (GTT) and (b) Insulin tolerance test (ITT) were performed at the end point of the HFD treatment and analyzed the area under the curve to determine statistical differences. Metabolic analysis included measurements of (c) CO<sub>2</sub> expelled, (d) active respiratory quotient, (e) active energy expenditure, (f) resting energy expenditure, (g) energy expenditure (h) running speed, (i) distance, (j) walking time and (k) still time. Values for each genotype are represented by scatter plot and mean ± standard error. Two-way ANOVA and post-hoc Tukey test, \*p<0.05, \*\*p<0.01, \*\*\*p<0.001, \*\*\*\*p<0.0001.

#### 6.4. Histological Analysis of Inguinal Adipose Tissue after HFD study

Inguinal white adipose tissue (iWAT) from mutant mice were significantly smaller than controls when they were both fed on HFD (Fig. 29 a). Preadipocytes isolated from mutant iWATs showed significantly less adipogenic capacity as shown by Oil Red O staining quantification (Fig. 29b, c). Thus, we think  $\alpha$ -Synuclein is fundamental for adipocyte function, either mediating commitment establishment or fatty acid storage.

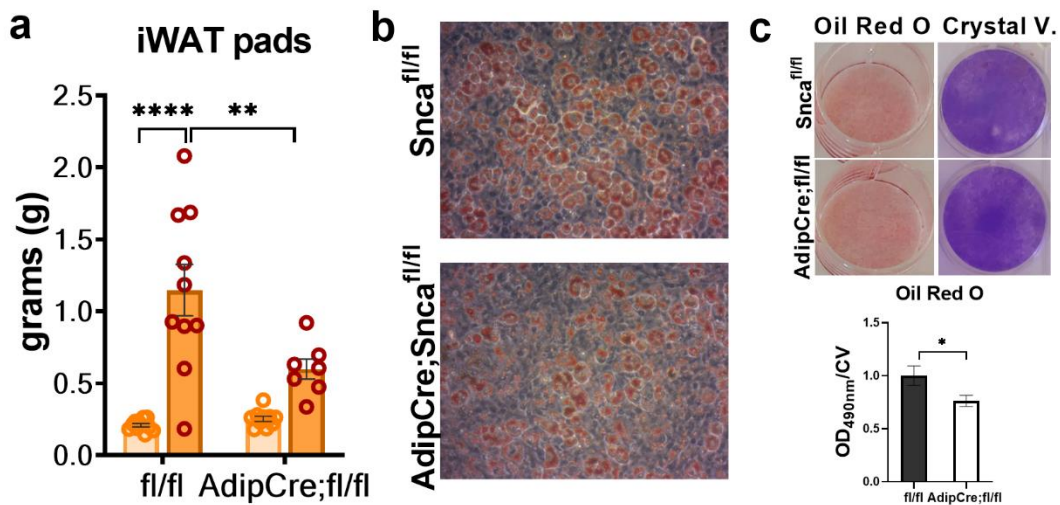


Figure 29. AdipoqCre; $Snc\alpha^{fl/fl}$  female iWATs showed an impaired adipogenic capacity. (a) Quantification of iWAT pads at the endpoint of the HFD study. (b) Representative images of *in vitro* culture of preadipocytes isolated from iWAT from mutants and control mice. Stromal vascular fraction (SVF) from iWAT was isolated and induced adipogenic differentiation and, were stained at day 8 with (c) Oil Red O (ORO) and crystal violet (CV). ORO staining was measured spectrophotometrically at OD= 490 nm and normalized by CV absorbance at 650 nm. For (a), Two-way ANOVA and post-hoc Tukey test, \*p<0.05, \*\*p<0.01, \*\*\*p<0.001, \*\*\*\*p<0.0001. For (c), T test, \*p<0.05.

## 6.5. AdipoqCre;Snca<sup>fl/fl</sup> Male Mice showed No Differences in Serum Catecholamines Compared to Control Mice

As we observed previously, Prrx1Cre;Snca<sup>fl/fl</sup> male mice showed altered levels of catecholamines that we attributed to Prrx1Cre off-target expression in the CNS. Here, in order to test whether our mice model AdipoqCre;Snca<sup>fl/fl</sup> was showing impaired sympathetic function, we measured catecholamines in serum at the endpoint of the HFD. Our results showed no significant difference for any of the three – epinephrine, norepinephrine, or dopamine- between the genotypes at any of the diets (Fig.30).

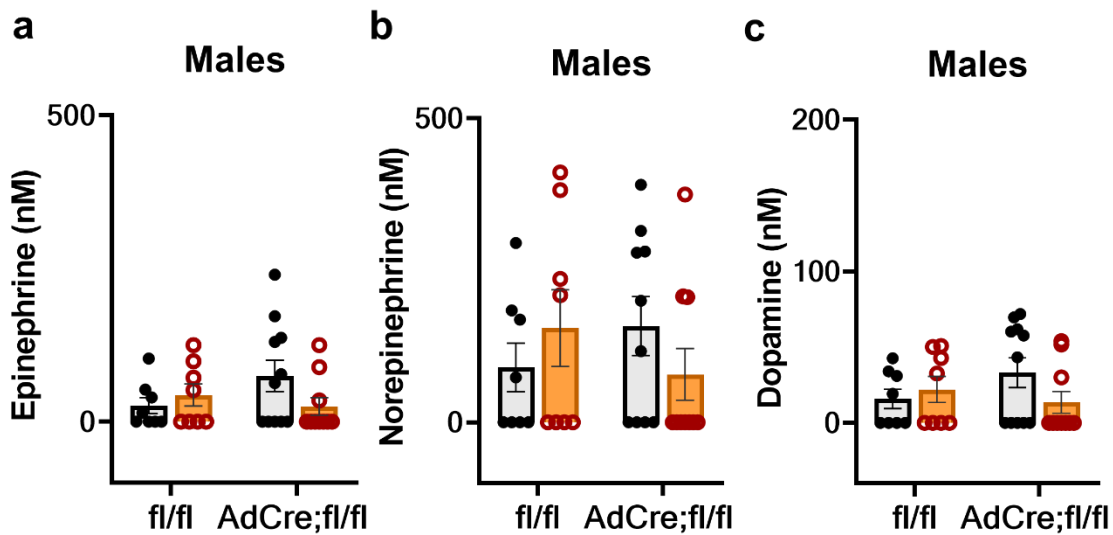


Figure 30. AdipoqCre;Snca<sup>fl/fl</sup> male mice showed no significant differences in catecholamines serum level compared to control mice.

Male mice from both genotypes were on a low fat diet (10%, black dots) and high fat diet (60%, red circles) for 15 weeks. Catecholamines levels were measured from serological samples at the end point (23 weeks old). (a) Epinephrine, (b) Norepinephrine and (c) Dopamine levels in males. Each genotype is represented by scatter plot and mean  $\pm$  standard error (black filled circles, LFD and brown circles, HFD). Two-way ANOVA and post-hoc Tukey test, \* $p < 0.05$ .

## CHAPTER 7

### IN VITRO STUDIES IN PRIMARY CULTURE OF LOSS AND GAIN OF FUNCTION

To better understand  $\alpha$ -Synuclein role in adipocyte function we added a few strains of mice to use in adipocyte primary culture and compare to our previous *in vitro* data. First, we crossed Sox-2 Cre enhancer to *Snca*<sup>fl/fl</sup> until we obtained litters with a null deletion of *Snca* and littermate controls. Second, we obtained a strain overexpression human mutant *Snca*. These homozygous mice expressed the endogenous mouse  $\alpha$ -Synuclein and overexpressed A53T missense mutation for the human *Snca* gene under the expression of the prion (*Prnp*) promotor (A53T*Snca*).

#### 7.1. Differentiation in Preadipocytes from Inguinal Adipose Tissue from *Snca*<sup>-/-</sup> Mice and A53T<sup>tg/tg</sup>

We isolated the preadipocytes from iWATs from both genotypes, and after 8 days of adipogenic differentiation, cells were fixed and stained. Oil Red O staining quantification (Fig. 31 a,b) showed that total deletion of *Snca* leads to a significant decrease in adipogenic differentiation, while A53T *Snca* showed a significantly higher adipogenic capacity.

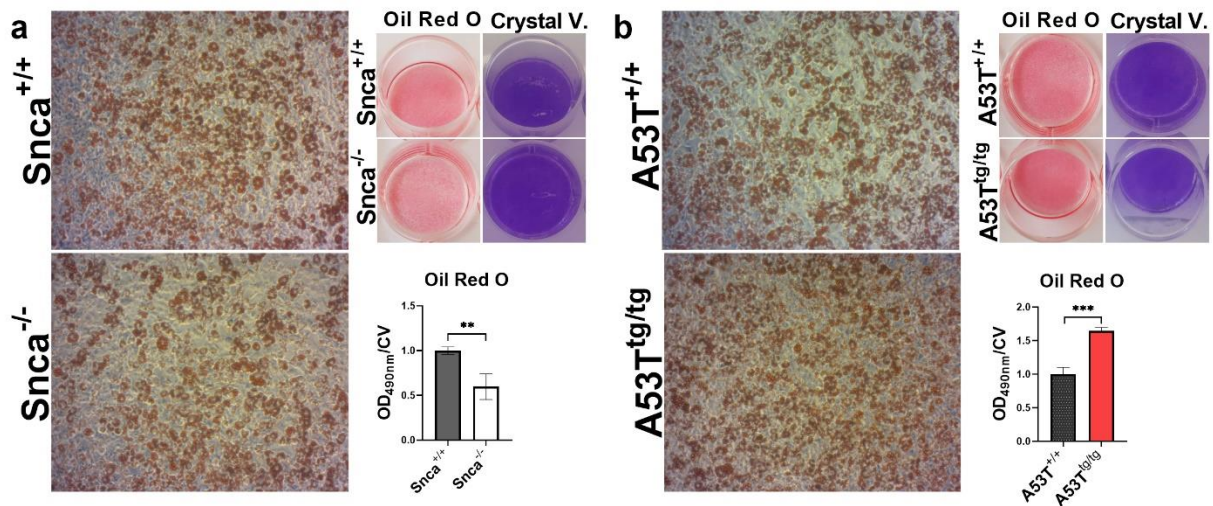


Figure 31. iWAT preadipocytes from null  $Snca^{-/-}$  mice and  $A53T^{tg/tg}$  showed an opposite adipogenic phenotype.

Representative images of *in vitro* culture of preadipocytes isolated from iWAT from (a) null mice for  $Snca^{-/-}$  and control  $Snca^{+/+}$ , (b) overexpressing A53T  $\alpha$ Synuclein mice after 8 days of adipogenic induction. ORO staining was measured spectrophotometrically at OD= 490 nm and normalized by CV absorbance at 650 nm. T test, \* $p < 0.05$ , \*\* $p < 0.01$ , \*\*\* $p < 0.001$ , \*\*\*\* $p < 0.0001$ .

## 7.2. Lipid Droplet in Preadipocytes from Inguinal Adipose Tissue from $Snca^{-/-}$ mice and $A53T^{tg/tg}$

As  $\alpha$ -Synuclein has been associated to lipid storage in neuronal models. We fixed preadipocytes after adipogenic differentiation and immunostained against Perilipin A (PLIN), found in lipid droplet membrane, quantified the size and number of lipid droplets in each phenotype. We found that  $AdipoCre;Snca^{fl/fl}$ , had lower lipid droplet number per cell and increased expression of phosphorylated Hormone Sensitive Lipase (pHSL) to total protein ratio. No changes in lipid droplet size or number were found in  $A53T^{tg/tg}$  adipocytes (Fig. 32).

### 7.3. Mitochondria Morphology in Preadipocytes from Inguinal Adipose Tissue from *Snca*<sup>-/-</sup> Mice and A53T<sup>tg/tg</sup>

PD has been associated with aberrant mitochondrial function. We fixed preadipocytes after adipogenic differentiation and immunostained against  $\alpha$ -Synuclein and co-stained mitochondria with MitoTracker. We found that *AdipoCre;Snca*<sup>fl/fl</sup>, had smaller fragments of mitochondria compared to control (Fig. 33a,b,c), but lower pDRP1S616/pDRP1637 (Fig. 33g) ratio than controls, suggesting inhibition of fission. A53T<sup>tg/tg</sup> adipocytes showed increased mitochondria fragment size (Fig. 33e, f, d), and coherently we observed decreased in pDRP1 (S616) levels (Fig. 33g), indicative of decreased mitochondrial fission.

### 7.4. Differential Subcellular Localization of $\alpha$ -Synuclein in iWAT Preadipocytes from *AdipoCre;Snca*<sup>fl/fl</sup> and A53T<sup>tg/tg</sup> mice

As  $\alpha$ -Synuclein has been shown to interact and even, be located within the mitochondria, we analyzed if partial deletion or overexpression of mutated protein would change its localization towards mitochondria. In control cells,  $\alpha$ -Synuclein significantly colocalizes to mitochondria (60%,  $p < 0.05$  compared to random distribution, percentages are values normalized by the amount of protein), however it does not seem to significantly change its distribution in partial absence of the protein (Fig. 34a, b, c) or in overexpressing mutant  $\alpha$ -Synuclein adipocytes (Fig. 34e, f, g).

As one of the most striking and consistent finding of our work was that our mice with partially loss of  $\alpha$ -Synuclein had significant alterations in the insulin sensitivity, we further

investigated if this phenotype could be a recapitulation of an aberrant insulin signaling, at a cellular level. Thus, we treated our preadipocytes with 2  $\mu$ M of insulin for 48 h before the endpoint of adipogenic differentiation.  $\alpha$ -Synuclein in control adipocytes seems to be evenly distributed in the cytoplasm and nuclei in vehicle conditions, however, it significantly changed its location to the nuclei after insulin treatment (Fig. 35g). Similar response we observed in A53T<sup>+/+</sup> control but A53T<sup>tg/tg</sup> does seem to be translocating protein to the nuclei, compared to controls (Fig. 35h). These results showed that  $\alpha$ -Synuclein can respond to insulin and can translocate to the nuclei under normal conditions.

#### 7.5. Insulin Signaling in Preadipocytes from AdipoCre;Snca<sup>fl/fl</sup> and A53T<sup>tg/tg</sup> mice

Immunoblots from total iWATs lysates from AdipoCre;Snca<sup>fl/fl</sup>, showed decreased pAKT and AKT levels (Fig. 36b,c) and increased in pAKT and total AKT in overexpressing A53T  $\alpha$ -Synuclein compared to controls (Fig. 36b, d). Snca<sup>-/-</sup> null preadipocytes showed the highest levels of total AKT and the lowest levels for pAKT (Fig. 36b, e), along with and increased in pIR $\beta$  and pShc (Fig. 36f, g, h). These results suggest that normal  $\alpha$ -Synuclein is necessary for an adequate insulin signaling in the adipocyte and that  $\alpha$ -Synuclein may be required in the nuclei to exert its regulatory role in the insulin response.

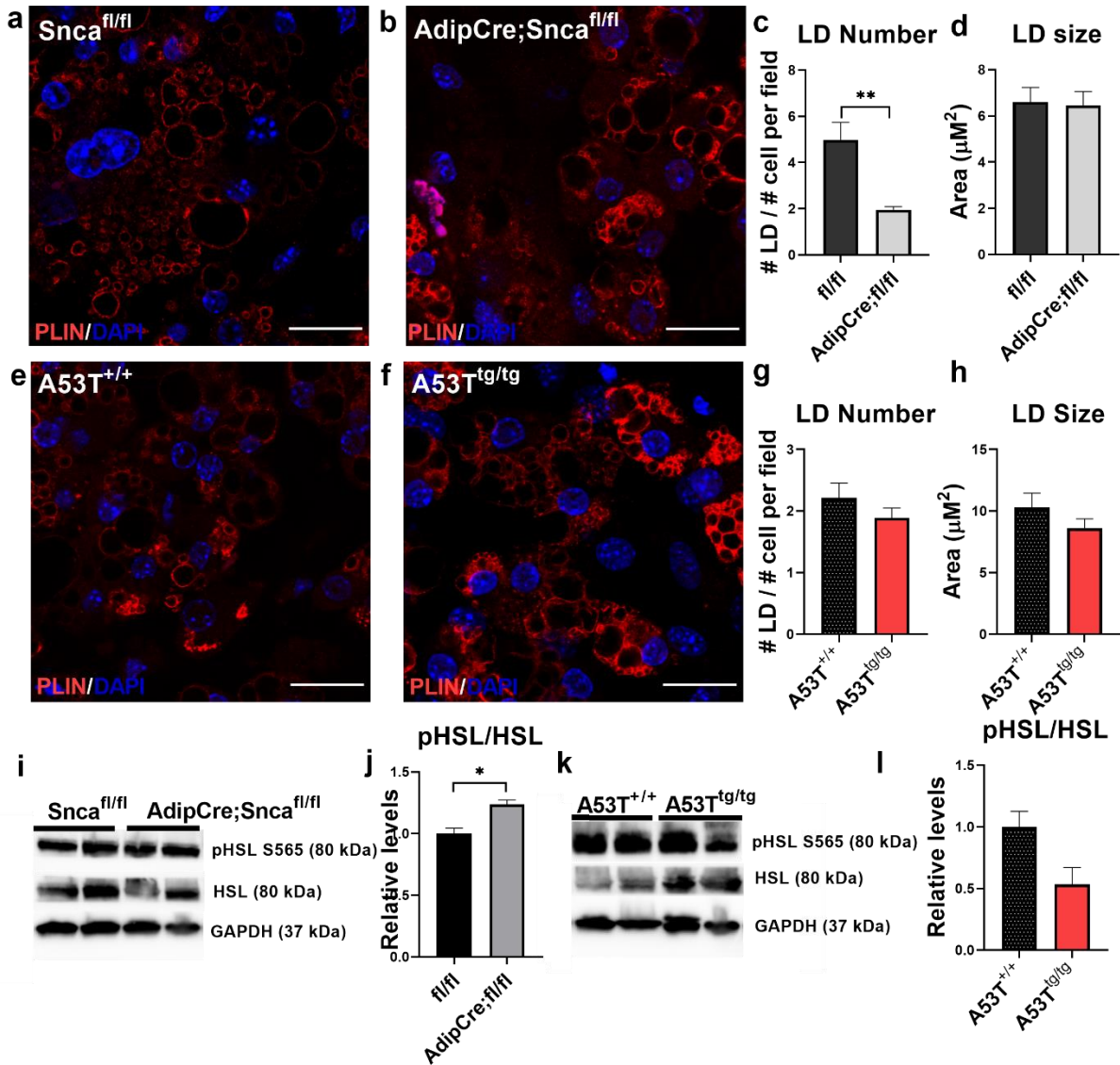


Figure 32. iWAT preadipocytes from *AdipoCre;Snca*<sup>fl/fl</sup> mice showed decreased lipid droplet formation and high expression of lipolytic marker.

Representative images of immunofluorescence against Perilipin A (PLIN) from *in vitro* culture of preadipocytes isolated from iWAT from (b) *AdipoCre;Snca*<sup>fl/fl</sup>, (a) control mice, (f) overexpressing A53T  $\alpha$ Synuclein or (e) control mice after 8 days of adipogenesis. Quantification of (c, g) lipid droplet number normalized per number of cells, (d, h) lipid droplet size for the different genotypes. Western blot analysis for (i, k) phosphorylated hormone sensitive lipase (pHSL), total HSL and GAPDH. (j, l) Quantifications of the intensity band and pHSL/HSL ratios. T test, \* $p < 0.05$ . Scale bar 20  $\mu$ M.

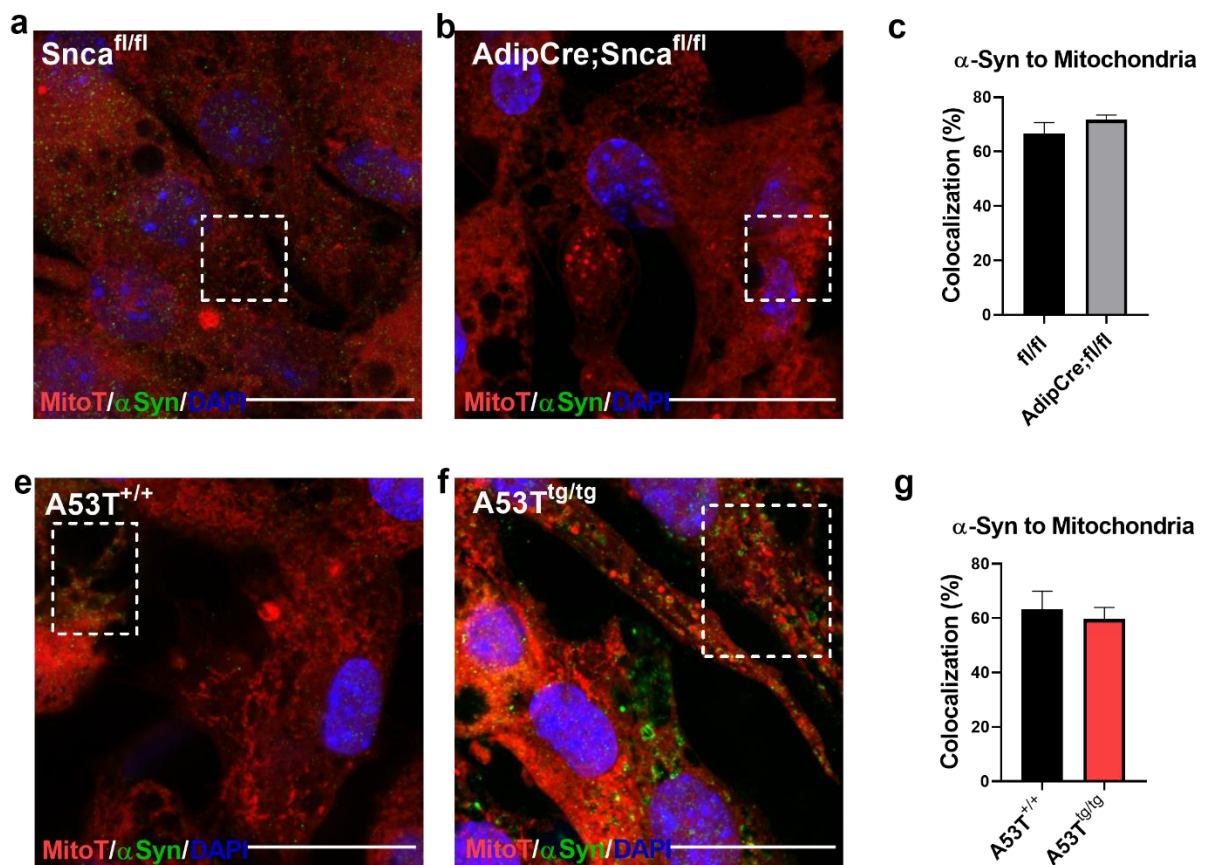


Figure 33. Differential expression of  $\alpha$ -Synuclein in iWAT preadipocytes from AdipoCre; $Snca^{fl/fl}$  and A53T<sup>tg/tg</sup> mice does not alter its location relative to mitochondria. Representative images of immunofluorescence against  $\alpha$ -Synuclein ( $\alpha$ Syn, in green) from *in vitro* culture of preadipocytes isolated from iWAT from (b) AdipoCre; $Snca^{fl/fl}$ , (a) control mice, (f) overexpressing A53T  $\alpha$ -Synuclein or (e) control mice after 8 days of adipogenesis and co-staining with the mitochondrial marker, MitoTracker. Quantification of (c, g) percentage of colocalization of  $\alpha$ -Synuclein to mitochondria for each genotype. T test, \* $p < 0.05$ . Scale bar 20 $\mu$ M.

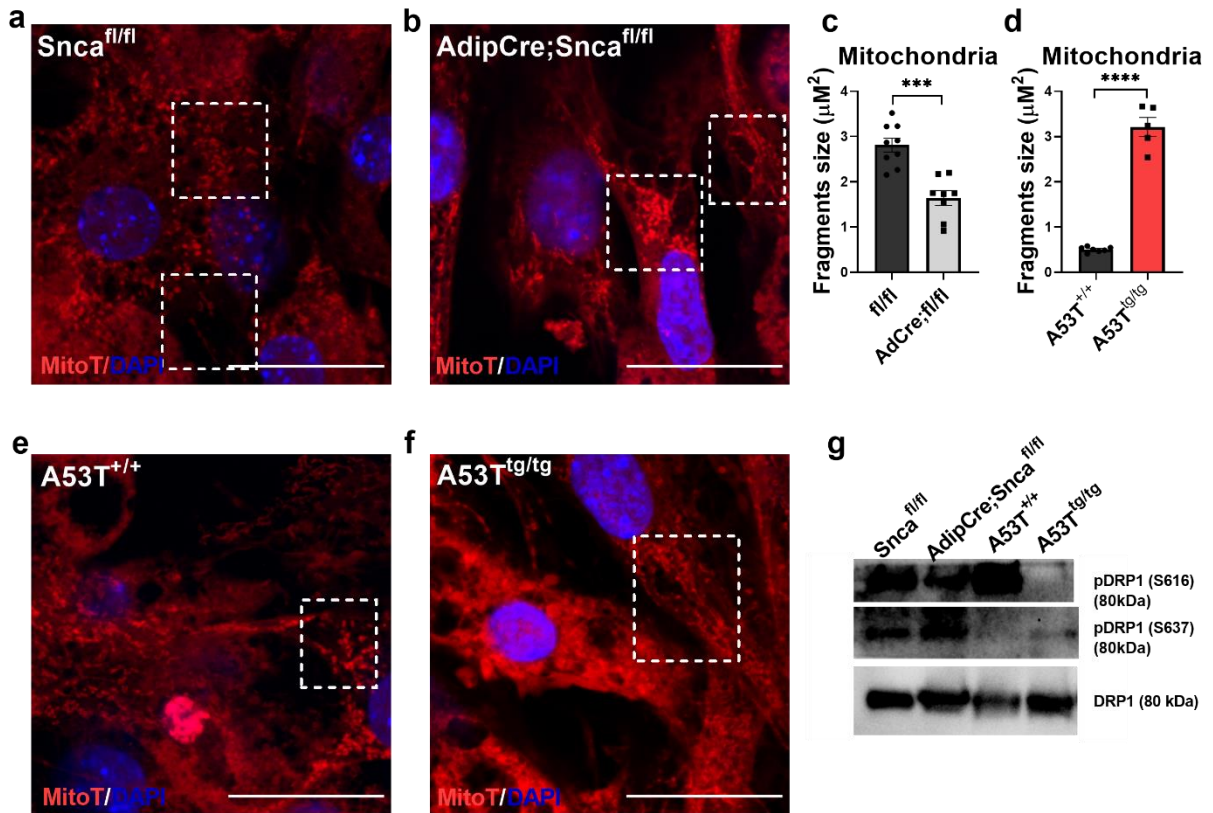


Figure 34. iWAT preadipocytes from *AdipoCre;Snca*<sup>fl/fl</sup> and *A53T*<sup>tg/tg</sup> showed opposite mitochondrial phenotype.

Representative images of *in vitro* culture of preadipocytes isolated from iWAT from (b) *AdipoCre;Snca*<sup>fl/fl</sup>, (a) control mice, (f) overexpressing A53T  $\alpha$ Synuclein or (e) control mice after 8 days of adipogenesis, after incubation with the mitochondrial staining, Mitotracker (Red). Quantification of (c, d) mitochondrial fragment size for the different genotypes. Western blot analysis for (g) pDRP1 (S616), pDRP1 (S637) and total DRP1. \**p*<0.05, \*\**p*<0.01, \*\*\**p*<0.001, \*\*\*\**p*<0.0001. Scale bar 20μM.

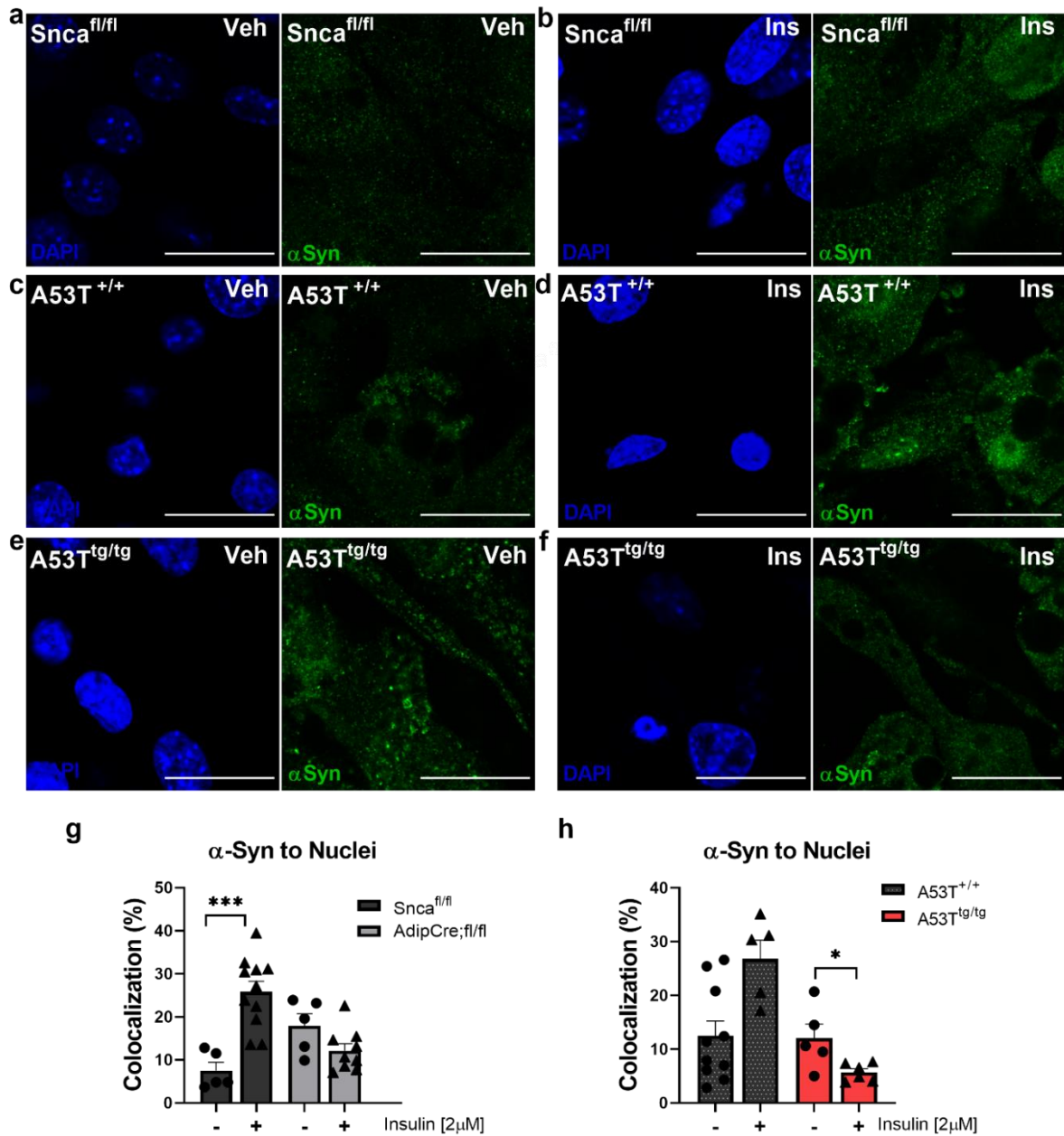


Figure 35.  $\alpha$ -Synuclein relocates to the nuclei after insulin treatment in control preadipocytes but not in A53T<sup>tg/tg</sup> preadipocytes.

Representative images of immunofluorescence against  $\alpha$ -Synuclein ( $\alpha$ Syn, in green) from *in vitro* culture of preadipocytes isolated from iWAT from control mice with (a, c) vehicle or (b, d) insulin treatment, overexpressing A53T  $\alpha$ Synuclein under (e) vehicle or (f) insulin treatment [2 $\mu$ M] at day 6 for 48 h. Quantification of (g, h) percentage of colocalization of  $\alpha$ -Synuclein to the nuclei for each genotype. T test, \* $p$ <0.05. Scale bar 20 $\mu$ M.

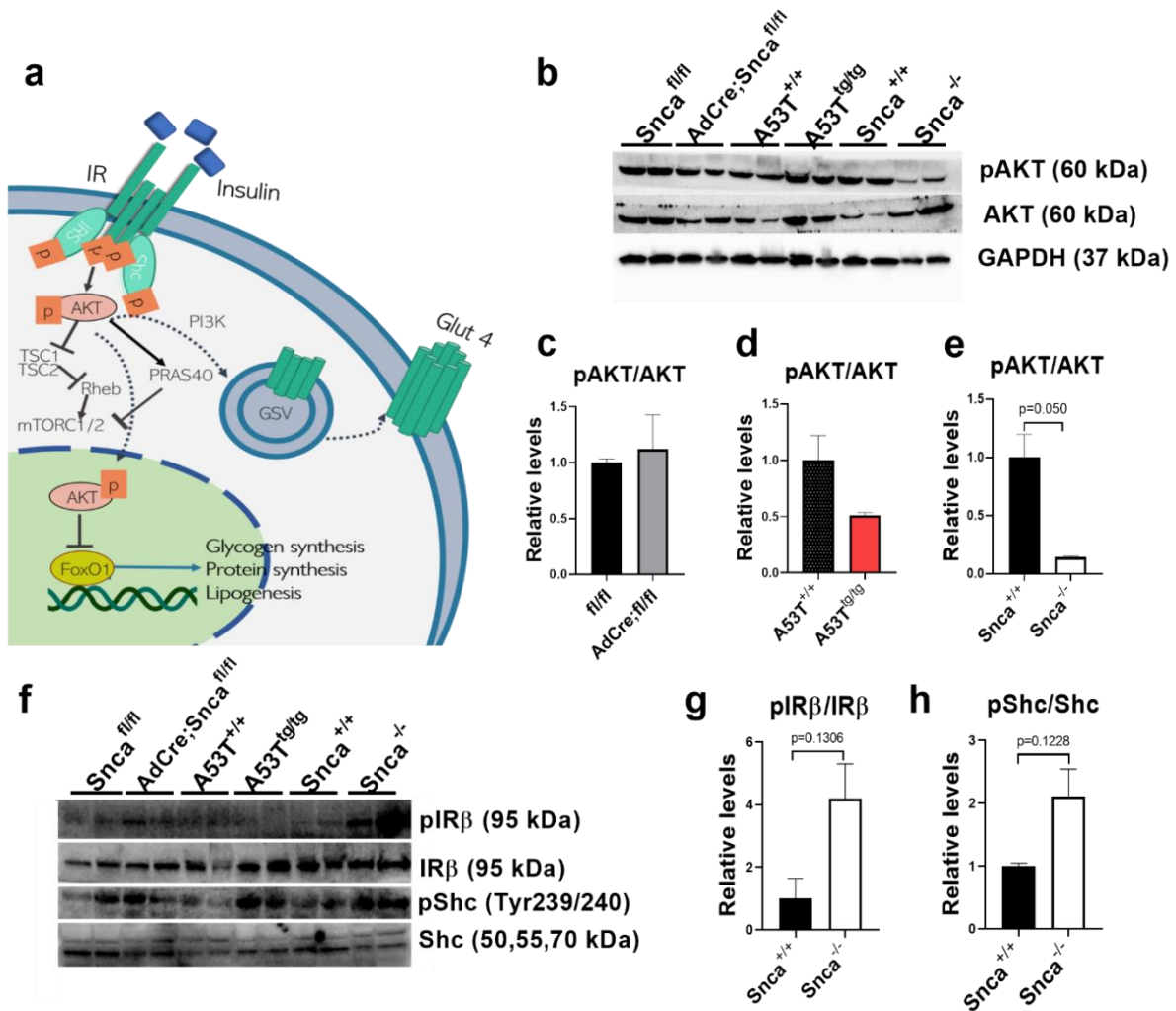


Figure 36. Differential levels of  $\alpha$ -Synuclein induces changes in insulin signaling through AKT.

(a) Scheme of insulin signaling. (b) Immunoblot from total iWATs lysates against pAKT, AKT, GAPDH, (f) pIR $\beta$ , IR $\beta$ , pShc and Shc and band quantification for (c) AdipoCre;Snca<sup>fl/fl</sup>, (d) overexpressing A53T  $\alpha$ Synuclein and (e, g, h) Snca<sup>-/-</sup> null, and respective controls. T test, \*p<0.05.

## CHAPTER 8

### DISCUSSION

#### 8.1. Discussion of the Effects of Deletion of $\alpha$ -Synuclein in Osteoprogenitor Cells

*Prrx1* (paired related homeobox 1) is expressed in the undifferentiated mesenchyme of the craniofacial and appendicular skeleton as well as the inguinal depots [109], and its loss of function in mice leads to defective growth of osteoprogenitor and severe limb abnormalities [109]. Our initial observations that *Snca* could be one of those target genes regulating remodeling led us to use the *PrrxCre* in ovariectomy experiments [110]. Importantly, this provided a link between *Snca* and bone turnover. *Snca* has been strongly implicated in the pathology of neurodegenerative disorders, especially PD, largely by forming molecular aggregates that impair the dopaminergic system [111, 112, 113]. Intriguingly, PD patients also exhibit non-neurological comorbidities such as sarcopenia, low bone mineral density and a much higher risk of fractures than age-matched control [114, 115, 116].

Here, we showed that partial deletion of  $\alpha$ -Synuclein in osteoprogenitors neither protects against estrogen deficiency-induced bone loss nor counters the effects of obesity. Even though  $\alpha$ -Synuclein seems to be playing a relevant role in the stress response in the bone marrow and bone, its partial absence does not explain the effects seeing in the *Snca*<sup>-/-</sup> null mice. We attribute the mild changes in bone microarchitecture (increase in trabecular bone volume fraction (Fig. 12f) and trabecular thickness (Fig. 12k) after fed with a HFD) to the indirect effects of higher lean and fat mass that in some

cases act as a mechanical stimulus to build bone after HFD. However, with dramatic loss of lean mass but associated fat mass gain, this may lead to lower bone mass and in humans, osteoporosis.

Moreover, as we discuss on the next section, we cannot discard alterations in the sympathetic tone as consequence of off target effects of Prrx1Cre in the CNS.

## 8.2. Discussion of the Implications of using Prrx1Cre as Enhancer to Target Deletion in the Skeletal Limb

The Prrx1Cre recombinase mouse is used in studies to test the function of skeletal genes *in vivo* by employing conditional genetic engineering. The current work provides new evidence supporting earlier, but often not recognized studies, that Prrx1Cre is expressed in adult brains.

There have been a few previous reports indicating that *Prrx1* is expressed early in the prenatal brain at E16.5 [117], and also in neural progenitor cells from the pituitary gland, forebrain and hippocampus [118, 103]. However, virtually all papers employing conditional deletion of skeletal and progenitor genes using the Prrx1 Cre driver failed to report on neural expression of the Cre transgene. In this study, we showed that *Prrx1* transcripts were present in several regions of the brain, leading to decreased *Snca* transcript levels and partial protein loss of  $\alpha$ -Synuclein in the frontal-motor area of the cortex (Ctx1), striatum and pons/medulla/brainstem. We noted that the Prrx1Cre;*Snca*<sup>fl/fl</sup>

mice exhibited impaired trabecular and cortical bone microarchitecture after OVX to the same extent as that observed in *Snca*<sup>fl/fl</sup> control mice. Therefore, protection against estrogen deficiency-induced bone loss observed in the global *Snca* knockout mice was neither regulated through osteoprogenitors nor by *Prrx1*Cre(+) *Snca*(+) cells in the CNS. However, it is worth noting that ovariectomies were done at 8 weeks of age, as reported previously in a number of protocols [119]. Ovariectomy in older mice might have demonstrated a different response although it would likely have been confounded by age-related trabecular bone loss which occurs in female C57BL6 mice after 16 weeks of age.

Due to the marked non-skeletal expression changes from the conditional deletion, we performed comprehensive metabolic and behavioral studies of the *Prrx1*Cre;*Snca*<sup>fl/fl</sup> and *Snca*<sup>fl/fl</sup> littermate control mice. We found important differences between genotypes. For example, male *Prrx1*Cre;*Snca*<sup>fl/fl</sup> on a LFD had higher water consumption than controls, but no changes in food intake. These changes could have been associated with decreased dopamine and norepinephrine levels found in their serum. Catecholamines have an inhibitory effect on fluid intake, in rats [220] by acting through the nucleus accumbens, one of the centers involved in regulation of hunger and thirst. It has been shown that bilateral lesions of accumbens and caudate nuclei result in significant and sustained increase in water intake [221]. Dopamine injections after inducing injury in accumbens and caudate nuclei, reestablished water intake in a dose dependent manner [222]. Similarly, norepinephrine injections in the nucleus accumbens increases water intake, without changes in food intake, in rats [221], thus

indicating that catecholamines regulate water intake through osmolarity/volumetric changes of a porto-hepatic feedback rather than through  $\beta$ -adrenergic stimulation [221].

The *nucleus accumbens* is part of the striatum, within the basal ganglia, and receives glutaminergic, dopaminergic and histaminergic input fibers from different regions in the brain. We found decreased expression of  $\alpha$ -Synuclein in the striatum of mutant mice that could lead to an abnormal regulation of the thirst feedback loop and increased fluid intake. In PD,  $\alpha$ -Synuclein aggregation causes death of dopaminergic cells in *substantia nigra pars compacta*, disrupting normal nigrostriatal circuits. We postulate that partial loss of  $\alpha$ -Synuclein in the striatum and pons/medulla/brainstem (P/MY/BS) region impairs central regulatory circuits of thirst, although *Snc* transcript levels were also decreased in the hypothalamus of *Prrx1Cre;Snc<sup>fl/fl</sup>* mice, and this could affect sensibility to detect tonicity and water intake through antidiuretic hormone (ADH) secretion. Interestingly, one of the major reasons for emergency hospitalization of PD patients is profound electrolyte disturbances [223]. Serological (Pathological??) levels of sodium and chloride levels have been associated with dyskinesia in PD patients [224], and dehydration has emerged as a mortality factor in PD [225]. However, peripheral catecholamine levels do not always correlate with cerebrospinal fluid (CSF) levels although there is evidence indicating that PD patients show lower CSF and serum levels of dopamine and norepinephrine, and that the decreased CSF dopamine level observed in PD can cross the blood brain barrier [226].

Low levels of epinephrine and norepinephrine can also result in physical and neural symptoms such as anxiety. PD patients often present with psychiatric symptoms (~60%), including signs of anxiety, depression (17-50%) and psychosis. Our data suggests that *Prrx1Cre;Snca<sup>fl/fl</sup>* male mice have an altered behavioral and activity phenotype that could be explained by lower levels of dopamine and norepinephrine in blood, and abnormal  $\alpha$ -Synuclein in key brain regions such as striatum, brainstem and hypothalamus. Locomotor control is attributed to the activity of ascending dopaminergic projections from the *substantia nigra* to the striatum within the basal ganglia, which projects to the mesencephalic locomotor region of the brainstem controlling locomotion. It was recently found that dopaminergic neurons can also innervate the mesencephalic locomotor region through descending inputs to control locomotion [227]. Therefore, slight changes in  $\alpha$ -Synuclein in these neurons could translate into dramatic changes in locomotor/activity pattern in mice.

Our physical-behavioral activity experiments showed that control animals, when switched from LFD to HFD, did not show any diet effects on the EPM; however, they decreased their distance traveled in the central and peripheral areas on the open field test. Female and male controls were less likely to climb their tails when fed with a HFD, however no differences in immobility latency were found. Lastly, the marble burying test, which measures the propensity of mice to engage in a digging behavior, is increased in models of anxiety [228]. There was no diet effect in the number of marbles buried in control mice. Additionally, control mice fed on a HFD decreased the time, distance and speed they spent running on the wheel in the metabolic cages, compared

to control mice on LFD. These results show an anxiety-type of behavior and/or activity switch when mice were on a HFD. Mice [220] and humans [229, 230], when undergoing a HFD and overfeeding, significantly reduce acute spontaneous activity and exhibit an anxiety-like phenotype in mice [231], as obesity and diabetes in humans is associated with increased rates of anxiety and depression [232, 233].

We noted other phenotypic differences in activity between the conditional deletion of *Sncα* and their littermate controls that reinforce the function of the *Prrx1* Cre in brain. For example, *Prrx1Cre;Sncα<sup>fl/fl</sup>* male mice on HFD dramatically decreased their ambulatory activity compared to LFD and to control mice under HFD (Fig. 10b), and contrary to evidence in control mice, there was no diet effect on the spontaneous running activity (Fig. 10c-e) and in distance travelled in center and periphery (not shown) of the open field (Fig. 10h). *Prrx1Cre;Sncα<sup>fl/fl</sup>* male mice also decreased the number of entries to the open areas when fed a HFD compared to LFD, but decreased time spent in the open area in respect to controls on a HFD. There was a subtle interaction factor for the genotype by diet effect ( $p=0.0981$ ) observed in the marble burying test. *Prrx1Cre;Sncα<sup>fl/fl</sup>* male mice on LFD buried higher number of marbles than when fed on a LFD and compared to control at any of the diets. It appears that diet effects on activity differ between mutant and control mice by two type of responses: changes in the type of preferred activity (ambulatory versus non-ambulatory) and despaired (anxiety-type) behavior. In sum, the phenotypic changes we observed provide strong support that there are functional consequences by using the *Prrx1Cre* driver for genes that are expressed in the brain.

### 8.3. Discussion of the Effects of Deletion of $\alpha$ -Synuclein in Adipocytes from the Inguinal Adipose Tissue

Prrx1Cre mice were partially protected against OVX-induced weight and fat mass gain, suggesting a possible cell autonomous role for  $\alpha$ -Synuclein in adipocyte metabolism.

Our primary intention was to determine if  $\alpha$ -Synuclein regulates BMD during estrogen deficiency by intrinsic mechanisms within the osteoblasts; but we could not ignore the fact that our first mouse model to target the limb showed off-target effects in the CNS, an organ that expresses significant amounts of  $\alpha$ -Synuclein. In an attempt to prove that the adipose phenotype was due to the intrinsic effects of  $\alpha$ -Synuclein preadipocytes, we performed a set of *in vitro* experiments to induce adipogenesis and to quantify if primary culture of preadipocytes, would show a phenotype correlative to our *in vivo* data. Indeed, mutant preadipocytes had higher oxidative capacity, and their capacity to differentiate into a mature adipocyte decreased, as their fat storage capacity did, as well.

To further investigate  $\alpha$ -Synuclein's role in adipose tissue, we moved to a second mouse model, AdiponectinCre, which demonstrated that mutant mice were recapitulating the *Snca* null phenotype in terms of adipose phenotype (Fig. 26a-b). These mice had improved insulin sensitivity, opposite to what we found in the Prrx1Cre;*Snca* study and possibly suggesting that  $\alpha$ -Synuclein regulate insulin response by cell autonomously and non-cell autonomously. Altogether, we conclude that  $\alpha$ -Synuclein is necessary to regulate insulin sensitivity (Fig. 17 a-b); systemically, enhancing insulin sensitivity (i.e.,

through  $\beta$  cell stimulus for insulin secretion) and locally -within the fat cell- reducing its sensitivity.

From our *in vitro* studies we infer  $\alpha$ -Synuclein is critical for proper insulin signaling as we observed that total deletion of *Snca* leads to increased levels of AKT but decreased levels of pAKT, suggesting adipocytes increased its levels of AKT, possibly, as a compensation to the decreased pAKT levels. Overexpression of the mutated form of *Snca* leads to more availability of the pAKT and total AKT. We hypothesize that *Snca* is necessary for a proper signaling transduction from the insulin receptor (IR) to AKT. When  $\alpha$ -Synuclein is completely absent, levels of phosphorylated IR beta (pIR $\beta$ ) and pShc increased, the later also increases when mutated A53TSnca (Fig. 34). These results suggest that at some point downstream to IR $\beta$  and Shc, the signal fails to transduce, thus, normal levels of  $\alpha$ -Synuclein is necessary but not sufficient for proper signal transduction. Preliminarily, we analyzed IRS1 and IRS2 protein levels, as they are important substrates of insulin signaling. We did not observe differences in IRS1 or 2, but in the absence of *Snca*, there was a decrease in pIRS1 (S612), while in the presence of mutated A53TSnca total IRS1 is decreased (Not shown).

There is a strong connection between PD and insulin resistance (IR). A recent study showed that nearly 60% of the non-diabetic participants may have undiagnosed insulin

resistance [25]. Others have shown that dysglycemia seems to be another nonmotor feature of PD, as insulin production is regulated by the autonomic nervous system, as sympathetic denervation might lead to  $\beta$ -cell dysfunction. The progression of PD could be correlated to blood glucose dysregulation [27].

Others have also shown PD patients have impaired insulin sensitivity as their *Snca* serum levels are inversely associated to IR indicators [234]. Similarly, when we partially deleted *Snca* in the central nervous system, we observed similar effects as in PD patients; insulin resistance. One possible explanation is that normal  $\alpha$ -Synuclein levels are needed to control insulin signaling at the neurological level and for peripheral control of insulin secretion as suggested by Marques et al (2018) [27]. A study showed  $\alpha$ -Synuclein interacts with Kir6.2 (a major subunit of the ATP-sensitive K channel), on insulin secretory granules, acting to downregulate insulin secretion in pancreatic beta cells [235]. They showed in islet cell cultures overlapping localization of  $\alpha$ -Synuclein with Kir6.2, but also with Sur1 (an ATP-binding cassette protein that functions as an ion channel regulator), insulin, and C peptide.

Neurological function is dependent on glucose metabolism. Moreover, it has been shown that insulin signaling contributes significantly to normal brain function and recently had been shown to be dysregulated in neurodegenerative diseases [236, 237,

238]. Previous studies have shown an association with mitochondrial dysfunction and insulin resistance [239, 240], such as alterations of mitochondria dynamics, polarization and ROS levels in insulin resistance [241]. Overexpression  $\alpha$ -Synuclein has been associated with high levels of pAKT in dopaminergic (DA) neurons [242], IR and increased reactive oxygen species (ROS) levels, as well as mitochondrial depolarization [243].

When we deleted *Snca* solely in the white adipose tissue using the AdipoCre which is not expressed in the CNS, *Snca* expression is physiologically normal, we observed an improvement in the insulin response, suggesting that  $\alpha$ -Synuclein could be regulating insulin sensitivity by inhibition in adipose depots but activation in the CNS.

Therefore, this work shows  $\alpha$ -Synuclein has a role in energy metabolism and lipid storage, by regulating insulin responsiveness.  $\alpha$ -Synuclein responds to insulin treatment by regulating insulin sensitivity, at least to a significant extent, by mechanisms intrinsic to the adipocyte.

## CHAPTER 9

### CONCLUSIONS AND CLINICAL IMPLICATIONS

The first part of our work provides new evidence supporting earlier, but often not recognized studies, that *Prrx1Cre* is expressed in adult brains. In this case, that expression led to partial deletion of the *Snca* gene in the CNS, which resulted in aberrant catecholamine levels, altered activity patterns and anxiety-types of behavior. Taken together, our data suggest that deletion of genes that are normally expressed in the CNS using the *Prrx1 Cre* could profoundly affect a mesenchymal phenotype of interest, whether it be skeletal or adipogenic. As such it provides a further cautionary note for investigators that seek to understand early osteoprogenitor differentiation in the marrow using the *Prrx1Cre* enhancer.

PD patients are at high risk of fracture and its association with  $\alpha$ -Synuclein remains unclear. Here we showed that decreased *Snca* expression in osteoprogenitors leads to a mild bone phenotype, suggesting *Snca* might be acting coordinately through bone cells (i.e. osteoblasts, osteocytes) and bone marrow cells (i.e. osteoclasts, adipocytes or hematopoietic-derived cells) to orchestrate the protection against low bone mass, as seen in *Snca*<sup>-/-</sup> mice.

Moreover, PD patients present a high incidence of insulin resistance and Type II DM is a risk factor for PD [244]. Only recently, researchers have started to focus their efforts on understanding the association between glucose metabolism and neurodegeneration.

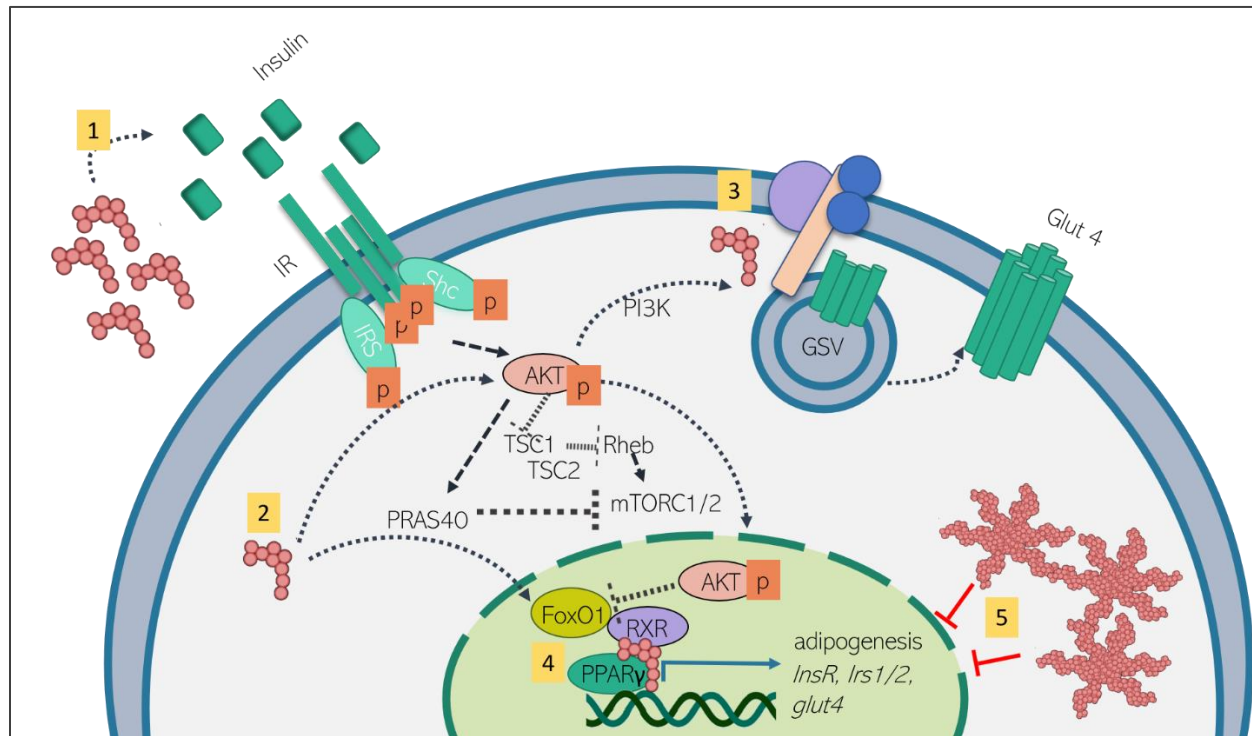


**Figure 37. Proposed Role of  $\alpha$ -Synuclein in Insulin Signaling Regulation.**

(1)  $\alpha$ -Synuclein mediate the binding of insulin to the insulin receptor (IR), (2)  $\alpha$ -Synuclein can be acting as a checkpoint by regulating AKT phosphatases or other downstream targets downstream IR. (3)  $\alpha$ -Synuclein can be found in the plasma membrane and complexed within lipid rafts to facilitate glucose transporter 4 (GLUT 4) translocation to the cell membrane. (4)  $\alpha$ -Synuclein can translocate to the nuclei and mediate gene activation/repression programming by binding to transcriptional factors. (5) A53T missense mutation in *Snca* favors aggregation and concomitantly loss of the normally functional  $\alpha$ -Synuclein.

However,  $\alpha$ -Synuclein connections to insulin response are still unclear. Here, we provided evidence that  $\alpha$ -Synuclein plays an important role in energy metabolism and insulin sensitivity by acting not only through the central nervous system but also directly in adipocytes.  $\alpha$ -Synuclein can respond to insulin stimuli and its absence leads to a

defective insulin pathway. Possible mechanisms of  $\alpha$ -Synuclein regulation of insulin response include binding to transcriptional factors to enable activation or repression of downstream targets by nuclear translocation in response to insulin exposure. Also  $\alpha$ -Synuclein could be acting in the cytoplasm as a checkpoint by regulating AKT phosphatases or other downstream targets of IR, and enabling proper protein interaction. Moreover,  $\alpha$ -Synuclein can be found in the plasma membrane and complexed within lipid rafts to facilitate GLUT 4 exocytosis and membrane translocation (Fig 37).

Our findings help to better understand the mechanisms by which  $\alpha$ -Synuclein regulates energy metabolism and insulin response. Additionally, our results contribute to an understanding of the possible mechanism that could explain the neuroprotective effects of antidiabetic drugs such as Exenatide, as recently demonstrated in a large clinical trial [245]. More studies are necessary to fully define the cellular role of  $\alpha$ -Synuclein in non-neural tissues.

## CHAPTER 10

### FUTURE DIRECTIONS

By using our *in vitro* models of loss of  $\alpha$ -Synuclein and overexpression of mutant  $\alpha$ -Synuclein we aim to further determine  $\alpha$ -Synuclein targets in the insulin pathway, particularly upstream AKT and establish if glucose transport 4 (GLUT 4) translocation or availability is impaired in any of our  $\alpha$ -Synuclein models as it occurs in diabetic patients [246].

We are particularly interested to analyze the location, possible presence of  $\alpha$ -Synuclein aggregates and lipid storage capacity, along with gene expression profile in subcutaneous fat biopsies from PD patients from the Alzheimer's Disease Center at Rush University.

We aim to metabolically phenotype A53T<sup>tg/tg</sup> mice, a clinically relevant mice model of PD, and compare it to the knock out *Snc*a<sup>-/-</sup> to better understand the role of  $\alpha$ -Synuclein in the regulation of insulin response (Supplemental grant, NIA/NIGMS).

## REFERENCES

- [1] Kinsella K, Wan H. U.S. Aging World: 2008. Census Bureau, International Population Reports, P95/09-1, An, U.S. Government Printing Office, Washington, DC, (2009).
- [2] Hiorth Y, Lode K and Larsen JP. Frequencies of falls and associated features at different stages of Parkinson's disease. *European Journal of Neurology*. 20, 160-166 (2013).
- [3] Jankovic J. Parkinson's disease: clinical features and diagnosis. *J Neurol Neurosurg Psychiatry*. 79, 368-376 (2008).
- [4] Chen H, Zhang S, Hernan M, et al. Weight loss in Parkinson's disease. *Ann Neurol*. 53, 676-679 (2003).
- [5] Bosco D, Plastino M, Cristiano D, et al. Dementia is associated with insulin resistance in patients with Parkinson's disease. *J Neurol Sci*. 315(1-2), 39-43 (2012).
- [6] Pouwels S, Bazelier MT, Boer A, et al. Risk of fracture in patients with Parkinson's disease *Osteoporos Int*. 24, 2283-2290 (2013).
- [7] Spillantini M, Schmidt M, Lee V et al.  $\alpha$ -Synuclein in Lewy bodies. *Nature* 388, 839-840 (1997).
- [8] Maroteaux L, Campanelli JT, Scheller R. Synuclein: a neuron-specific protein localized to the nucleus and presynaptic nerve terminal. *Journal of Neuroscience*. 8, 2804-2815 (1988).
- [9] Tredici K, Braak H. Idiopathic Parkinson's disease: staging an  $\alpha$ -synucleinopathy with a predictable pathoanatomy. *Madame Curie Bioscience Database, Austin (TX) Landes Bioscience*; 2000-2013.
- [10] Claassen DO, Josephs KA, Ahlskog JE, et al. REM sleep behavior disorder preceding other aspects of synucleinopathies by up to half a century. *Neurology*. 75, 494-499 (2010).

- [11] Shen Y, Liu CF. Sleep disorders in Parkinson's disease: present status and future prospect. *Chin Med J (Engl)*. 131, 883-885 (2018).
- [12] Maiga B, Diop MS, Sangare M, et al. Sleep quality assessment in 35 Parkinson's disease patients in the Fann Teaching Hospital, Dakar, Senegal. *Rev Neurol (Paris)*.172, 242-7 (2016).
- [13] Niccolini F, Wilson H, Giordano B. et al. Sleep disturbances and gastrointestinal dysfunction are associated with thalamic atrophy in Parkinson's disease. *BMC Neurosci*. 22,20(1), 55 (2009).
- [14] Niwa F, Kuriyama N, Nakagawa M, et al. Circadian rhythm of rest activity and autonomic nervous system activity at different stages in Parkinson's disease. *Auton. Neurosci*. 165,195-200 (2011).
- [15] Jellinger K. Neuropathobiology of non-motor symptoms in Parkinson disease. *J Neural Transm*.122, 1429-1440 (2015).
- [16] Stiasny-Kolster K, Doerr Y, Möller JC, et al. Combination of 'idiopathic' REM sleep behaviour disorder and olfactory dysfunction as possible indicator for alpha-synucleinopathy demonstrated by dopamine transporter FP-CIT-SPECT. *Brain*. 128,126-37 (2005).
- [17] Edwards LL, Quigley EM, Pfeiffer RF. Gastrointestinal dysfunction in Parkinson's disease: frequency and pathophysiology. *Neurology*.42, 726-32 (1992).
- [18] Lebouvier T, Chaumette T, Damier P, et al. Pathological lesions in colonic biopsies during Parkinson's disease. *Gut*. 57(12), 1741-3 (2008).
- [19] Senard JM, Raï S, Lapeyre-Mestre M, et al. Prevalence of orthostatic hypotension in Parkinson's disease. *J Neurol Neurosurg Psychiatry*. 63(5),584-9 (1997).
- [20] Magerkurth C, Schnitzer R, Braune S. Symptoms of autonomic failure in Parkinson's disease: prevalence and impact on daily life. *Clin Auton Res*. 15, 76-82 (2015).
- [21] Kim HJ, Oh ES, Lee JH, et al. Relationship between changes of body mass index (BMI) and cognitive decline in Parkinson's disease (PD). *Arch Gerontol Geriatr*. 55,70-72 (2012).

- [22] Akbar U, He Y, Dai Y, et al. Weight loss and impact on quality of life in Parkinson's disease. *PLoS ONE*. 10(5): e0124541 (2015).
- [23] Gao H, Wei X, Liao J, et al. Lower bone mineral density in patients with Parkinson's disease: a cross-sectional study from Chinese Mainland. *Front. Aging Neurosci*. 7, 203 (2015).
- [24] Tandberg E, Larsen JP, Aarsland D, et al. The occurrence of depression in Parkinson's disease. A community-based study. *Arch Neurol*. 53,175-9 (1996).
- [25] Hogg E, Athreya K, Basile C, Tan EE, Kaminski J, Tagliati M. High Prevalence of Undiagnosed Insulin Resistance in Non-Diabetic Subjects with Parkinson's Disease. *J Parkinsons Dis*. 8(2), 259-265 (2018).
- [26] Yang YW, Hsieh TF, Li CI, et al. Increased risk of Parkinson disease with diabetes mellitus in a population-based study. *Medicine (Baltimore)*. 96(3), e5921 (2017).
- [27] Marques A., Dutheil F Duran E et al. Glucose dysregulation in advanced Parkinson's Disease: too much glucose or not enough insulin?. *Parkinsonism Relat Disord*.55, 122-127 (2018).
- [28] Marinus J, Leentjens A, Visser M, et al. Evaluation of the Hospital Anxiety and Depression Scale in Patients with Parkinson's Disease. *Clinical Neuropharmacology*. 25, 318-324 (2002).
- [29] Papapetropoulos S. Factors associated with drug-induced visual hallucinations in Parkinson's disease. *Journal of Neurology*.252, 1223-1228 (2005).
- [30] Weintraub D, Koester J, Potenza MN, et al. Impulse control disorders in Parkinson disease: a cross-sectional study of 3090 patients. *Arch Neurol*. 67,589-95 (2010).
- [31] Zhang G, Zhang Z, Liu L, et al. Impulsive and compulsive behaviors in Parkinson's Disease. *Front Aging Neurosci*. 6, 318 (2014).
- [32] Kanis JA et al. A new approach to the development of assessment guidelines for osteoporosis. *Osteoporosis International*.13, 527-536 (2002).

- [33] Johnell O, Gullberg B, Kanis JA. The hospital burden of vertebral fracture in Europe: a study of national register sources. *Osteoporosis International*. 7, 138-144 (1997).
- [34] Taggard H, Crawford V. Reduced bone density of the hip in elderly patients with Parkinson's disease. *Age and Ageing*. 24, 326-328 (1995).
- [35] Zhao Y, Shen L, Ji HF. Osteoporosis risk and bone mineral density levels in patients with Parkinson's disease: a meta-analysis. *Bone*. 52, 498-505 (2013).
- [36] Hagenau T, Vest R, Gissel TN, et al. Global vitamin D levels in relation to age, gender, skin pigmentation and latitude: an ecologic meta-regression analysis. *Osteoporos Int*. 20, 133-140 (2009).
- [37] Karsenty G. Convergence between bone and energy homeostasis: leptin regulation of bone mass. *Cell Metab*. 4(5), 341-8 (2006).
- [38] Glass DA, Bialek P, Ahn JD, et al. Canonical Wnt signaling in differentiated osteoblasts controls osteoclast differentiation. *Dev Cell*. 8, 751-64 (2005).
- [39] Kondo A, Togari A. *In vivo* stimulation of sympathetic nervous system modulates osteoblastic activity in mouse calvaria. *Am J Physiol Endocrinol Metab*. 285, E661-7 (2003).
- [40] Webber RH, DeFelice R, Ferguson RJ, et al. Bone marrow response to stimulation of the sympathetic trunks in rats. *Acta Anat (Basel)*. 77, 92-7 (1970).
- [41] Asada N, Katayama Y, Sato M, et al. Matrix-Embedded Osteocytes Regulate Mobilization of Hematopoietic Stem/Progenitor Cells. *Cell Stem Cell*. 12, 737-747 (2013).
- [42] Handa K, Kiyohara S, Yamakawa T, et al. Bone loss caused by dopaminergic degeneration and levodopa treatment in Parkinson's disease model mice. *Scientific Reports*. 9, 13768 (2019).
- [43] Rittweger J, Frost HM, Schiessl H, et al. Muscle atrophy and bone loss after 90 days' bed rest and the effects of flywheel resistive exercise and pamidronate: results from the LTBR study. *Bone*. 36, 1019-29 (2005).

- [44] Verschueren S, Gielen E, O'Neill TW, et al. Sarcopenia and its relationship with bone mineral density in middle-aged and elderly European men. *Osteoporos Int.* 24, 87-98 (2013).
- [45] Johannesdottir F, Aspelund T, Siggeirsdottir K, et al. Mid-thigh cortical bone structural parameters, muscle mass and strength, and association with lower limb fractures in older men and women (AGES-Reykjavik Study). *Calcif Tissue Int.* 90, 354-64 (2012).
- [46] Peball M, Mahlkecht P, Werkmann M, et al. Prevalence and associated factors of sarcopenia and frailty in Parkinson's disease: a cross-sectional study. *Gerontology.* 65, 216-228 (2019).
- [47] Olney RC. Regulation of bone mass by growth hormone. *Med Pediatr Oncol.* 41, 228-34 (2003).
- [48] Isaacs CM, Zaidi M, Blair HC. ACTH is a novel regulator of bone mass. *Ann N Y Acad Sci.* 1192, 110-6 (2010).
- [49] Chiodini I, Scillitani A. Role of cortisol hypersecretion in the pathogenesis of osteoporosis. *Recenti Progressi in Medicina.* 99, 309-313 (2008).
- [50] Bellomo G, Santambrogio L, Fiacconi M, et al. Plasma profiles of adrenocorticotrophic hormone, cortisol, growth hormone and prolactin in patients with untreated Parkinson's disease. *J Neurol.* 238, 19-22 (1991).
- [51] Lim, Shen Yang, Fox, Susan H, Lang, Anthony E. Overview of the Extranigral Aspects of Parkinson Disease. *Arch Neurol.* 66, 167-172 (2009).
- [52] Langston W, Forno L. The hypothalamus in Parkinson disease. *Annals of Neurology.* 3, 129-133 (1978).
- [53] Conte-Devolx B, Pfister B, Viallet F, Rey M, et al. The anterior pituitary endocrine function in Parkinson's disease. *Presse Med.* 16, 566-568 (1987).
- [54] Ding H, Dhima K, Lockhart KC, et al. Unrecognized vitamin D3 deficiency is common in Parkinson disease. *Neurology.* 22, 1531-1537 (2013).

- [55] Evatt ML, DeLong MR, Khazai N, et al. Prevalence of vitamin D insufficiency in patients with Parkinson disease and Alzheimer disease. *Arch Neurol.* 65,1348-1352 (2008).
- [56] Wang L, Evatt ML, et al. Vitamin D from different sources is inversely associated with Parkinson disease. *Mov Disord.* 30, 560-566 (2015).
- [57] Sato Y, Kikuyama M, Oizumi K. High prevalence of vitamin D deficiency and reduced bone mass in Parkinson's disease. *Neurology.* 49, 1273-8 (1997).
- [58] Tan L, Wang Y, Zhou L, et al. Parkinson's disease and risk of fracture: a meta-analysis of prospective cohort studies. *PLoS One.* 9, e94379 (2014).
- [59] Goodwin V, Richards SH, Henley W, et al. An exercise intervention to prevent falls in people with Parkinson's disease: a pragmatic randomized controlled trial. *J Neurol Neurosurg Psychiatry.* 82, 1232e1238 (2011).
- [60] Allen NE, Sherrington C, Paul SS, Canning CG. Balance and falls in Parkinson's disease: a meta-analysis of the effect of exercise and motor training. *Mov Disord.* 26,1605-15 (2011).
- [61] Silva de Lima AL, Smits T, Darweesh SKL, et al. Home-based monitoring of falls using wearable sensors in Parkinson's disease. *Mov Disord.* 35, 109-115 (2020).
- [62] Woodford H, Walker R. Emergency hospital admissions in idiopathic Parkinson's disease. *Mov Disord.* 20, 1104e8 (2005).
- [63] Otomune H, Mihara M, Hattori N, et al. Involvement of cortical dysfunction in frequent falls in patients with Parkinson's disease. *Parkinsonism and Related Disorders.* 64,169-174 (2019).
- [64] Braak H, Braak E. Pathoanatomy of Parkinson's disease. *J Neurol.* 247, II/3-II/10 (2000).
- [65] Harris-Hayes M, Willis A, Klein S, et al. Relative Mortality in U.S. Medicare beneficiaries with Parkinson disease and hip and pelvic fractures. *J Bone Joint Surg Am.* 96, e27(1-7) (2014).

[66] Coomber R, Alshameeri Z, Masia AF, Mela F, Parker MJ. Hip fractures and Parkinson's disease: A case series. 48, 2730-2735 (2017).

[67] Leisman G, Braun-Benjamin O, Melillo R. Cognitive-motor interactions of the basal ganglia in development. *Front Syst Neurosci.* 8, 16 (2014).

[68] Kucinskia A, Albin R, Lustig C, et al. Modeling falls in Parkinson's disease: Slow gait, freezing episodes and falls in rats with extensive striatal dopamine loss. *Behavioural Brain Research.* 282, 155-164 (2015).

[69] Vetrano DL, Pisciotta MS, Laudisio A, et al. Sarcopenia in Parkinson disease: Comparison of different criteria and association with disease severity. *J Am Med Dir Assoc.* 19, 523-527 (2018).

[70] Sharir A, Stern T, Rot C, et al. Muscle force regulates bone shaping for optimal load-bearing capacity during embryogenesis. *Development* 138,3247-59 (2011).

[71] Bonewald LF, Kiel DP, Clemens TL, et al. Forum on bone and skeletal muscle interactions: summary of the proceedings of an ASBMR workshop. *J Bone Miner Res.* 28, 1857-65 (2013).

[72] Li M, Li C, Parkhouse WS. Age-related differences in the des IGF-I-mediated activation of Akt-1 and p70 S6K in mouse skeletal muscle. *Mechanisms of Ageing and Development.* 124, 771-778 (2003).

[73] Liu JM, Zhao HY, Ning G, et al. IGF-1 as an early marker for low bone mass or osteoporosis in premenopausal and postmenopausal women. *J Bone Miner Metab.* 26,159-64 (2008).

[74] Prasad KN. Oxidative Stress, Pro-Inflammatory Cytokines, and Antioxidants Regulate Expression Levels of MicroRNAs in Parkinson's Disease. *Curr Aging Sci.* 10,177-184 (2017).

[75] Godau J, Herfurth M, Kattner B, et al. Increased serum insulin-like growth factor 1 in early idiopathic Parkinson's disease. *J Neurol Neurosurg Psychiatry.* 81, 536-538 (2010).

- [76] Godau J, Knauel K, Weber K, et al. Serum Insulinlike Growth Factor 1 as possible marker for risk and early diagnosis of Parkinson disease. *Arch Neurol.* 68, 925-931 (2011).
- [77] Fleming SM, Tetreault NA, Mulligan CK, et al. Olfactory deficits in mice overexpressing human wildtype alpha-synuclein. *Eur. J. Neurosci.* 28, 247-256 (2008).
- [78] Koprach JB, Johnston TH, Huot P, Reyes MG, Espinosa M, et al. Progressive neurodegeneration or endogenous compensation in an animal model of Parkinson's disease produced by decreasing doses of Alpha-Synuclein. *PLOS ONE.* 6, e17698 (2011).
- [79] Crabtree DM, Zhang J. Genetically engineered mouse models of Parkinson's disease. *Brain Res Bull.* 88,13-32 (2012).
- [80] Emmer KL, Waxman EA, Covy JP, et al. E46K human alpha-synuclein transgenic mice develop Lewy-like and tau pathology associated with age-dependent, detrimental motor impairment. *J Biol Chem.* 286, 35104-18 (2011).
- [81] Zimprich A, Müller-Myhsok B, Farrer M, et al. The PARK8 locus in autosomal dominant parkinsonism: confirmation of linkage and further delineation of the disease-containing interval. *Am J Hum Genet.* 74,11-19 (2004).
- [82] Berwick DC, Javaheri B, Wetzell A, et al. Pathogenic LRRK2 variants are gain-of-function mutations that enhance LRRK2-mediated repression of  $\beta$ -catenin signaling. *Mol Neurodegener.* 12, 9 (2017).
- [83] Calabrese G, Mesner LD, Foley PL, et al. Network analysis implicates alpha-synuclein (*snca*) in the regulation of ovariectomy-induced bone loss. *Sci Rep.* 6, 29475 (2016).
- [84] Nakaia M, Fujitaa M, Waragaia M, et al. Expression of  $\alpha$ -synuclein, a presynaptic protein implicated in Parkinson's disease, in erythropoietic lineage. *Biochem Biophys Res Commun.* 358,104-10 (2007).
- [85] Reid IR, Bolland MJ, Grey A. Effects of vitamin D supplements on bone mineral density: a systematic review and meta-analysis. *Lancet.* 383, 146-55 (2014).

[86] Zhu K, Austin N, Devine A, et al. A Randomized controlled trial of the effects of vitamin d on muscle strength and mobility in older women with vitamin d insufficiency. *J Am Geriatr Soc.* 58, 2063-8 (2010).

[87] Dhesi JK, Jackson SH, Bearne LM, et al. Vitamin D supplementation improves neuromuscular function in older people who fall. *Age Ageing.* 33, 589-95 (2004).

[88] Murad MHElamin KB, Abu Elnour NO, et al. The effect of vitamin D on falls: a systematic review and meta-analysis. *J Clin Endocrinol Metab.* 10, 2997-3006 (2011).

[89] Bolland MJ, Grey A, Avenell A. Effects of vitamin D supplementation on musculoskeletal health: a systematic review, meta-analysis, and trial sequential analysis. *Lancet Diabetes Endocrinol.* 6, 847-858 (2018).

[90] Burt LA, Billington EO, Rose MS, et al. Effect of high-dose vitamin D supplementation on volumetric bone density and bone strength: A Randomized Clinical Trial. *JAMA.* 27, 736-745 (2019).

[91] Keen R. Osteoporosis: strategies for prevention and management. *Best Pract Res Clin Rheumatol.* 21(1),109-122 (2007).

[92] MacLean C, Newberry S, Maglione M, et al. Systematic review: comparative effectiveness of treatments to prevent fractures in men and women with low bone density or osteoporosis. *Ann Intern Med.* 148,197-213 (2008).

[93] Reid I, Brown JP, Burckhardt P, et al. Intravenous zoledronic acid in postmenopausal women with low bone mineral density. *N Engl J Med.* 346, 653-61(2002).

[94] Black DM, Delmas PD, Eastell R, et al. Once-yearly zoledronic acid for treatment of postmenopausal osteoporosis. *N Engl J Med.* 356, 1809-22 (2007).

[95] Eastell R, Christiansen C, Grauer A, et al. Effects of denosumab on bone turnover markers in postmenopausal osteoporosis. *J Bone Miner Res.* 26, 530-7 (2011).

[96] Lindsay R, Nieves J, Formica C, et al. Randomized controlled study of effect of parathyroid hormone on vertebral-bone mass and fracture incidence among postmenopausal women on oestrogen with osteoporosis. *Lancet.* 350, 550-5 (1997).

- [97] Dobnig H, Sipos A, Jiang Y, et al. Early changes in biochemical markers of bone formation correlate with improvements in bone structure during teriparatide therapy. *J Clin Endocrinol Metab.* 90, 3970-7 (2005).
- [98] Fontalis A, Kenanidis E, Kotronias RA, et al. Current and emerging osteoporosis pharmacotherapy for women: state of the art therapies for preventing bone loss. *Expert Opin Pharmacother.* 20, 1123-1134 (2019).
- [99] Miller PD, Hattersley G, Riis BJ, et al. Effect of Abaloparatide vs placebo on new vertebral fractures in postmenopausal women with osteoporosis: a randomized clinical trial. *JAMA.* 316, 722-33 (2016).
- [100] Bhasin S, Gill TM, Reuben DB, et al. Strategies to reduce injuries and develop confidence in elders (stride): a cluster-randomized pragmatic trial of a multifactorial fall injury prevention strategy: design and methods. *J Gerontol A Biol Sci Med Sci.* 73, 1053-1061 (2018).
- [101] Cummings SR, Eastell R. Risk and prevention of fracture in patients with major medical illnesses: a mini-review. *J Bone Miner Res.* 31, 2069-72 (2016).
- [102] Figueroa CA & Rosen CJ. Parkinson's disease and osteoporosis: basic and clinical implications, *Expert Review of Endocrinology & Metabolism*, 15:3, 185-193 (2020).
- [103] Ninkina N, Connor-Robson N, Ustyugov AA, Tarasova TV, Shelkownikova TA, Buchman VL. A novel resource for studying function and dysfunction of alpha-synuclein: mouse lines for modulation of endogenous *Sncα* gene expression. *Sci Rep.* 5, 16615 (2015).
- [104] Malcolm Logan, James F. Martin, et al. Expression of Cre recombinase in the developing mouse limb bud driven by a *Prxl* enhancer. *Genesis.* 33, 77-80 (2002)
- [105] Eguchi J; Wang X; Yu S; Kershaw EE; Chiu PC; Dushay J; Estall JL; Klein U; Maratos-Flier E; Rosen ED. Transcriptional control of adipose lipid handling by IRF4. *Cell Metab* 13(3), 249-59 (2011).

- [106] Ji C, Walton J, Su Y, Tella M. Simultaneous determination of plasma epinephrine and norepinephrine using an integrated strategy of a fully automated protein precipitation technique, reductive ethylation labeling and UPLC-MS/MS. *Anal Chim Acta.* 670(1-2), 84-91 (2010).
- [107] Bradley D, Liu J, Blaszcak A, et al. Adipocyte DIO2 Expression Increases in Human Obesity but Is Not Related to Systemic Insulin Sensitivity. *J Diabetes Res.* 2018, 2464652 (2018).
- [108] Kun Liu, Shengli Zhou, Ji-Young Kim, Kristin Tillison, et al. Functional analysis of FSP27 protein regions for lipid droplet localization, caspase-dependent apoptosis, and dimerization with CIDEA. *Am J Physiol Endocrinol Metab.* 297, E1395-E1413, (2009).
- [109] Martin JF, Bradley A, Olson EN. The paired-like homeo box gene M<sub>Hox</sub> is required for early events of skeletogenesis in multiple lineages. *Genes Dev.*, 9,1237-1249 (1995).
- [110] Calabrese G, Mesner LD, Foley PL, et al. Network analysis implicates alpha-Synuclein (*Snca*) in the regulation of ovariectomy-induced bone loss. *Sci Rep.* 6, 29475. (2016).
- [111] Maroteaux L, Campanelli J, and Scheller R. Synuclein: a neuron-specific presynaptic nerve terminal protein localized to the nucleus. *The Journal of Neuroscience.* 8, 2804-2815 (1988).
- [112] Spillantini MG, Schmidt ML, Lee V, Trojanowski JQ.  $\alpha$ -Synuclein in Lewy bodies. *Nature.* 388, 839-840 (1997).
- [113] Irizarry MC, Growdon W, Gomez-Isla T, et al. Nigral and cortical Lewy bodies and dystrophic nigral neurites in Parkinson's disease and cortical Lewy body disease contain alpha-synuclein immunoreactivity. *J Neuropathol Exp Neurol.* 57,334-337 (1998).
- [114] Drey M, Hasmann S, Krenovsky JP, Hobert MA, Straub S et al. Associations between Early Markers of Parkinson's Disease and Sarcopenia. *Frontiers in Aging Neuroscience.*9, 53 (2017).
- [115] Gao H, Wei X, Liao J, et al. Lower bone mineral density in patients with Parkinson's disease: a cross-sectional study from Chinese Mainland. *Front Aging Neurosci.* 7, 203. (2015).

- [116] Tan L, Wang Y, Zhou L, et al. Parkinson's disease and risk of fracture: a meta-analysis of prospective cohort studies. *PLoS One*. 9, e94379 (2014).
- [117] Higuchi, M., Yoshida, S., Ueharu, H. et al. PRRX1 and PRRX2 distinctively participate in pituitary organogenesis and a cell-supply system. *Cell Tissue Res*, 357, 323-335 (2014).
- [118] Shimozaki K, Clemenson GD Jr, Gage FH. Paired related homeobox protein 1 is a regulator of stemness in adult neural stem/progenitor cells. *J Neurosci*. 33, 4066- 4075. (2013).
- [119] Souza V.R., Mendes E., Casaro M., Antiorio A.T.F.B., Oliveira F.A., Ferreira C.M. Description of ovariectomy protocol in mice. In: Guest P. (eds) *Pre-Clinical Models. Methods in Molecular Biology*, vol 1916. Humana Press, New York, NY. (2019).
- [220] Vellers HL, Letsinger AC, Walker NR, Granados JZ, Lightfoot JT. High fat high sugar diet reduces voluntary wheel running in mice independent of sex hormone involvement. *Front Physiol*. 8, 628 (2017).
- [221] Russek M, Soto-Mora LM, T. Uriostegui, R. Racotta, Effects of catecholamines on water intake in rats. *Physiology & Behavior*. 49, 201-206 (1991).
- [222] Pal K, Bharathi B, Thombre DP. Modulation of daily water intake by dopamine in caudate and accumbens nuclei in rats, *Physiology & Behavior*. 51, 851-856 (1992).
- [223] Guneyssel O, Onultan O, Onur O. Parkinson's disease and the frequent reasons for emergency admission. *Neuropsychiatr Dis Treat*. 4,711-714 (2008).
- [224] Mao CJ, Zhong CK, Yang Y, et al. Serum sodium and chloride are inversely associated with dyskinesia in Parkinson's disease patients. *Brain Behav*. 7, e00867 (2017).
- [225] Menezes-Rodrigues FS, Scorza CS, Fiorini AC, et al. Sudden unexpected death in Parkinson's disease: why is drinking water important?. *Neurodegenerative Disease Management*. 9, 241-246 (2019).

- [226] Andersen AD, Blaabjerg M, Binzer M, et al. Cerebrospinal fluid levels of catecholamines and its metabolites in Parkinson's disease: effect of L-DOPA treatment and changes in levodopa-induced dyskinesia. *J Neurochem.*,141, 614-625 (2017).
- [227] Ryczko D, Grätsch S, Auclair F, Dubé C, Bergeron S, et al. Descending dopaminergic inputs control locomotion. *Proceedings of the National Academy of Sciences*, 110, e3235-e3242 (2013).
- [228] Njung'e K, Handley SL. Evaluation of marble-burying behavior as a model of anxiety. *Pharmacol Biochem Behav.*, 38, 63-7 (1991).
- [229] Levine JA, McCrady SK, Lanningham-Foster LM, Kane PH, Foster RC, Manohar CU. The role of free-living daily walking in human weight gain and obesity. *Diabetes*. 57, 548-54 (2008).
- [230] Schmidt SL, Harmon KA, Sharp TA, Kealey EH, Bessesen DH. The effects of overfeeding on spontaneous physical activity in obesity prone and obesity resistant humans. *Obesity (Silver Spring)*. 20, 2186-93 (2012).
- [231] Sharma S, Fulton S. Diet-induced obesity promotes depressive-like behaviour that is associated with neural adaptations in brain reward circuitry. *Int J Obes (Lond)*. 37, 382-389 (2013).
- [232] Lykouras L, Michopoulos J. Anxiety disorders and obesity. *Psychiatriki*. 22, 307-313 (2011).
- [233] De la Cruz-Cano E, Tovilla-Zarate CA, Reyes-Ramos E, et al. Association between obesity and depression in patients with diabetes mellitus type 2; a study protocol. *F1000Res*. 4, 7 (2015).
- [234] Rodriguez-Araujo, G., Nakagami, H., Takami, Y. et al. Low alpha-synuclein levels in the blood are associated with insulin resistance. *Sci Rep* 5, 12081 (2015).
- [235] Geng X, Lou H, Wang J, et al.  $\alpha$ -Synuclein binds the K(ATP) channel at insulin-secretory granules and inhibits insulin secretion. *Am J Physiol Endocrinol Metab*. 300(2), E276-E286 (2011).

- [236] Theresa R. Bomfim, Sergio T. Ferreira, Fernanda G. De Felice et al. An anti-diabetes agent protects the mouse brain from defective insulin signaling caused by Alzheimer's disease-associated A $\beta$  oligomers. *J Clin Invest.* 122(4),1339-1353 (2012).
- [237] Bamji-Mirza M, Callaghan D, Najem D, Shen S, Hasim MS, Yang Z, et al. Stimulation of insulin signaling and inhibition of JNK-AP1 activation protect cells from amyloid-beta-induced signaling dysregulation and inflammatory response. *J Alzheimers Dis.* 40,105-122 (2014).
- [238] Gao H, Wei X, Liao J, et al. Lower bone mineral density in patients with Parkinson's disease: a cross-sectional study from Chinese Mainland. *Front Aging Neurosci.* 7, 203. (2015)
- [239] Sripetchwandee, J.; Chattipakorn, N.; Chattipakorn, S.C. Links between obesity-induced brain insulin resistance, brain mitochondrial dysfunction, and dementia. *Front. Endocrinol.* 9, 496 (2018).
- [240] Ruegsegger, G.N.; Crea, A.L.; Cortes, T.M.; Dasari, S.; Nair, K.S. Altered mitochondrial function in insulin-deficient and insulin-resistant states. *J. Clin. Investig.* 128, 3671-3681 (2018).
- [241] Kim, B.; Feldman, E.L. Insulin resistance in the nervous system. *Trends Endocrinol. Metab.*,23, 133-141 (2012).
- [242] Seong Su Kang, Zhentao Zhang, Xia Liu, Fredric P. et al. Alpha-synuclein binds and inhibits TrkB receptors. *Proceedings of the National Academy of Sciences Oct 114 (40) 10773-10778 (2017).*
- [243] Hong CT, Chen KY, Wang W, et al. Insulin resistance promotes Parkinson's disease through aberrant expression of  $\alpha$ -Synuclein, mitochondrial dysfunction, and deregulation of the polo-like kinase 2 signaling. *Cells.* 9(3):740 (2020).
- [244] Camargo Maluf F, Feder D, Alves de Siqueira Carvalho A. Analysis of the relationship between type ii diabetes mellitus and Parkinson's disease: a systematic review. *Parkinsons Dis.* 4951379 (2019).

[245] Athauda, D., Maclagan, K., Skene, S.S., Bajwa-Joseph, M., et al. Exenatide once weekly versus placebo in Parkinson's disease: A randomized, double-blind, placebo-controlled trial. *Lancet*. 390, 1664-1675 (2017).

[246] Gaster M, Staehr P, Beck-Nielsen H, et al. GLUT4 Is Reduced in Slow Muscle Fibers of Type 2 Diabetic Patients *Diabetes*. 50 (6), 1324-1329 (2001).

## BIOGRAPHY OF THE AUTHOR

Carolina Andrea Figueroa Amenábar was born in Punta Arenas, Chile in 1985. She graduated with honors from Bachelor in Science, biology major from University of Chile in 2009.

While doing her Bachelor's, she joined Dr. Miguel Concha Laboratory, in the Faculty of Medicine in University of Chile and in 2009 became a Research Assistant at his lab.

There she worked in several projects, such as "Role of E- and N-cadherins in migration of embryonic cell layers during epiboly" using the teleost fish *Cyngolebias nigripinnis*, as *in vivo* model. Later, she took over a few projects of Dr. Concha's collaborator, Dr. Steffen Härtel to work in the "Quantification of morphological changes in collective migration of neural crests" using *Danio rerio* (zebrafish) as *in vivo* model, a collaboration with Dr. Claudia Linker at King's College London.

In 2011, at Dr. Härtel's Lab and together with informatic engineers, she worked to develop a "Computed-assisted evaluation of DNA fragmentation of human sperm" as a tool for infertility diagnosis.

In 2013, she gets accepted in the Master of Science, major in Nutrition and Food program at University of Chile and in 2014 she joined Dr. Juan Pablo Rodriguez Laboratory to study "The role of BMP-2 in lineage commitment in bone mesenchymal stem cells from postmenopausal osteoporotic women" as a Master's thesis project.

With intentions to continue in the bone field and her scientific training, she joined the University of Maine Graduate School of Biomedical Science and Engineering and began her work in the lab of Dr. Clifford Rosen at the Maine Medical Center Research Institute in 2015.

At the Rosen lab she worked on the role of  $\alpha$ -Synuclein in bone and adipose tissue. She has two first author publications and two supporting author publications. She is currently working in her third first author publication. She is a candidate for the Doctor of Philosophy degree in Biomedical Sciences and Engineering from The University of Maine in August 2020.